INFORMATION TO USERS

While the most advanced technology has been used to photograph and reproduce this manuscript, the quality of the reproduction is heavily dependent upon the quality of the material submitted. For example:

- Manuscript pages may have indistinct print. In such cases, the best available copy has been filmed.

- Manuscripts may not always be complete. In such cases, a note will indicate that it is not possible to obtain missing pages.

- Copyrighted material may have been removed from the manuscript. In such cases, a note will indicate the deletion.

Oversize materials (e.g., maps, drawings, and charts) are photographed by sectioning the original, beginning at the upper left-hand corner and continuing from left to right in equal sections with small overlaps. Each oversize page is also filmed as one exposure and is available, for an additional charge, as a standard 35mm slide or as a 17"x 23" black and white photographic print.

Most photographs reproduce acceptably on positive microfilm or microfiche but lack the clarity on xerographic copies made from the microfilm. For an additional charge, 35mm slides of 6"x 9" black and white photographic prints are available for any photographs or illustrations that cannot be reproduced satisfactorily by xerography.

Order Number 8725193

Prediction and analysis of basic gravitational microlensing phenomena

Nemiroff, Robert J., Ph.D.

University of Pennsylvania, 1987

U·M·I
300 N. Zeeb Rd.
Ann Arbor, MI 48106

PLEASE NOTE:

In all cases this material has been filmed in the best possible way from the available copy. Problems encountered with this document have been identified here with a check mark __✓__.

1. Glossy photographs or pages _____
2. Colored illustrations, paper or print _____
3. Photographs with dark background _____
4. Illustrations are poor copy _____
5. Pages with black marks, not original copy __✓__
6. Print shows through as there is text on both sides of page _____
7. Indistinct, broken or small print on several pages __✓__
8. Print exceeds margin requirements _____
9. Tightly bound copy with print lost in spine _____
10. Computer printout pages with indistinct print _____
11. Page(s) _____ lacking when material received, and not available from school or author.
12. Page(s) _____ seem to be missing in numbering only as text follows.
13. Two pages numbered _____. Text follows.
14. Curling and wrinkled pages __✓__
15. Dissertation contains pages with print at a slant, filmed as received __✓__
16. Other _____

_____

_____

University
Microfilms
International

PREDICTION AND ANALYSIS OF BASIC GRAVITATIONAL MICROLENSING PHENOMENA

Robert J. Nemiroff

A DISSERTATION

in

ASTRONOMY AND ASTROPHYSICS

Presented to the Graduate Faculty of the University of Pennsylvania in Partial Fulfillment of the Requirements for the Degree of Doctor of Philosophy

1987

Robert H. Koch
Supervisor of Dissertation

Kenneth Lande
Graduate Group Chairperson

Acknowledgements

Although my name is the only one that appears on the thesis, the efforts of many people are actually represented here. The formulation and realization of this thesis were the result of a comedy of unlikely situations, and without the specific influence of several people, it would not have materialized as it did.

Specifically, in chronological order, Drs. Ftaclas, Wiita, Koch, and Paczynski all were a great help and influence, both in criticism of my work and in general advice and counsel. I also owe a great deal to the Zaccheus Daniel Foundation for their several years of financial support, which gave me enormous freedom to work on what I choose.

I would also like to acknowledge the 'general positive influence' of the (then) graduate students of the Department of Astronomy and Astrophysics. Particularly meritorious in this respect are J. Goldstein, V. Migenes, and M. Corcoran. We frequently worked feverishly as a team in a quest to understand the universe for the betterment of mankind, a quest usually successful as shown by our handing our homework in on time.

Abstract

Prediction and Analysis of Basic Gravitational Microlensing Phenomena

Robert J. Nemiroff

Supervisor: Robert H. Koch

The phenomena of gravitational microlensing are described, and predictions are made about its possible future detection. A mathematical formalism is developed which exploits gravitational lensing effects in terms of photometric measuring capability. This formalism is then used to outline the most probable places to look for microlensing.

Basic microlensing induced light curves are calculated for a variety of possible lens-source configurations. These configurations include that of a single star acting as a lens, and that of a double star acting as the lens. The light curve signatures of the double star lens are themselves indicators of the microlensing phenomenon. Light curve signatures for a single star acting on a uniform extended source are presented. Analysis is described listing methods by which parameters taken from this light curve could be used to recover both lens and source information.

The effect of microlensing on the shape of the spectral lines originating in the broad line emission region (BLR) of an active galactic nucleus (AGN) is analyzed. For various possible dynamical models of AGN make-up, it is shown that microlens-

ing could distort the shape of a spectral emission line. Microlensing typically amplifies the center of the BLR emission line, but, for some models, it can amplify the wings, or shift the central peak instead.

A sample finding list of QSO's is presented for observers. For the assumption of galaxies made up entirely of compact objects, calculations are presented for each QSO on the list, listing optical depth for microlensing, the average time between microlensing events of various amplitudes, and the expected duration of an event. Possible observing programs are described.

Much could be learned from the identification and analysis of microlensing induced photometric and spectroscopic variations. Recoverable information includes AGN structure at 10^{-6} arcsec resolution, galaxy proper motion at 10^{-6} arcsec/year, and the number and mass density of lensing stars in galaxies.

Table of Contents

List of Tables

List of Figures

Chapter 1

Introduction

1.1) Historical Perspective

The concept of gravitational lensing - that objects may gravitationally affect the light from sources behind them - can be traced back to the early 1800's, specifically to Soldner (1801). Combining Newtonian gravitational theory with the particle theory of light, Soldner predicted that a star could be imaged twice if another star lay close to the light path to the observer. One of these images would appear on one side of the lensing star, while the gravity of the lens would pull another image around the other side. No example of this was observed at the time.

Gravitational lensing ideas gained importance when Einstein predicted that the Sun would noticeably deflect starlight passing just outside its limb. Einstein actually made this prediction at two different times of his career. The first time (Einstein 1908) he incorporated a somewhat Newtonian calculation predicting the solar deflection would be 0".88. Later (Einstein 1916), with the advent of General Relativity (GR), he predicted a solar deflection at the limb of 1".76. The later prediction was roughly confirmed by expeditions to the 1919 solar eclipse (Eddington 1919), where the results of the Newtonian calculation were definitely ruled out.

Much later, R. W. Mandl approached Einstein and asked him to calculate the parameters involved in measuring gravitational lensing by stars other than the Sun (Einstein 1936). Einstein did this and concluded that although it was possible for

stars to split, deflect, or distort the images of stars behind them, these effects were not measurable in practice. The main reason for this, he wrote, was the obscuring effect of the brightness of the star that acts as the lens.

Others soon began to think about gravitational lensing. Tikhov (1937) worked out many of the mathematical properties of a point lens acting on a point source. Zwicky (1937a, 1937b, 1957) became convinced that galaxies could eclipse each other and hence act as lenses. He estimated that the probability of observing this effect was very high. But the analysis of Einstein had cast a shadow on the search for lensing outside the solar system, and no major advance in the subject would appear for more than a decade.

The subject was revived in 1964 with the emergence of two separate works: Liebes (1964) and Refsdal (1964). Both worked out more of the mathematics of a point lens acting on a point source and applied their calculations to a more modern knowledge of the Milky Way galaxy. Both estimated the probability of measuring such a gravitational lens effect for stars in our galaxy. In these works it was concluded that a gravitational lens effect caused by stars within our own galaxy was a relatively rare event, but with long and careful observations, such an event might be detected.

In the later 1960's, J. and M. Barnothy tried to invoke gravitational lensing as the explanation for several of the outstanding astrophysical problems of the day. They predicted that stars within our own galaxy could gravitationally affect the

light from quasars at cosmological distances. They also proposed that QSO's, N galaxies, and Seyfert Nuclei were anomalously bright because they were in fact being lensed by intermediate galaxies (Barnothy and Barnothy 1969). Another of their models explained pulsars as artifacts of a stellar lens in a nearby binary system acting to modulate the flux from distant quasars (Barnothy 1968). Although most of their models have fallen out of favor today, the ideas behind them were ahead of their time.

In the early 1970's, papers on stellar gravitational lensing were relatively few. There seemed, however, to be a growing realization that gravitational lensing *should* be seen if some models of the mass distribution in the universe were correct. Press and Gunn (1973) showed that if the universe were uniformly populated with certain types of objects, and the density of such objects were comparable to the visible mass, several gravitational lens effects should be observable. These effects include a change in the number density of quasars seen in magnitude intervals of different redshifts, and double imaging of the background quasars.

Maeder (1973) showed how the resulting flux from a binary system could be altered by gravitational lensing. He calculated the amplification of a point lens on a circular source. He also computed light curves for various hypothetical binary systems. He concluded that most binary systems do not show any measurable gravitational lens effects. Only the systems which show eclipses and in which one star is compact and widely separated from another star would be expected to show

noticeable gravitational lens effects in the resultant light curve.

The detection of the first extra-solar system gravitational lens event came in 1979 with the discovery by Walsh, Carswell, and Weymann (1979) of two gravitationally induced images of the same quasar 0957 + 561. The two images were interpreted as that of a single quasar whose light is split by a galaxy along the line of sight. Since then, eight other gravitational lens candidates have been put forward, all of them caused by lenses of galactic mass or greater. These cases have come to be known as macrolensing. They are important to the present work in that they are also quite likely to show lensing by stars within the lensing galaxy: microlensing. It is not the purpose of this thesis, however, to study macrolensing, and so that specific work will not be reviewed in detail.

In 1979 microlensing began to gain popularity. Chang and Refsdal (1979, 1984) showed that a single star, with the addition of the gravitational shear (discussed later) of the host galaxy, could split the image of a quasar into very close components and either magnify or diminish the flux from the original quasar image.

Gott (1981) discussed the possibility that the haloes of spiral galaxies could be composed of low mass stars that could themselves lens background quasars. The paper predicted the likelihood and time scale of such events, and suggested that observations of quasar 0957 + 561 might show this microlensing phenomenon.

More recently, Paczynski (1986) calculated the effect of many stars in a galaxy acting at once as a lens. These effects were shown to be much more complicated

than that due to each stellar lens individually. The corresponding light curves were calculated and displayed.

Since the discovery of macrolensing systems, the number of papers written on gravitational lensing has increased dramatically. Although most papers attempt to model the mass distribution needed for macrolens systems, there has been a major conspicuous attempt to understand the effects of microlensing. To date, however, no unambiguous microlensing detection has been made.

1.2) Principles of Gravitational Lensing

According to GR, gravitation acts on light as well as upon matter. The result of this interaction is to deflect a photon away from a path that would appear straight as viewed by an observer at infinity. In this way, non-uniform gravitational fields can act as lenses.

A particular gravitational field that merits study in the way it deflects light is the field of a point mass. Far from a point mass, a linear approximation to GR is valid. The angular deflection of a photon is very nearly $i = 2R_s/R$, where R_s is the Schwarzschild radius of the point mass, and R, the impact parameter, is the distance of closest approach of the photon to the mass. It is a good approximation to assume that the photon is deflected discretely when it crosses the lensing plane (the plane containing the lensing mass perpendicular to the line connecting the source to the observer, see Refsdal 1964 on this point).

If the lens (assumed spherical) has a finite radius L greater than R_s, a unique

focal length can be defined. Light traveling parallel to the axis connecting the observer to the center of the lens and incident on the lensing plane at a given b is deflected so that it will cross this axis. Clearly, the smaller is b, the closer to the lens the ray crosses the axis. At $b = R$, the ray passes just outside the surface of the lensing mass. The distance between the lens and the point the ray crossed the axis is then at a minimum, hence this distance could be called the minimum focal length of the lens, or just the focal length F. The geometry is shown in Figure 1.2.1. The focal length is easily shown to be

$$F = 538\left(\frac{R}{R_\odot}\right)^2\left(\frac{M_\odot}{M}\right)AU. \qquad (1.2.1)$$

Table 1.2.1 shows the focal lengths for different astronomical objects. It is evident that an observer must be a distance greater than F away from the lens for the lens to be able to deflect light so that a source far behind it becomes visible. Alternatively, the source must be a distance F or greater from the lens so that an observer far behind the lens can see it. If these conditions are not met, light from the source will not be bent sufficiently around the limb of the lens to make it visible to the observer.

It is important to note that in the majority of cases that will be considered here, the observer-lens distances and the lens- source distances involved are all much greater than F. The lenses are thus incapable of blocking light by a classical eclipse effect. Only for objects inside the solar system and objects in close binary systems can light be decreased by an eclipse effect with three body alignment. All

other three body alignments, with each body pair separated by more than the focal length of the intermediate body, will show a flux-increasing gravitational lens effect.

An important mathematical consequence of gravitational lensing is the conservation of surface brightness (Misner, Thorne, and Wheeler 1973). This consequence derives directly from conservation of phase space in the bundle of rays coming to the observer. Continuous, uniform-brightness images of source objects seen by an observer have the same surface brightness after passing a gravitational lens as before. What a lens does is distort the area of the solid angle of the image as seen by the observer. With the same surface brightness but different angular extent, an unresolved object can appear to have a different overall apparent brightness to an observer.

For total source flux to be conserved, there must be observers who see an increased source flux due to gravitational lensing, and other observers who receive a decreased amount. For near exact observer-lens source alignment, there are observers that receive a substantially greater flux from the source than without a lens. There are, however, no positions that would receive a substantially *smaller* amount of flux than without the lens.

To visualize this more clearly, consider a set of observers occupying a sphere at infinity watching a point lens and a point source near the center. Those observers close to observer-lens- source alignment would see an increased flux from the source. The closer they are to the source-lens line, the greater the increase of flux they

receive. Those very few observers extremely close to this line measure a dramatically increased flux from the source.

There are many more observers, however, who receive a slightly reduced flux from the source than in the absence of lensing. If one integrates the total flux leaving the fictitious sphere, one finds that it is the same as in the absence of the lens: total flux is conserved. As expected, gravitational lensing does not *create* flux, it merely distorts its distribution.

At perfect observer-lens-source alignment, a point source is distorted by a point lens into a circle: a thin angular ring centered on the source (Einstein 1936). At this configuration the flux from the source to the observer is maximized. The angular radius of this circle is a scale unit which is naturally defined by the problem. This scale unit will be referred to as the Einstein Ring Unit (ERU). The ERU is

$$ERU = \frac{2R_s(d - D)}{Dd}, \tag{1.2.2}$$

where R_s is the Schwarzschild radius of the lens, D is the distance to the lens and d is the distance to the source. Lens variables will usually be designated in upper case and source variables in lower case. The geometry is shown in Figure 1.2.2.

Note that only at perfect collinear alignment does the Einstein ring appear (Einstein 1936). If the alignment is not exact, two images of the source appear. When the alignment is close to exact, the two images are separated by nearly two ERU. Their exact position with respect to the source object is well defined and is

given by

$$R_{\pm} = \frac{1}{2}[(R_o^2 + 1)^{1/2} \pm R_o], \tag{1.2.3}$$

where R_o is the original position of the source in the absence of lensing, and $R_{\pm}$ represent the position of the two images (for a derivation, see e.g. Liebes 1964). These variables are given in ERU. The position of the source, lens, and lens images are all contained on a single great circle on the observer's sky. The case of a single lens will be discussed in more detail in Chapter 4.

There is also typically a time delay between the two images. The magnitude of the time delay is of the order of the time it takes light to cross the Schwarzschild radius of the lensing mass. The images are not precise replicas of each other. One image is a scaled, inverted mirror image of the other. The difference in the apparent brightnesses of the images is always the original apparent brightness of the source (Liebes 1964).

What happens to the image character when more than one lens is present? To discuss this in the context of the modern mathematical language of gravitational lensing, it is necessary to introduce the concepts of optical depth and shear. Optical depth can be defined in a gravitational lensing sense as the number of lensing masses per ERU. If there is a distribution with lenses spaced by only a couple of ERU or less, the net effect on the source light will be more complex than from the linear addition of the individual lenses.

If the average separation between lenses is much greater than the ERU, it is

usually a good approximation to consider the lenses one at a time and add their respective contributions. In this case however, only one lens will significantly affect the image flux.

If a large mass is near to a stellar lens in the lensing plane, the mass can distort the image characteristics of an individual lens in non-trivial ways. This can be the case when stars close to the center of a galaxy act on the flux from a distant quasar, the host galaxy of the star exerts a gravitational influence distorting the lens effect of the individual star. This effect is called a shear effect. Shear is important when a lens is within a few ERU of the near large mass. When the star is many ERU (of the massive object) distant, shear effects of the massive objects are minimal.

In the presence of high optical depth and shear terms, the location of the images and the calculation of their brightnesses become more complex. To calculate these one may invoke Fermat's Principle (Blandford and Narayan 1986). Fermat's Principle states that real images take paths where the time of travel is an extremum, either maximized or minimized (or both as with a saddle point). In the absence of lensing, the critical path is a straight line between the source and the observer, and the travel time is obviously a minimum. In the presence of lensing, time is slowed in the vicinity of the gravitational fields of the lenses, making the the critical paths more numerous and complex. Fermat's Principle and its application to gravitational lensing will be discussed more specifically and in more detail in Chapter 5 when dealing with the lensing of two stars simultaneously.

References

Barnothy, J. M. 1968, *A. J.* **73**, S.164.

Barnothy, J., and Barnothy, M. F. 1969, *Nature* **222**, 759.

Blandford, R., and Narayan, R. 1986, *Ap. J.* **310**, 568.

Chang, K., and Refsdal, S. 1979, *Nature* **282**, 561.

Chang, K., and Refsdal, S. 1984, *A. Ap.* **132**, 168.

Eddington, A. S. 1919, *Observatory* **42**, 119.

Einstein, A. 1908, *Jahrb. Radioaktivitat und Electronik* **4**, 11.

Einstein, A. 1916, *Ann. Phys.* **49**, 769.

Einstein, A. 1936, *Science* **84**, 506.

Gott, J. R. III 1981, *Ap. J.* **243**, 140.

Liebes, S., Jr. 1964, *Phys. Rev.* **133B**, 835.

Maeder, A. 1973, *A. Ap.* **26**, 215.

Misner, C. W., Thorne, K. S., and Wheeler J. A. 1973, Gravitation, San Francisco: W. H. Freeman.

Paczynski, B. 1986, *Ap. J.* **301**, 503.

Press, W. H., and Gunn, J. E. 1973, *Ap. J.* **185**, 397.

Refsdal, S. 1964, *M.N.R.A.S.* **128**, 295.

Soldner, J. 1801, *Berliner A. Jahrb.* **1804**, 161.

Tikhov, G. A. 1937, *Bull. Obs. Central a Poulkovo* **16**, 1.

Walsh, D., Carswell, R. F., and Weymann, R. J. 1979, *Nature* **279**, 381.

Zwicky, F. 1937a, *Phys. Rev.* **51**, 290.

Zwicky, F. 1937b, *Phys. Rev.* **51**, 679.

Zwicky, F. 1957, Morphological Astronomy, Berlin: Springer-Verlag.

Focal Lengths of Astronomical Objects

Object	Typical Radius	Typical Mass	F
Sun	1 $R_\odot$	1 $M_\odot$	538 AU
O5 V Star	18 $R_\odot$	40 $M_\odot$	4630 AU
M5 V Star	0.32 $R_\odot$	0.2 $M_\odot$	275 AU
White Dwarf	6000 km	1 $M_\odot$	0.04 AU
Neutron Star	15 km	1 $M_\odot$	40 km
Jupiter	0.1 $R_\odot$	$10^{-3} M_\odot$	6000 AU
Earth	$10^{-2} R_\odot$	$3x10^{-6} M_\odot$	15000 AU
Asteroid	100 km	10^{20} gm	10 pc
Baseball	5 cm	1000 gm	30 Mpc
Dust Grain	10^{-5} cm	$4x10^{-15}$ gm	2600 Mpc
Proton	10^{-13} cm	$2x10^{-24}$ gm	650 pc

Figure Captions

Figure 1.2.1: The lensing geometry depicting the concept of minimum focal length. Collimated light rays approach the lens. Those rays with impact parameter b equal to the spherical lens radius R pass tangent to the lens surface. These rays pass the closest of all the rays without getting absorbed or scattered by the lens; hence they are deflected by the greatest angle and travel the shortest converging distance in order to reach the axis of the lens. Along the axis, the distance from the lens is defined to be F, the minimum focal length of the lens.

Figure 1.2.2: The lensing geometry depicting the two images an observer would see with a single point lens and source. Two light paths lead to the observer from the source. It is a good approximation to assume that the light rays travel along a straight path until they are deflected in the lens plane. After a discrete change in direction, the rays then travel again on a straight path to the observer. The observer thus sees two images of the same source object.

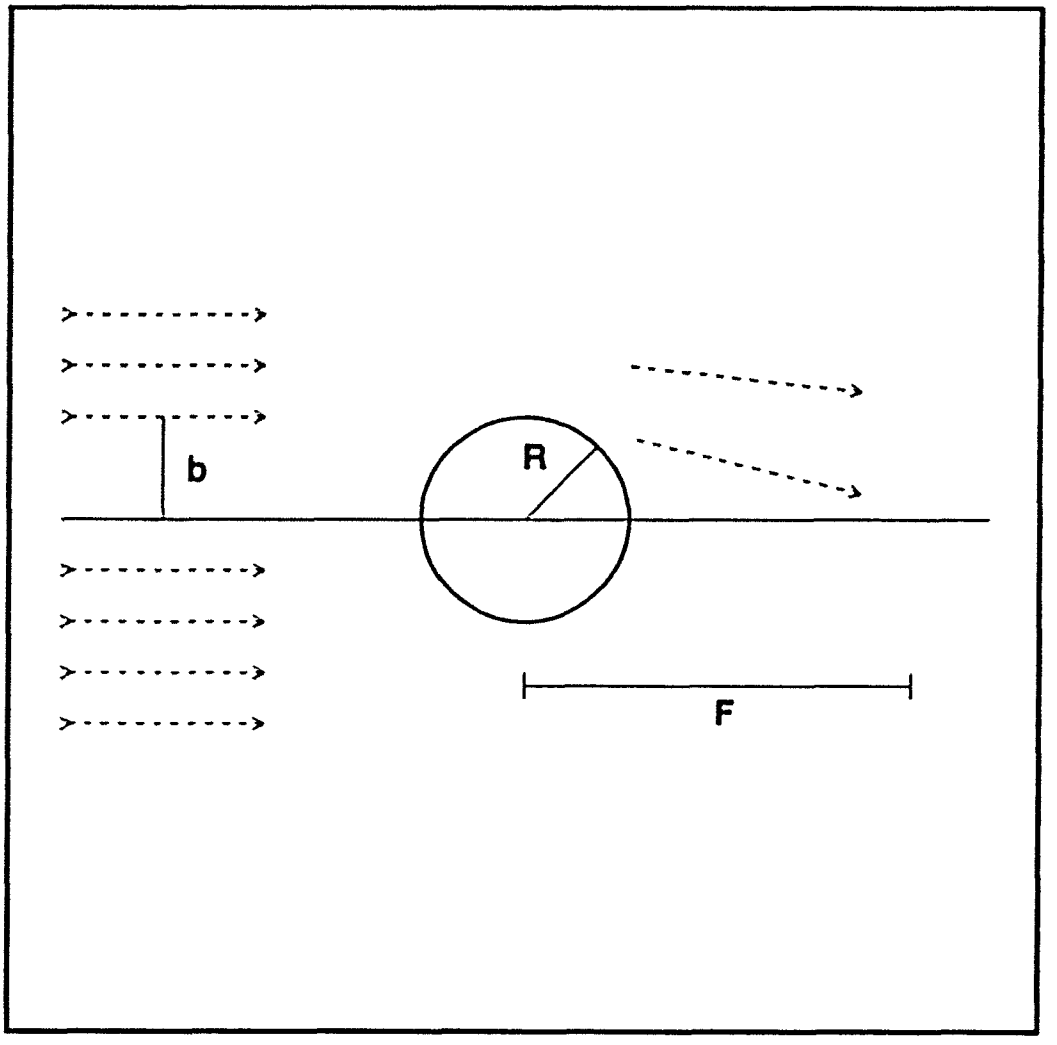

Figure 1.2.1

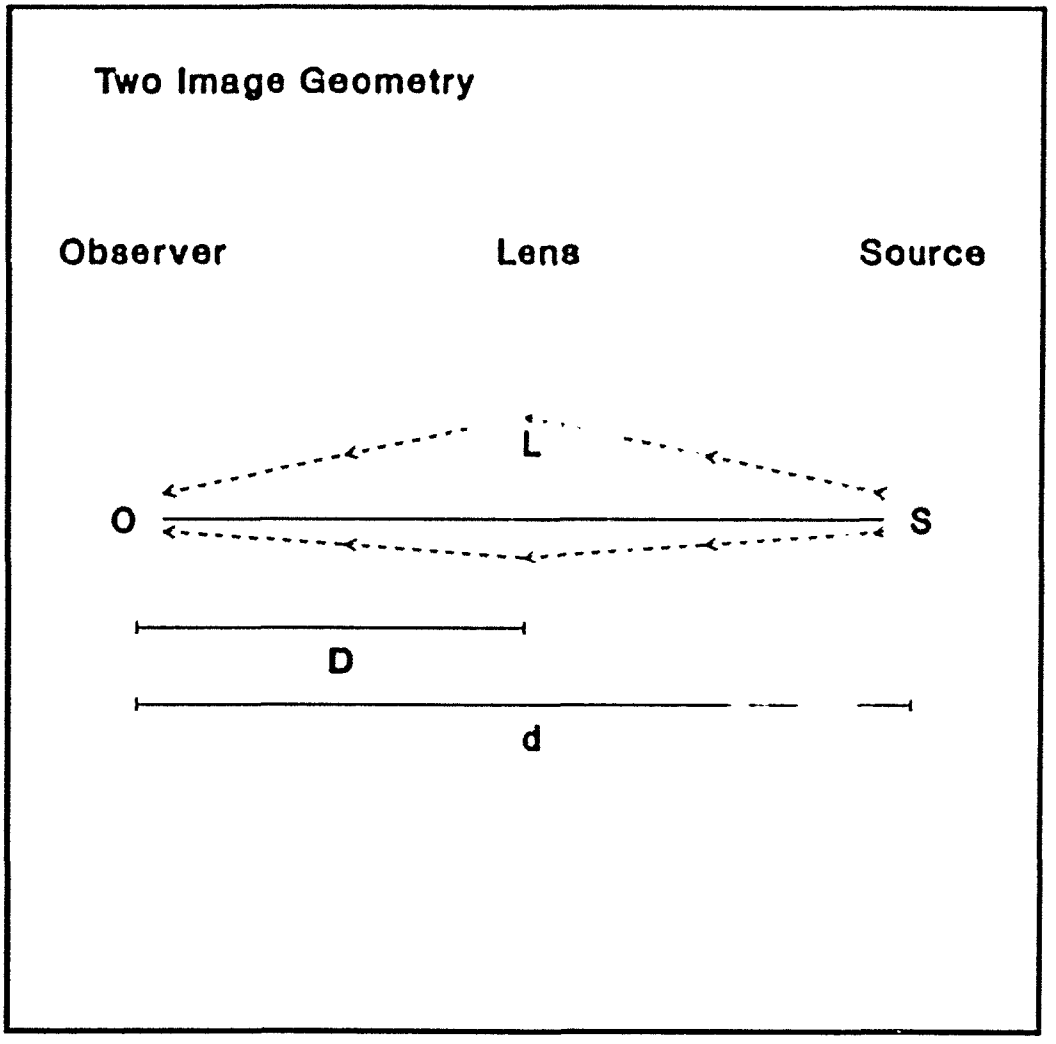

Figure 1.2.2

Chapter 2

Definition and Use of the Lensing Ellipsoid

When is Lensing Important?

2.1) Introduction

In this Chapter we will evaluate the probability of detecting gravitational lensing photometrically. As stars are the most numerous lens candidates for this type of lensing, we will assume stars as the lenses, unless explicitly stated otherwise. Much of the work in this Chapter is based on Nemiroff (1986).

For typical stellar lenses, the angular separation between images is well below modern angular resolution. This can be seen by inspection of the angular size of the ERU for stellar lens cases. Typical image separations will be of the order of two ERU. Even for an 'optimistic' case of a star of 10 $M_{\odot}$ at 100 pc distance acting as a lens for a source much further behind it, we can see from Equation 1.2.2 that the ERU has an angular size of only 10^{-2} arcseconds. For stars in nearby galaxies, the situation is even less hopeful. A 10 $M_{\odot}$ star at a distance of 1 Mpc has an ERU of about 10^{-4} arcsec. Since modern optical telescopes cannot go below 0.1 arcsec at best, the chance of angular resolution of images due to stellar lenses is small.

Photometrically, however, the effects of stellar lensing can be well above detection threshold. Image brightnesses can get measurably greater even while images remain unresolved. In this Chapter we therefore concentrate specifically on the photometric observability of stellar lensing.

The mathematical tools defined in this section will work only under specific assumptions. These assumptions are: (a) a single lens acts at a given time, (b) the lens is considered to be space singular: a point, and (c) the source is also to be considered a point.

With stellar lenses, assumption (a) is quite reasonable when there are no other lenses within an angular distance much greater than the ERU from the original lens (this is demonstrated by lensing analysis at high optical depth; on this point see Young 1981, Paczynski 1986a and references within). It is also a valid approximation when lenses are randomly distributed with average angular distances between them much greater than the ERU of any individual lens.

For stellar lenses, the angular radius of a star is typically several orders of magnitude less than its corresponding ERU. In typical lens scenarios, the lens must come to within about an ERU of the source for lensing to be detectable photometrically (Liebes 1964). At that distance the photons pass, at closest, about 1/100 of an ERU from the center of the lensing star. Since the typical stellar radius subtends an angle much smaller than this, photons will not typically intersect the surface of the star; hence (b) is also a valid assumption.

For circular sources, the maximum amplitude of lensing is given by (Nottale 1986)

$$A_{max} = \left[1 + \frac{4}{R^2}\right]^{1/2}, \qquad (2.1.1)$$

where R is the radius of the source in ERU. For amplifications much smaller than

the maximum amplitude, a point source is a good approximation. Since the angular size of the source is typically small compared to the ERU, and the amplifications we will be dealing with in this section are for A greater than but approximately equal to a few, (c) will usually be a good assumption.

For the case of a single point lens between the observer and the source, the photon flux reaching the observer from the source is always greater than if the lens were not present. As we consider only one lens at a time, we, therefore, are dealing with an increase in photometric flux from the source, never a decrease. A decreases in flux does become possible with multiple lenses (Chang and Refsdal 1984).

Other works investigating the general probability of stellar gravitational lens encounters include Liebes (1964), Refsdal (1964), and Press and Gunn (1973), and Gott (1981). Our treatment is more accurate in that we give a fully three dimensional treatment: the lens can be at any location between the observer and the source. Our approach also allows calculations with any amplification, not just specific ones. This approach is easy enough to use that it can be invoked to indicate in a quick and simple manner whether or not gravitational lens effects are important.

2.2) Definition of the Lensing Ellipsoid

A point lens splits a point source into two images. As derived originally by Tikhov (1937), the total amplification is

$$A = \frac{1}{2}\left[\frac{\alpha}{\Delta\alpha} + \frac{\Delta\alpha}{\alpha}\right], \qquad (2.2.1)$$

where α is the unlensed angular separation of the lens and the source in the observers

sky, and $\Delta\alpha$ is the observed angular separation of the two lensed images. A is the total amplification of the source, combining the light from the two images. Note that A is a multiplicative factor of the original source brightness.

One can check that Equation 2.2.1 is correct in the asymptotic limit of large angular separations. As α becomes large, one of the images moves closer to the lens, while the other approaches the unlensed source position. Therefore $\Delta\alpha$ becomes α. This, in turn, from inspection of Equation 2.2.1 causes A to become unity, which we expect for large separations.

Defining R to be the distance from the lens to the source- observer line, and D to be the distance from the observer to the lens, we can see from Figure 1.2.1 that $\alpha = R/D$. Liebes (1964) and Refsdal (1964) have shown that

$$\Delta\alpha = \left[\left[\frac{R}{D}\right]^2 + \left[\frac{8R_s(d-D)}{Dd}\right]\right]^{1/2}. \qquad (2.2.2)$$

Here d is the distance from the observer to the source, and R_s is the Schwarzschild radius of the lens. We can combine Equations 2.2.1 and 2.2.2 with $\alpha = R/D$ to give an expression for A in terms of distance parameters for the lens and the source:

$$A = \frac{1}{2}\left[\left[1 + \frac{8R_sD(d-D)}{R^2d}\right]^{1/2} + \left[\frac{1+8R_sD(d-D)}{R^2d}\right]^{-1/2}\right]. \qquad (2.2.3)$$

If we invert this equation to get R in terms of A we find that

$$R = [4R_sD(1-D/d)\Phi]^{1/2} \qquad (2.2.4)$$

where Φ is related to A through the equation

$$\Phi = \left[\frac{A^2}{A^2-1}\right]^{1/2} - 1. \qquad (2.2.5)$$

The distance R is measured perpendicular to the optical axis connecting the observer to the source. Were the lens to be placed closer to the optical axis than R, the amplitude of lensing would be greater than A. Similarly, were the lens to be placed further away, the amplification of source light is not as great.

Note that when Φ is equal to $1/2$, R is equivalent to the ERU. R represents a more general radius in the problem than the ERU, as it incorporates the amplitude of lensing being considered. R will also be found to be useful in generalizing the concept of optical depth in a similar manner.

Plotting, in dimensionless units, the distance from the optical axis as a function of the distance from the lens to the observer, we obtain an ellipse for each amplitude A. This is shown graphically in Figure 2.2.1. By rotating the ellipse around the optical axis, we obtain an ellipsoid. Because the source distance is usually much greater than R, this ellipsoidal volume is typically a prolate spheroid. We will refer to this ellipsoid as the Lensing Ellipsoid, or LE.

The LE can be an instructive diagnostic and indicator of gravitational lens effects. Any lens of Schwarzschild radius R_s that falls inside the LE amplifies the source by the amount A or greater. The volume inside the LE is the volume this lens must fall into in order to have a specific minimum photometric gravitational lens effect. This volume is

$$V = \frac{2}{3}\pi R_s d^2 \Phi. \qquad (2.2.6)$$

A simple result that can be shown immediately is the relative probability for

lensing to occur at different amplitudes. For a homogeneous isotropic distribution of lensing objects, the relative probability is simply the ratio of the volumes of the LE's, which simplifies to the ratio of the Φ factors. So, for example, one would find, by use of Equation 2.2.6, that lensing between amplitudes of $A = 1.01$ and 10 is about 1200 times more likely than lensing with $A \geq 10$.

2.3.1) Local Gravitational Lensing

An interesting use of the LE formalism is to check whether there can be noticeable gravitational lens effects on stars inside our own galaxy. Assume there is a bright star that can be seen at a distance of 1 kpc. What is the chance that this specific star will be lensed by a 1 $M_\odot$ star to an $A > 2$? If we use $A = 2$ in Equation 2.2.5 we see that $\Phi = 0.155$. Taking Φ, d, and R_s ($\approx$ 3 km) in Equation 2.2.6, we see that the volume of the LE is $V \approx 3.0x10^{-8}\,pc^3$. In our solar neighborhood we see a number density of stars equivalent to one star in every $10\,pc^3$. As the lensing volume is about 9 orders of magnitude smaller than the local average stellar volume interval, we would *not* expect to find this star, or any individual star inside our galaxy, being gravitationally amplified by a factor of 2 or more at any given time.

We can also take the reverse approach and ask: to what level do we expect this star to be gravitationally lensed by the known stellar distribution? To answer this question, we set the volume per star equal to the LE volume and solve for Φ. With the parameters above defining the LE, we find that the average star at 1 kpc is lensed by the amount $\Phi = 10^7$ corresponding to $A = 1 + 10^{-15}$. The detection of

this small amplitude seems unlikely for the indefinite future because of quantum effects of measurement.

But if stars are always moving, won't lensing become detectable if we wait long enough? To estimate this time, we will have to make several more approximations. We add to the uniformity of population by adding uniformity of motion: we treat stars as a three-dimensional gas. We can then approach this problem with mean free path arguments. A static LE 'collides' with a gas of stars.

It is a good approximation to take the mean cross section of the LE to be $\sigma = (\pi R_s d^3 \Phi)^{1/2}$. This is derived by taking the cross section to be the area of the LE that has major axis d and minor axis $(R_s d\Phi)^{1/2}$. If the mean free path is $L = 1/(n\sigma)$, where n is the number density of lenses, and the mean transverse speed of the stars is v, then the mean time between collisions is $T = L/v$. Therefore, the mean time between collisions is

$$T = (R_s d^3 n^2 v^2 \Phi)^{-1/2} \beta \qquad (2.3.1)$$

where β is a constant that depends on the geometry and is of order unity. Watching a source at the distance d, we expect to see it vary in brightness due to gravitational lensing, reaching the amplitude A every T time units.

How long do the lensing events last? Again we employ the picture of an LE colliding with a star, as shown in Figure 2.3.1. Here we see that if a star 'starts' at position 1 causing a small lensing amplitude Φ_1, its distance to the optical axis is $(R_s d\Phi_1)^{1/2}$. The stellar lens moves so that its closest approach to the optical axis is

$(R_s d\Phi_2)^{1/2}$ at position 2, where its lensing amplitude is Φ_2. The time the observer measures for the lens to go from position 1 to position 2 is $(2R_s d(\Phi_1 - \Phi_2))^{1/2}/v$, where v is the transverse velocity of the lens. The duration of the lens event is twice this, namely,

$$t = [8R_s d(\Phi_1 - \Phi_2)]^{1/2}. \qquad 2.3.2$$

Watching a source at a distance d, we expect a lensing event of amplitude A to last t time units.

Even the most optimistic Galactic estimates show that lensing events of a particular star are rare. A typical observer would have to wait a million years to see an amplitude change of 1.2 over the period of a month. These results are comparable with those of Liebes (1964).

The LE puts us in a good position to solve other problems just as simply. At what distance from the observer does one expect to see *any* source lensed by an amount A or greater? Assume a uniform distribution of stars of Schwarzschild radius R_s and number density n and a lensing amplitude A. When the sum of the volumes of all the LE's of stars out to a distance b is equal to the average volume per star $1/n$, lensing becomes probable. The mathematical statement of this is

$$\frac{1}{n} = \int_0^{\Gamma} (n)(\frac{2}{3}\pi R_s d^2\Phi)(4\pi d^2)\,\mathrm{d}d, \qquad (2.3.3)$$

so that

$$\Gamma = \left[\frac{15}{8n^2\pi^2 R_s \Phi}\right]^{1/5}. \qquad (2.3.4)$$

For the stellar densities assumed above, the relationship between Γ and A is plotted in Figure 2.3.2. One can see from inspection of this graph that at distances on the order of 1 kpc, lensing at a noticeable amplitude becomes likely.

There are, however, at least three major confounding factors that would obscure a lensing detection. (a) The lens would probably be brighter than the source, making it hard even to detect the luminosity of the lensed star altogether, let alone its increase in brightness (Einstein 1936, Feibelman 1966, 1986). (b) There are *hundreds of millions* of stars within 1 kpc of the Sun, it would be very difficult to isolate the one star undergoing lensing. (c) Even if we were lucky enough to witness the lensing event, it could be hard to distinguish the gravitational lens variability from the many causes of variable light in stars and stellar systems already known. These confounding factors make small the chance of a local source undergoing detectable gravitational lensing.

What is the chance that a star inside our galaxy could lens objects outside our galaxy, say QSO's at cosmological distances? Paczynski (1986b) recently considered a similar problem of halo stars in our galaxy lensing stars in nearby galaxies. Again the LE can be invoked to answer this question. Assuming $d >> D$, Equation 2.2.4 simplifies to $R = (4R_s D\Phi)^{1/2}$. By interpreting R as the radius of a disk, we can integrate the areas of all the disks out to the edge of the galaxy, Ω, to give a volume of

$$V = \int_0^{\Omega} \pi R^2 n \, dD = 2\pi R_s n \Phi \Omega^2. \qquad (2.3.5)$$

Even if we assume that our galaxy contains a uniform distribution of 0.1 $M_{\odot}$ lenses out to 100 kpc with number density 0.1 pc^{-3}, and that we could detect amplitude changes of $A = 1.1$, the volume of the LE is of the order of 10^{-4} pc^3, five orders of magnitudes smaller than the average volume per star. Therefore only one source in 10^5 should be expected to show this lensing effect. This result is comparable to that of Paczynski (1986b). We conclude that the probability of detection of stars in our own galaxy lensing QSO's is small.

2.3.2) Macrolensing Probability

Although it is out of the mainstream of this thesis to deal with lensing by objects other than stars, the discovery and popularity of macrolensing, the lensing effects of galaxies, suggests a brief digression on how the LE can be used to estimate the probability of the detection of this phenomenon. Gravitational lens effects by galaxies were predicted by Zwicky (1937).

The LE assumptions are now much cruder than with stellar lensing. To use the LE formalism, we must assume that galaxies are point lenses and sources, and this is not a good approximation in either case. Also, the LE deals implicitly with the photometric effects of gravitational lensing, which are the most important when dealing with stars at present angular resolution, while the most notable effects of macrolensing are angular splitting and distortion effects.

Galaxies do not make good point lenses because their typical angular size is larger than their corresponding ERU. A spiral galaxy at a distance of 100 Mpc with

a massive halo of radius 50 kpc has an angular size of about 100 arcseconds. If we assume a mass of $10^{12}\ M_{\odot}$, the angular size of the ERU is, as given by Equation 1.2.2, about 5 arcseconds.

Similarly, galaxies do not make good point sources, as they are large compared to their ERU. Inspection of Equation 2.1.1 shows that amplification should not be larger than $A = 2$ no matter how exact the observer-lens-source alignment. For angularly smaller objects, however, such as the continuum regions of quasars and AGN, larger amplifications can be generated.

Nevertheless, to make the LE formalism somewhat valid, we will limit our discussion to lensing events where $A > 2$. This amplitude reflects an alignment of observer-lens-source that would generate two images of comparable brightnesses. Therefore, if one image is visible, the other should be discernible to the observer also. At $A > 2$ the two images should be separated by 2 ERU, which according to the above estimation, is typically about 5 arcseconds, i.e. within modern angular resolution. We do not expect $A > 2$ since, even if the alignment is more exact, the angular extent of the source object works to diminish any amplification above this point.

With these constraints in mind, we ask: what is the probability of a random distribution of galaxies lensing quasars at cosmological distances? We assume lensing is detectable for $A > 2$, for this amplification would generally precipitate the creation of two, separate detectable images. Using a quasar distance of 10^9 pc

being lensed by a galaxy of 10^{12} $M_{\odot}$ in a Euclidean universe, we again calculate the volume for the LE by Equation 2.2.6. This volume is about 0.03 Mpc^3. The average free volume associated with a single galaxy in space is about is about 30 Mpc^3. From these numbers we see that we would expect about one quasar per 1000 to show significant gravitational lens effects.

At what distance must we look to see any galaxy gravitationally distorted by a foreground galaxy? Again we consider that a photometric effect of $A > 2$ (when considering the galaxy to be a point) is commensurate with coincident angular effects that could be seen on an extended object. Use of Equation 2.3.3 with galaxy parameters replacing stellar ones shows that the sum of the LE's becomes equal to the average volume per galaxy at a distance of about 100 Mpc. Galaxies at this distance can be seen with modern telescopes, so it is possible that a galaxy currently visible to us is being gravitationally distorted significantly by a foreground galaxy. The number of galaxies out to this distance is on the order of 100,000.

The angular size of the distortion would be about 5 arcseconds. Since the visible (non-halo) angular size of a galaxy at 100 Mpc can be as large as about 20 arcseconds, we would expect the distortion to be typically within the image of the galaxy, not angularly removed from it. This distortion should be hard to document when one recollects the large number of peculiar galaxies already catalogued.

2.3.3) Lensing of QSO's by Stars in Intervening Galaxies: Microlensing

In this section we will use the LE to estimate, under a range of assumptions, the magnitude of the gravitational lens effect of stars in nearby galaxies on quasars and AGN at cosmological distances. We do *not* assume that galaxies have massive halos containing lensing candidates. More specific cases, in which the effect of a massive halo containing lensing stars is considered, will be discussed in Chapter 3.

In microlensing, the assumptions of a point lens and point source are good ones. The lens is assumed to be a single star acting alone in a galaxy at 10^8 pc, while the source is a QSO behind it at about 10^9 pc. The angular size of the ERU is then 10^{-6} arcsec, while the size of the stellar lens is about $5x10^{-12}$ arcsec. So the assumption of a point lens is a good one. The angular size of the continuum region of quasar light is estimated to be on the order of 10^{-7} arcsec (Wiita 1985); therefore, the assumption of quasars as point sources is also reasonable for amplifications $A \leq 20$.

When a quasar is seen through a galaxy, the intersection of the LE with the galaxy is a cylinder. We shall calculate the volume of this cylinder and compare it to the average volume per star in the galaxy. From Equation 2.2.4, when the quasar distance is much greater than that of the galaxy, one can see that the radius of the cylinder is $R = (4R_s D\Phi)^{1/2}$. The thickness of the galaxy will be given by the variable b. Therefore, in this case, the volume of the LE is

$$V = \pi R^2 b = 4\pi R_s D\Phi b \qquad (2.3.6)$$

For a quasar at 10^9 pc being lensed by a 1 $M_\odot$ star in a galaxy at 10^8 pc with a thickness of 1 kpc to an amplitude $A > 2$, the volume of the LE is 0.02 pc^3. Assuming a star density similar to the solar neighborhood giving 10 pc^3 per star, we see that one quasar in 500 being seen through a galaxy should currently be undergoing a measurable gravitational lens effect.

But this calculation was static: it did not include the relative motion of the lens. High lens velocities, generated by the motion of the galaxy dragging the stellar lens across the quasar, may cause a quasar not being detectably lensed now to become a lensed source in the future. So again we ask, what is the mean time between lensing events?

Again consider the cylindrical LE colliding with a gas of stars. The collision cross-section of the LE is $\sigma = 2Rb = (16R_sDb^2\Phi)^{1/2}$, so the mean free path is $L = 1/(n\sigma) = (16R_sn^2Db^2\Phi)^{1/2}$. The mean time between collisions is then

$$T = \frac{L}{v} = (\frac{16}{3}R_sn^2Db^2v^2\Phi)^{-1/2} \qquad (2.3.7)$$

We add to the above assumptions by giving the host galaxy of the lens a transverse velocity of 500 km/sec. The time between lensing events where $A > 2$ is about 4000 years. If 100 quasars behind galaxies are being monitored, the mean time between events of $A > 2$ is 40 years.

What are the durations of such events? We will estimate the duration of the event to be the time it takes for the lens to cross the diameter of the LE. If the diameter of the LE is $2R = (16R_sD\Phi)^{1/2}$, and the lenses move with transverse

velocity v, then the duration of the event is

$$t = \left[\frac{16 R_s D \Phi}{v^2}\right]^{1/2}. \tag{2.3.8}$$

For all the assumptions above, the duration of a typical lensing event is about 10 years. This number is comparable to that calculated by Gott (1981). These calculations will be made in more detail and for specific systems in Chapter 3.

2.4) Comments

In this Chapter we have introduced a simple formalism in order to estimate the probability of gravitational lensing by chance superposition of observer, lens, and source. The definition and use of the Lensing Ellipsoid can give a quick first estimate of cases when random gravitational lensing is important. As indicated in earlier works, we find that the chance of detecting lensing locally is small, but that the chances are much better on the extragalactic distance scale.

It should be stressed that the LE formalism assumes both a point lens and a point source. Only the gravitational potential field of a single point lens is considered in the calculations. Galaxies were not assumed to have dark, stellar halos. In later Chapters we will investigate the relaxation of some of these requirements. In the next Chapter, Chapter 3, we will reproduce some of the calculations given here under the assumption that galaxies are primarily made up of dark, stellar halos.

References

Chang, K., and Refsdal, S. 1984, *A. Ap.* **132**, 168.

Einstein, A. 1936, *Science* **84**, 506.

Feibelman, W. A. 1966, *Science* **151**, 73.

Feibelman, W. A. 1986, *P.A.S.P.* **98**, 1199.

Gott, J. R. III 1981, *Ap. J.* **243**, 140.

Liebes, S. Jr. 1964, *Phys. Rev.* **133B**, 835.

Nemiroff, R. J. 1986, *Ap. Sp. Sci.* **123**, 381.

Nottale, L. 1986, *A. Ap.* **157**, 383.

Paczynski, B. 1986a, *Ap. J.* **301**, 503.

Paczynski, B. 1986b, *Ap. J.* **304**, 1.

Press, W. H., and Gunn, J. E. 1973, *Ap. J.* **185**, 397.

Refsdal, S. 1964, *M.N.R.A.S.* **128**, 295.

Tikhov, G. A. 1937, *Bull. Obs. Central a Poulkovo* **16**, 1.

Wiita, P. J. 1985, *Phys. Rep.* **123**, 117.

Young, P. 1981, *Ap. J.* **244**, 756.

Zwicky, F. 1937, *Phys. Rev.* **51**, 290.

Figure Captions

Figure 2.2.1: Rotating each curve about the D/d axis creates an ellipsoidal volume: the Lensing Ellipsoid. Any point lens of Schwarzschild radius R_s that falls in the volume will gravitationally amplify the background source by *at least* the amount A labelled on the enclosing curve. The observer is located at $(R, D) = (0, 0)$ in the lower left hand corner.

Figure 2.3.1: A plane cut of two LE's is shown on the observer's sky. The lens L moves from position 1 to position 2 while the source S, at the center, remains fixed.

Figure 2.3.2: For an isotropic uniform distribution of point stars at 0.1 star pc^{-3} out to a distance of b, one expects to see of the order of one lensing event of amplitude A to be visible at any given time. The upper curve indicates 1 $M_\odot$ lenses, while the lower curve indicates 0.01 $M_\odot$ lenses.

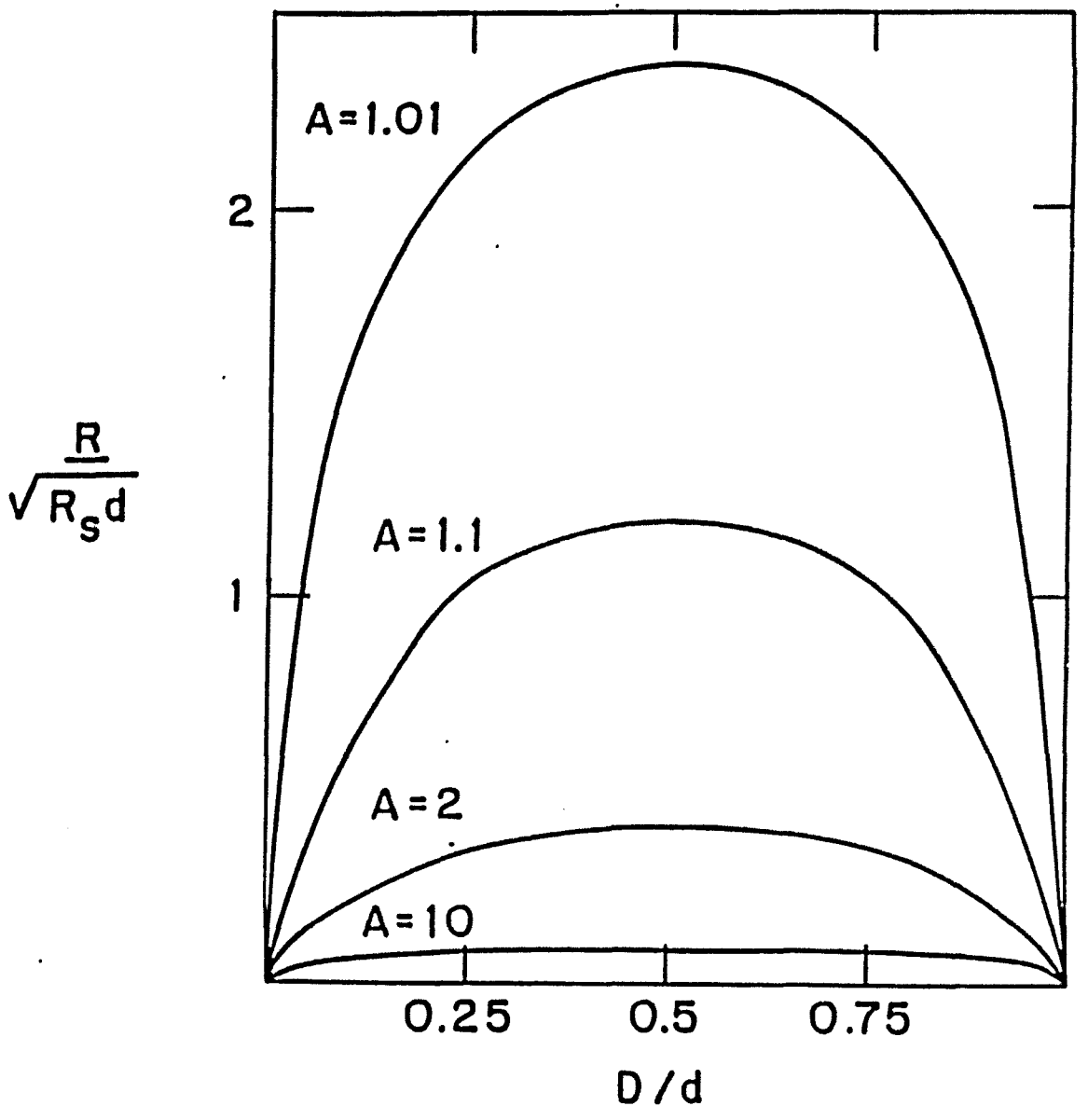

Figure 2.2.1

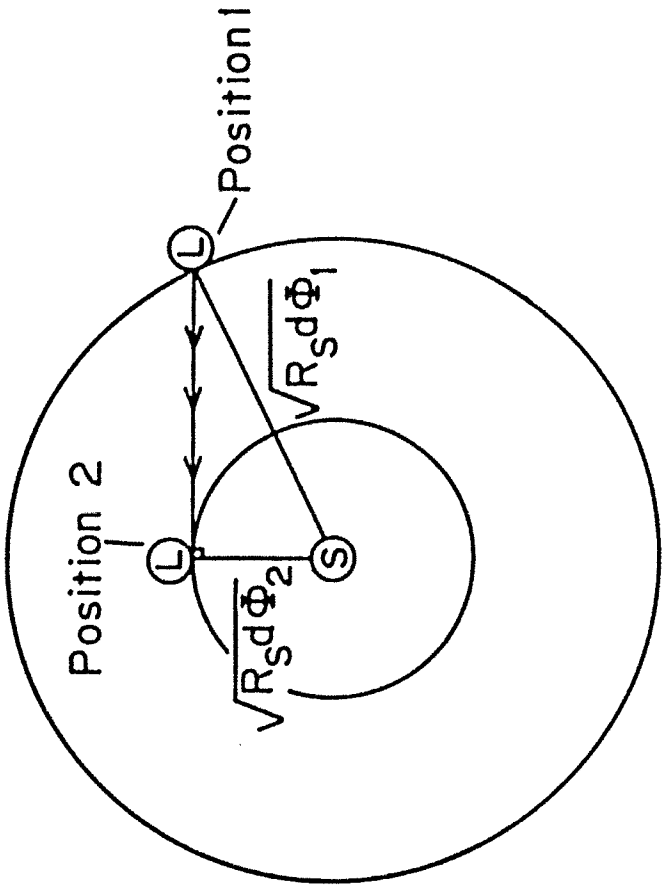

Figure 2.3.1

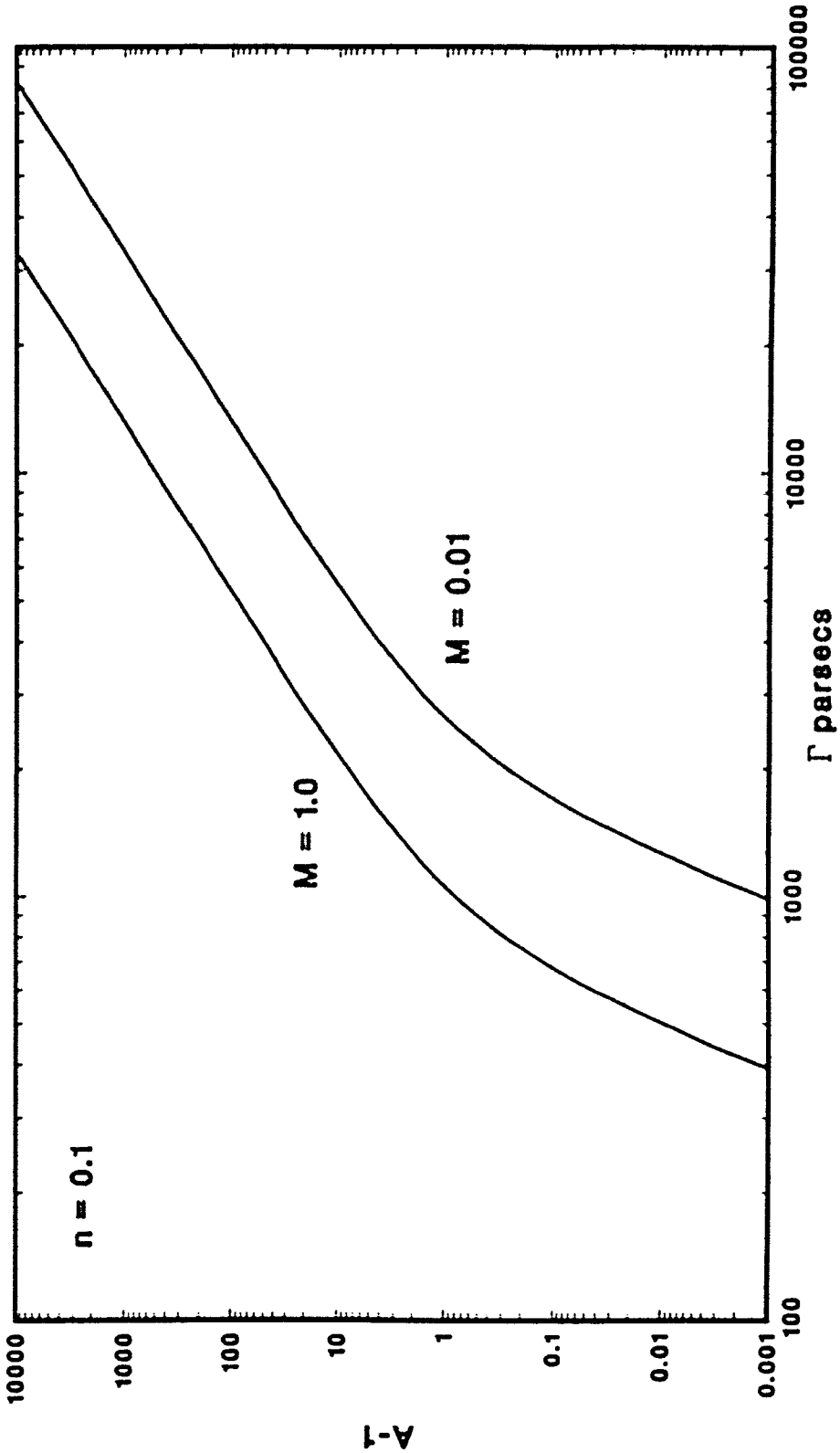
n = 0.1
M = 1.0
M = 0.01
A-1
Γ parsecs
10000
1000
100
10
1
0.1
0.01
0.001
100
1000
10000
100000

Figure 2.3.2

Chapter 3

Microlensing: Analysis for Observers

3.1) Quasar - Galaxy Associations

For the microlensing phenomena to exist, a star must move close to the light path of a quasar. There are at least three situations which will allow this to happen. In the first, the star is a member of a host galaxy, itself gravitationally deflecting light from the background quasar. In the second, the lensing star may be outside a galaxy itself housed in a cluster of galaxies. In a third situation, the eclipsing star may be a member of a uniform cosmological density of intergalactic stars. In this Chapter we will calculate, for each case, the probability of occurrence, the mean time between lensing events, and the duration of an event. We will apply, where possible, these calculations to actual systems.

Press and Gunn (1973) have previously studied the effects of a cosmological density of objects on background point sources. They concentrated on predicting the angular separations expected for the source objects. Turner, Ostriker, and Gott (TOG 1984) also considered a uniform density of objects in different cosmologies. They calculated optical depths for both compact and isothermal objects, predicting the number of gravitational lens pairs of objects likely to be seen per unit of angular separation per magnitude interval.

Gott (1981) predicted the likely effects of a halo of compact objects on background quasars. He considered the time transients of these effects on the background

emitted light, and calculated their magnitude and duration for the double quasar 0957 + 561.

In this Chapter, we will again frequently use the LE formalism (Nemiroff 1986). In Chapter 2 the LE formalism was shown to be valid for stars outside the galaxy which lens the continuum regions of distant quasars. The term 'quasar' here is used in a general sense, indicating QSO's, BL Lac's, and AGN's in general. We again stress that it is typically the optical continuum region of quasars that is under consideration to show microlensing effects. Another frequency band that may be expected to show microlensing effects is the X-ray. Other bands, including the radio, are typically too large; however some objects may indeed show structure in some bands.

In this first section we will work under the assumption that a star within a host galaxy acts gravitationally to lens a background quasar. We will begin by assessing the probability that a galaxy itself would be seen in front of a quasar. We assume a quasar is seen at a distance of d_9 (in units of 10^9 pc) in a flat Newtonian universe. We also assume the universe is filled with spherical galaxies with radii of R_4 (in units of 10^4 pc). With these assumptions we ask: what volume of space must a galaxy fall into in order to be seen superimposed in front of this quasar?

The shape of the volume which the galaxy must fall into to be seen in front of the quasar is a cylinder whose axis is the line connecting the source to the observer. If the center of a galaxy falls within R_4 of the source-observer line, the quasar will

be seen through the galaxy. The volume of this cylinder is

$$V = \pi R^2 d = \pi R_4^2 d_9 = 3.14x10^{17} R_4^2 d_9 pc^3 = 0.314 R_4^2 d_9 Mpc^3. \qquad (3.1.1)$$

The average volume per galaxy in the vicinity of the local group is about $100 Mpc^3$ per galaxy (Lang 1980). To find the probability of a galaxy being superimposed on a quasar, we divide the volume in which the galaxy must fall by the average volume per galaxy. Equivalently, we define the probability P of one of a class of objects, uniformly dispersed with number density n, falling into a volume V as $P = nV$. This probability calculation technique will be used frequently in this Chapter.

If a typical quasar lies at a distance of 10^9 pc, and the typical diameter of galaxies is 10^4 pc, we then see that better than three quasars in 1000 would be expected to be seen through an intermediate galaxy. If galaxies have extended halos out to 10^5 pc, as many astronomers believe, then, typically, every quasar at a cosmological distance has a reasonable chance of being seen through the halo of an intervening galaxy.

We now begin with the premise that a galaxy is superimposed on a background quasar and ask: what chance is there that the quasar light comes close enough to a star so that its brightness is significantly increased? A number created to express this is called the optical depth (τ , Vietri and Ostriker 1983). Optical depth is defined as the number of stars per Einstein ring. When τ becomes of the order of unity, the quasar light path is dramatically split and altered by the foreground

distribution of stars. When τ is much less than unity, typically no stars are close to the light path, but if one were, it would effect the quasar light by itself.

Typical values for τ will be calculated under several assumptions. First, assume galaxies have spherical halos, that the halos are made up solely of stars with mass M, and these halos dominate the probability for microlensing in these galaxies. We assume these halos have a singular isothermal density distribution, with no core, so that their density is described by $\rho = \sigma^2/2\pi G r^2$. Here r signifies distance from the galaxy center and σ denotes dispersion velocity.

We assume the halo ends abruptly at a radius r_o from the center. We also assume the impact parameter of the light from the center of the galaxy is R. Because the galaxy is small compared to the observer-quasar distance, and deflection angles are small compared to the angular extent of the galaxy, we assume all the stars in the galaxy lie in a single lens plane.

To find τ, we integrate over the line-of-sight extent of the galaxy to find how much mass per distance squared there is in the lens plane. We then divide by the mass per star M to obtain the number of stars per distance squared. Lastly we multiply by the area of the Einstein ring in the lensing plane. This gives us the number of stars per Einstein ring, which is defined as the optical depth. The analytical result of this computation is

$$\tau = \frac{2\sigma^2 D(1 - D/d)}{c^2 R} arctan\left[\frac{r_o^2}{R^2} - 1\right]^{1/2}. \qquad (3.1.2)$$

As before, D is the distance to the lensing galaxy, and d is the distance to the

quasar.

A simple and practical formula can be extracted from Equation 3.1.2. If we assume the lensing galaxy is relatively close ($D << d$), and the halo is effectively infinite (not a bad assumption when the quasar and galaxy are closely aligned), the formula becomes

$$\tau = 0.01 \frac{\sigma_{250}^2}{\theta_{min}}. \tag{3.1.3}$$

The variable θ_{min} is the angle between the center of the galaxy and the quasar position measured in arcminutes. The quantity σ_{250} refers to the velocity dispersion within the galaxy in units of 250 km/sec.

We find several things surprising about the above equation. First, it is not a function of the mass of the lensing star. This is because of the relation between the size of the Einstein ring and the number density of stars along the line of sight. As we consider more massive lenses, the Einstein ring is larger, so one would expect τ to increase. But also when we consider more massive lenses, fewer objects are needed along the line of sight to make the mass density fill out the density formula $\rho = \sigma^2/2\pi G r^2$. These effects cancel exactly, as one is proportional to $M^{1/2}$, while the other is proportional to $M^{-1/2}$.

Secondly, in Equation 3.1.3, τ is not a function of the distance to the galaxy, the distance to the source, or the angular extent of the galaxy. Also, we should note that τ is typically small. It is for this reason that the approximation of a single star affecting the light from the quasar is usually valid.

Neither of the last two equations incorporate cosmological effects. From Gott (1981) and TOG, the correct cosmological equation for optical depth is

$$\tau = 9.55x10^{-3}\frac{\sigma_{250}^2(1+z_{gal})}{\theta_{min}}\Sigma\Psi. \tag{3.1.4}$$

Here we define

$$\Sigma = \left[1 - \frac{z_{gal}Q_{gal}}{z_{qso}Q_{qso}}\right], \tag{3.1.5}$$

and

$$\Psi = arctan\left[1.3x10^{-4}\left[\frac{R_4 h}{\theta_{min}z_{gal}Q_{gal}}\right]^2 - 1\right]^{1/2}. \tag{3.1.6}$$

R_4 refers to the radius of the galaxy in units of 10^4 pc.

Q is a cosmological term which converts distances to angular diameter distance units, and approaches unity as z approaches zero. Q is given by

$$Q = \frac{zq_o + (q_o - 1)[(2zq_o + 1)^{1/2} - 1]}{z(1+z)^2}, \tag{3.1.7}$$

where q_o is the local deceleration parameter. Most of the galaxies that are catalogued currently are at low z, and hence the cosmological effects are not significant for this discussion.

A number that describes the effect of the whole galactic potential on the quasar light is called shear. Shear, here designated γ, is a measure of the effect of the mass of the host galaxy on the gravitational distortion produced by star(s) along the light path. Shear is the inverted square of the impact parameter (here the distance between the center of the galaxy and the light path), measured in the ERU of the host galaxy.

To calculate the magnitude of this term we first note that an (infinite, singular) isothermal sphere deflects light by a bending angle independent of the impact parameter (Bourassa, Kantowski, and Norton 1973). The bending angle for an infinite isothermal galaxy is $\alpha = 4\pi\sigma^2/c^2$. We can calculate the effective mass interior to the light path by also noting the effect if all the mass were concentrated in the center. The bending angle is then $\alpha = 4R_s/R$. Setting these equal for a given impact parameter R, we find the mass internal to this R which deflects the photon by a (small) amount α. If we then calculate the square of the radius of the Einstein ring for this mass and divide it by the square of the impact parameter, we have the number of ERUs the light passes from the center. The inverse of this number squared is γ.

For an isothermal sphere, we find that the shear is exactly equal to the optical depth. We will therefore not present calculations of γ in this or the following sections. Since τ was shown to be typically small, we conclude that τ is equally small, so it is a good approximation to ignore the effects of the host galaxy in these lensing calculations: the LE criterion is upheld.

Next we find the duration of an event of amplitude Φ. We will define the time of duration as the time it takes for the amplitude to go from 2Φ to Φ and back to 2Φ again. We can then generalize Equation 2.3.3 for a discrete lens distance between the observer and the source to find that

$$t = [16R_s D\Phi(1 - D_l'd)]^{1/2}/v. \qquad (3.1.8)$$

If we now add cosmological effects we find that the duration of an event is

$$t = (130 years) z_{gal}(1 + z_{gal}) \left[\frac{(M/M_{\odot}) Q_{gal}}{h} \right]^{1/2} \Sigma \frac{\Phi^{1/2}}{v_{500}}, \qquad (3.1.9)$$

where M is the mass of the lens, v_{500} is the transverse velocity of the lens in units of 500 km/sec, and h is the Hubble constant in units of 100 km/sec/Mpc.

When $\Phi = 1/2$, t is equivalent to the time it takes the lens to cross the Einstein ring. If we divide this time by the optical depth, we get the mean time between events of amplitude $\Phi = 1/2$. This is because optical depth is a measure of the number of stars per Einstein ring. If there is typically one star every Einstein ring, the time between events would be the same as the duration of the event. The fewer stars per Einstein ring, the lower the optical depth, and the longer the time between events.

We can generalize this argument to all Φ by noting that $2\tau\Phi$ is the number of stars per ring where the least lensing amplitude is Φ. When $\Phi = 1/2$ we recover the normal optical depth. As τ is also the probability of lensing at the amplitude $\Phi = 1/2$ or brighter, $P = 2\tau\Phi$ is then the generalized probability of lensing at the amplitude Φ or brighter. We can then find the mean time between events T by dividing t by P. The result is

$$T = (6900 years) \frac{z_{gal}\theta_{min}}{\sigma_{250}^2 \Psi v_{500}} \left[\frac{(M/M_{\odot}) Q_{gal}}{h\Phi} \right]^{1/2}. \qquad (3.1.10)$$

This method gives results equivalent to the mean free path arguments given in Chapter 2.

As quasars are typically brighter than galaxies, they can be seen at much greater distances. Quasars can presently be seen to a redshift of $z = 4.0$, while galaxies can be seen to a redshift of only $z = 1.0$. It is therefore a typical situation for a quasar to be seen without a discernable galaxy near the line of sight. But this is not proof that there is no galaxy there. A good way to be sure that there is a quasar - galaxy superposition is to detect this observationally.

The derived equations can thus be applied to a distribution of nearby galaxies that are seen to be angularly close to quasars. A catalogue of such angular associations has been recently published by Monk et al. (1986). The purpose of this catalogue was to create a finding list for observers wishing to study absorption lines from foreground galaxies on background quasars. Quasar - galaxy associations have been a topic of interest since quasars were first discovered, especially for those believing a real physical connection between the two. For recent discussion of such theories, see Burbidge (1979).

Tables 3.1.1 list galaxies taken from Monk et al. (1986) for which we have calculated r, t, and T. We include only those quasar - galaxy pairs which have a redshift measured for both the galaxy and the quasar. The galactic halo is always taken to extend to 100 kpc in the galaxy's own frame. Those quasar - galaxy associations separated by more than 100 kpc are not included. The value of σ_{250} was taken to be 1, as was the value of v_{500}.

The table is broken up into two sections. Table 3.1.1a includes spiral and

lenticular galaxies, while 3.1.1b includes elliptical and irregular galaxies.

In Table 3.1.1, column 1 refers to the quasar number, column 2 to the name of the galaxy, if it exists. Column 3 lists *tau*, the optical depth. Column 4 lists event duration time t for 0.1 magnitude events, while column 5 lists time between events of magnitude 0.1 of greater (T). Column 6 and 7 list t and T for a 1.0 magnitude event.

From inspection of these tables we again see that the assumptions inherent in the use of the lensing ellipsoid are validated: low optical depth and shear frequently occur. We feel that a dedicated observing program might detect the luminosity changes if they exist: this point will be further discussed in Chapter 7. It is also evident that, were a search program carried out that could identify more quasar - galaxy associations, a more comprehensive observing program might be possible.

Inspection of these tables also shows that previous detection of the microlens effect is not a certainty. Although it is possible, as noted above, that a small fraction of quasars currently being observed are undergoing microlensing, the effect may not be so easy to identify.

As speculated by Ostriker and Vietri (1985) and Barnothy (1986), it is possible that some BL Lacertae type objects are actually Optically Violently Variable (OVV) quasars whose continuum has been greatly amplified by microlensing. With the present results, we can limit the mass range of the lens from the duration of the events, as the mass of the lens is the variable in Equation 3.1.9 that has the widest

range of possible values. If these events are quickly transient, on the order of weeks, as noted in Nottale (1986), the mass of the lens should be small: a fraction of a solar mass. If, however, the BL Lac has maintained its current brightness over a baseline of 10 years or more, the mass of the lens is probably large, over 100 $M_\odot$.

3.2) Quasar - Cluster Associations

Another situation where a star could lens a background quasar is when this star is part of a cluster of galaxies. We assume here that the 'dark matter' in clusters of galaxies is in the form of compact objects: either small mass stars or massive black holes. We model clusters as 'big galaxies': isothermal spheres, except that the cluster velocity dispersion is on the order of 1000 km/sec instead of 250 km/sec. Also, we give clusters larger radial extent. We assume all clusters are the same and they all have a radius of 1 Mpc, at which point the cluster ends abruptly.

The above Equations, 3.1.4, 3.1.9, 3.1.10 can be used to find r, t, and T for microlensing in clusters. We find that clusters are indeed good places to look for microlensing. These equations become

$$r = (0.1)\,\frac{\sigma_{1000}^2(1+z_{cls})}{\theta_{min}}\Sigma\Psi, \tag{3.2.1}$$

$$t = (130\,years)\,z_{cls}(1+z_{cls})\left[\frac{(M/M_\odot)Q_{cls}}{h}\right]^{1/2}\Sigma\frac{\Phi^{1/2}}{v_{500}}, \tag{3.2.2}$$

$$T = (430\,years)\,\frac{z_{cls}\theta_{min}}{\sigma_{1000}^2\Psi v_{500}}\left[\frac{(M/M_\odot)Q_{cls}}{h\Phi}\right]^{1/2}. \tag{3.2.3}$$

Here the velocity dispersion of the cluster is likely to be higher than that of a galaxy, of the order of 1000 km/sec. The subscript cls refers to a cluster of galaxies.

Inspection of these equations shows that, if the dark matter that exists in clusters is compact in nature, they are better candidates for microlensing (per object) than galaxies. This is because clusters allow larger internal velocities than galaxies, as well as being physically larger in both radial and angular extent. Also, there is a good chance that a galaxy (or even several) can act simultaneously in conjunction with the cluster to increase the chance of observing microlensing.

3.3) A Cosmological Density of Jupiters

Many cosmologists believe that the density of the universe is equal to the critical density needed to close it. If this is true, then much of the matter in the universe is not in luminous form. One hypothesis holds that this dark matter is in the form of compact baryonic matter distributed uniformly throughout the cosmos. Would such a cosmological density express itself in the form of microlensing effects on background quasars?

A temporary assumption we first make to estimate the answer to this question quickly is the LE formalism. We also assume that the universe is static and Euclidean.

Assume a quasar is visible at $d_8\ 10^8$ pc. The volume of the LE is

$$V = \frac{2}{3}\pi R_s d^2\Phi = (2000\,pc^3)(M/M_\odot)d_8^2\Phi. \qquad (3.3.1)$$

The critical mass density of the universe is is $\rho = 3H_0^2/8\pi G$ which means the critical number density is

$$n = (2.83x10^7\,pc^{-3})(M_\odot/M). \qquad (3.3.2)$$

The probability of finding lensing at amplitude Φ is thus found to be

$$P = nV = (5.66x10^{-4})\, d_8^2\, \Phi. \qquad (3.3.3)$$

This equation agrees with the results in TOG at low optical depth.

We see that, since the large majority of quasars is at a distance greater than 10^8 pc, *at least* one quasar in 1800 should currently be undergoing lensing at amplitude $\Phi = 1$ or brighter. This number is independent of the lensing mass, and the speed of the lenses. Since 10^8 pc is a small number in a cosmological sense, and since cosmological effects would only act to increase the density of lenses, we see that Equation 3.3.3 is a lower limit to the probability of gravitational lensing independent of cosmology. When $\Phi = 1/2$, $P = \tau$ and one quasar in 3600 is undergoing an event of magnitude increase of 0.3 or brighter (0.9 in the mean, for a true point source). Since of the order of 10,000 quasars are currently known, it seems probable that, if $\Omega = 1$ with compact lenses, at least one quasar undergoing microlensing has been seen (but, as before in the galaxy case, not necessarily identified with the gravitational phenomenon).

Note that the shear from a uniform density of objects is, on the average, zero. Nityananda and Ostriker (1985) have shown that for a uniform distribution of lenses, the largest fluctuations of the shear come from nearby objects and will affect only events whose amplitude of lensing A is on the order of of $1/\tau^2$ or greater. Shear effects are hence negligible for the calculations presented here.

Once again we will calculate the time scale of gravitational lens-induced vari-

ability. In this instance, however, we understand that the variability arises not from random motions of the cosmological objects, but from large bulk motions with respect to the observer, source, and rest velocity as defined by the microwave background. Random motions thought to exist in massive, baryonic, cosmological objects are thought to be small, of the order of 50 km/sec (Sandage 1972; Sandage and Tammann 1975). The dipole moment of the microwave background shows our (an observer in the Local Group) motion to be of the order of 700 km/sec (Smoot et al. 1977). This alone adds an effective lens velocity of $(700\,km/sec)(1 - D/d)$ to the lens (see Equation 4.3.1). Furthermore, if this velocity is typical, we can expect bulk lens velocities of the order of 700 km/sec. These velocities, will, on the average, add to the effective relative motion of the lens. In our calculations, we will consider the typical transverse lens velocity (actually a superposition of observer, lens, and source velocity via Equation 4.3.2) to be 500 km/sec.

If, however, we consider our velocity of 700 km/sec to be unusual in the universe, and that the typical transverse cosmological lens velocity is much less than this, then an unusual effect may arise. Quasars along our line of motion would show fewer transient lens effects than those perpendicular to our line of motion.

We will estimate the duration of a lensing event from the maximum duration, which occurs (typically) at the most likely place for the lensing event: halfway between the observer and the source ($D = d/2$). Again we define the duration of an event of amplitude Φ or greater as the time it takes for the amplitude to go from

Φ to 2Φ, and back down again to Φ. We can thus generalize Equation 2.3.3 to read

$$t = (4R_s d\Phi)^{1/2}/v \tag{3.3.4}$$

which in more convenient form is

$$t = (12.2\,years)\,\frac{[(M/M_\odot)d_8\Phi]^{1/2}}{v_{500}}. \tag{3.3.5}$$

The time between events of amplitude Φ or brighter can be calculated by the above method: dividing the duration by P, the probability of lensing at Φ or brighter, given in Equation 3.3.3. We find this time to be

$$T = (21,500\,years)\left[\frac{(M/M_\odot)}{d_8^3\Phi v_{500}^2}\right]^{1/2}. \tag{3.3.6}$$

TOG have calculated τ as a function of z for several cosmological scenarios. We generalize their calculation of τ to the probability of lensing at amplitudes of all Φ. For an empty universe, this probability is

$$\mathrm{P} = \Omega_L \Phi \frac{z_{qso}^2}{z_{qso} + 2}, \tag{3.3.7}$$

where Ω_L is the cosmological density of lenses divided by the critical density (at the present epoch).

The most probable redshift for lensing is at half the source distance for non-cosmological source objects. This can be seen by noting that the LE has the largest cross-section at this point. For cosmologically distant objects, the most probable redshift is found by TOG to be $z_{prob} = (1 + z_{qso})^{1/2} - 1$. When calculating a typical

duration of a lensing event, we will place the lens at redshift z_{prob}. We again assume the duration is the time it takes the lens to move from 2Φ to Φ and back to Φ again. The duration time is calculated to be

$$t = (47.3\,years)\left[\frac{(M/M_\odot)\Phi z_{qso}(1+z_{qso})^{1/2}}{v_{500}^2 h}\right]^{1/2}. \tag{3.3.8}$$

A characteristic time between lensing events of amplitude Φ or brighter is

$$T = t/P = (47.3\,years)\left[\frac{(M/M_\odot)(2+z_{qso})(1+z_{qso})^{1/2}}{\Omega_L^2 \Phi z_{qso}^3 v_{500}^2 h}\right]^{1/2}. \tag{3.3.9}$$

If the universe is filled with a cosmological density of lenses such that $\Omega = \Omega_L = 1$, a different τ is relevant. Again generalizing from results in TOG, we find the probability of lensing at an amplitude Φ or greater is

$$\tau = \frac{6}{5}\Phi\left[\frac{(1+z_{qso})^{5/2}+1}{(1+z_{qso})^{5/2}-1} ln(1+z_{qso}) - \frac{4}{5}\right]. \tag{3.3.10}$$

TOG find that when z_{qso} goes to infinity, the most probable lens distance is relatively close: $z_{prob} = 0.65$. z_{prob} is not a strong function of z_{qso} at large z: even at $z_{qso} = 2$, $z_{prob} = 0.48$. As small z cases were covered above, we will assume a high z_{qso} here and take $< z_{prob} >= 0.5$.

For the above assumptions we then find that a characteristic duration time for a lens event brighter than Φ is

$$t = (71.1\,years)\left[\frac{(M/M_\odot)\Phi}{v_{500}^2 h}\right]^{1/2} \tag{3.3.11}$$

and a characteristic time between lensing events of

$$T = t/P = (59.3\,years)\left[\frac{(M/M_\odot)}{v_{500}^2 h\Phi}\right]^{1/2}\left[\frac{(1+z_{qso})^{5/2}+1}{(1+z_{qso})^{5/2}-1} ln(1+z_{qso}) - \frac{4}{5}\right]^{-1} \tag{3.3.12}$$

3.4) Discussion

Could microlensing be invoked to explain all or most of quasar variability? Only when τ approaches unity, or when T approaches the time scale of a month, could microlensing produce the continual luminosity changes found in some quasars. We do not believe that lensing is the dominant cause for quasar variability, but we find the hypothesis interesting enough to examine further. This hypothesis has also been examined by Canizares (1982), and Schneider and Weiss (1987).

We will consider only the case where $\tau << 1$ but T is of the order of a month. Schneider and Weiss (1987) considered a case of higher average optical depth. The only range of parameter space that could allow such speculation is that of very small lenses which are moving very quickly. The situation calls for Jupiter- size masses or smaller moving transversely at 1000's of km/sec. The smaller the lens, the smaller its ERU, and the faster it can traverse its own ERU at a given velocity. Also, given a fixed ERU, the faster the lens, the shorter the wait between lensing events and the shorter the duration of the lensing events.

Even with these unusual assumptions, there are still discrepancies between theory and observation that indicate microlensing is not to be credited as the dominant cause of quasar variability. We will place these discrepancies into three categories. The first category involves light curve shape, the second involves individual quasar variability histories, and the third discusses discrepancies involving comparative quasar variability histories.

First, the light curves of individual lens events, shown in Figure 4.3.2, are not typical of what is seen. No quasar variation light curve has, to date, been strongly indicative of one of these curves. Quasar variations are typically different and more complicated (for a review of quasar properties, see, for example, Wiita 1985). One defense against this argument is to invoke a source that is complicated and extended in structure. Such a source would necessitate the production of more complicated light curves.

Discrepancies with individual quasar light histories may also discredit microlensing as an explanation of quasar variability. Why would a single quasar be highly variable over some period and relatively quiet over others? Shouldn't a uniform density of lenses act with similar effects over a large range of time? A defense against this argument is to suppose that either the density along the line of sight can change (say a star cluster passes in front of a quasar), or that the size of the lensing region changes, so as to damp out lens-induced variability.

Individual quasars are thought to echo light variations in their small internal compact regions to outlying regions (Wiita 1985). If the outlying regions are spherically symmetric and centered on the central regions, one would expect them to vary at the same time, not at a later time. If the outlying regions were not spherically symmetric, then lensing would predict an equal probability of the outlying region varying *first*, if not both before and after the inner region lensing event. This point is considered in more detail in Chapter 6.

Another major problem with believing that all quasar luminosity changes are due to microlensing is that of the relative light histories of quasars. If we invoke a cosmological density of objects for the lenses, why do some quasars vary greatly, while others are relatively quiet? Again, there are two possible explanations of this. The first is to suppose a higher lens density along the line of sight to some quasars than to others. The second is to suppose that some quasars have continuum regions significantly larger than others.

Gravitational lensing effects would also predict variability to be a function of quasar distance. We expect this because the more distant the quasar, the higher the average density of lenses that would be expected along the line of sight. This effect is not seen. It is also difficult to explain why some nearby quasars are highly variable.

Canizares (1982) compared the continuum luminosity of quasars to the broad emission line luminosity. He argued that if microlensing were a dominant cause of quasar variability, and if microlensing affected the continuum emission much more strongly than the broad line emission, then one would expect a large scatter in the continuum-to-line ratio measures between quasars. Since he did not find such an affect from inspection of several quasar data sets, he concluded that microlensing was *not* a dominant cause of quasar variability.

Although there are strong arguments against all or most quasar variability being tied to microlensing, we feel there is definitely room for *some* fraction of it to be

so explained. If much of dark matter can be explained by Jupiter-sized compact objects, a careful search for their gravitational lens effects could be fruitful.

References

Barnothy, J. M., 1986, *A. J.* **91**, 755.

Bourassa, R. R., Kantowski, R., and Norton, T. P. 1973, *Ap. J.* **185** 747.

Burbidge, G. R. 1979, *Nature* **282**, 451.

Canizares , C. R. 1982 *Ap. J.* **263**, 508.

Gott, J. R. III 1981, *Ap. J.* **243**, 140.

Lang, K. R. 1980, Astrophysical Formulae, Springer-Verlag: Berlin.

Monk, A. S., Penston, M. V., Pettini, M., and Blades, J. C. 1986, *M.N.R.A.S.*, preprint.

Nemiroff, R. J. 1986, *Ap. Sp. Sci.* **123**, 381.

Nityananda, R. and Ostriker, J. P. 1985, *J. Ap. A.* **5**, 235.

Nottale, L. 1986, *A. Ap.* **157**, 383.

Ostriker, J. P., and Vietri, M. 1985, *Nature* **318**, 446.

Press, W. H., and Gunn, J. E. 1973, *Ap. J.* **185**, 397.

Sandage, A. 1972, *Ap. J.* **178**, 1.

Sandage, A. and Tammann, G. A. 1975, *Ap. J.* **196**, 313.

Schneider, P., and Weiss, A. 1987, *A. Ap.* **171**, 49.

Smoot, G. F., Gorenstein, M. V., Muller, R. A. 1977, *Phys. Rev. Lett.* **39**, 898.

Turner, E. L., Ostriker, J. O., and Gott, J. R. III 1984, *Ap. J.* **284**, 1.

Vietri, M., and Ostriker, J. P. 1983, *Ap. J.* **267**, 488.

Wiita, P. J. 1985, *Phys. Rep.* **123**, 117.

Table 3.1.1a

Quasar Name	Galaxy Name	τ	t (0.1 mag, years)	T	t (1.0 mag, years)	T
0026+129	Anon	0.0021	1.177	216.	0.295	863.
0039-256	NGC 253	0.0001	0.508	3291.	0.127	13147.
0041-261	NGC 253	0.0002	0.508	1159.	0.127	4632.
0042-248	NGC 253	0.0002	0.508	1192.	0.127	4763.
0050-253	NGC 253	0.0001	0.508	1700.	0.127	6792.
0051-253	NGC 253	0.0001	0.508	2652.	0.127	10595.
0048-396	NGC 300	0.0001	0.398	2154.	0.100	8606.
0056-363	NGC 300	0.0001	0.397	1651.	0.099	6595.
0056-394	NGC 300	0.0001	0.398	1621.	0.100	6475.
0151+045	IC 1746	0.0134	2.435	71.	0.609	284.
0219+428	UGC 1832	0.0042	2.194	204.	0.549	816.
0219+428	NGC 891	0.0001	0.772	2537.	0.193	10135.
0336-248	NGC 1385	0.0004	1.012	1069.	0.253	4272.
0446-208	Anon	0.0643	3.864	25.	0.967	98.
0838+770	Anon	0.0050	1.741	136.	0.436	542.
0918+512	NGC 2841	0.0005	0.757	579.	0.189	2314.
0955+326	NGC 3067	0.0074	1.089	56.	0.273	226.
1049+616	NGC 3407	0.0035	2.014	221.	0.504	884.
1103-006	NGC 3521	0.0000	0.723	6233.	0.181	24901.
1206+459	NGC 4144	0.0002	0.524	928.	0.131	3708.
1219+755	NGC 4319	0.0190	1.186	24.	0.297	96.
1254+047	NGC 4765	0.0005	0.757	534.	0.190	2133.
1327-206	Anon	0.0217	2.085	37.	0.522	149.
1341+258	Anon	0.0056	1.924	133.	0.482	531.
1425+267	Anon	0.0020	1.829	349.	0.458	1394.
1428+498	NGC 5660	0.0011	1.398	493.	0.350	1969.
1749+701	NGC 6503	0.0027	0.500	71.	0.125	284.
2020-370	Anon	0.0495	0.847	7.	0.212	26.

Table 3.1.1b

Quasar Name	Galaxy Type	τ	t (0.1 mag, years)	T	t (1.0 mag, years)	T
0112-017	E	0.0008	1.287	611.	0.322	2440.
0137+060	Anon	0.0035	4.415	589.	1.105	2355.
0219+428	E	0.0019	2.290	471.	0.573	1882.
1011-040	Im	0.0002	0.315	483.	0.079	1929.
1208+322	Anon	0.0089	4.460	221.	1.117	885.
1233+125	E7/S0	0.0204	0.500	9.	0.125	37.
1246-057	E6	0.0008	0.947	431.	0.237	1723.
1302-102	Anon	0.0071	3.945	242.	0.988	968.
1302-102	Anon	0.0102	3.795	156.	0.950	623.
1355-416	Im	0.0002	0.499	1091.	0.125	4356.
1510-089	Anon	0.0050	3.874	370.	0.970	1478.
2020-370	E	0.0197	0.842	16.	0.211	66.
2305+187	Anon	0.0227	3.310	69.	0.829	277.
2305+187	Anon	0.0015	3.315	1046.	0.830	4180.

Chapter 4

Single Star Light Curves

4.1) Previous Work

Single star light curves have been studied previously by Liebes (1964), and Refsdal (1964). Liebes and Refsdal calculated analytically the basic effects of a single star on a point source behind it. Maeder (1973) considered a binary system with one star gravitationally lensing the light from the other star. Bontz (1979) calculated source changes that result from the lensing of a massive opaque lens. Chang and Refsdal (1979, 1984) considered the light curves of a star in a galaxy acting in conjunction with the gravitational field of its host galaxy (equivalent to working at large shear).

More recently Nottale (1986, NTL) considered the effect of a foreground star, acting alone on a background circular quasar of uniform brightness. NTL modeled a specific light increase of the quasar W0815+234. Paczynski (1986a) calculated the probable effect of single stars in our own galaxy lensing stars in nearby ones. He calculated and displayed single-star light curves for a wide range of magnitude brightenings due to a single star lensing a point source.

Our main goal in this Chapter is not directed toward generating a more realistic library of typical microlensing events, but toward the information latent in simple microlensing events. We focus on a simple light curve generated under basic (but not improbable) assumptions, and analyse the lens and source information which

can be recovered.

The scenario requires the LE formalism to be valid so that, in general, a point lens acts to amplify the light emitted from a point source. Later we will relax this assumption to include a uniform circular source, and lastly a uniform elliptical source. These simple cases seem to us the ones which preserve the most lens and source information in the most easily recoverable form. We give a step-by-step procedure to show how a photometric observer can recover this lens and source information from measurement of the light curve. We will find that such analysis leads to angular resolution at the angular scale of the ERU or smaller. This corresponds to measurement of source size and impact parameter between lens and source center of the order of 10^{-6} arcsec, and of velocity of the lens to a scale of 10^{-6} arcsec per year.

In section 4.2 we outline the mathematical and numerical techniques needed to calculate the light curves under these assumptions. Section 4.3 presents the light curves for a circular uniform source and discusses the information to be recovered from such a light curve. In section 4.4 we present and discuss the light curves for an uniform elliptical source.

4.2) Mathematics of Extended Source Lensing

As derived in Liebes and Refsdal, the total amplification of a point source by a point lens is

$$A = \frac{r^2 + 2}{r(r^2 + 4)^{1/2}} \qquad (4.2.1)$$

where the amplification factor A represents the ratio of lensed to unlensed brightnesses, and r is the distance between the lens and the source in terms of the ERU.

Following the analyses in Maeder (1973) and NTL, we calculate the amplification of an extended source by integrating equation 4.2.1 over the source distribution, assumed to be of uniform surface brightness. With a polar coordinate system centered on the point lens, the amplification A is

$$A = \frac{\int\int \frac{r^2+2}{r(r^2+4)^{1/2}}\, r\, dr\, d\phi}{\int\int r\, dr\, d\phi}, \qquad (4.2.2)$$

where r is the distance from the lens to a given point on the source, and ϕ is the azimuthal angle measured in the plane of the sky. The geometry of the situation is depicted in Figure 4.2.1. Numerical evaluation of Equation 4.2.2 was one method used to generate light curves.

An alternative but equivalent numerical approach to recovering A for an extended source, and hence generating light curves, is to use the property that gravitational lensing conserves surface brightness (Misner, Thorne, and Wheeler 1973). For a uniform source we calculated the area of the source after lensing and compared it to the area of the source before lensing, the ratio of the two being the amplitude A. Although the mathematical and physical principles involved are equivalent to the above technique, the details of the numerical processes are quite different. In the surface brightness approach, one chooses points on the boundary of the unlensed source and calculates the two positions into which the lens maps each point. The equation for calculating the displacement is Equation 1.2.3.

It is not numerically efficient to pick points equally spaced on the original source boundary when calculating the new lensed source boundary. Because of the non-linear way the lens redistributes boundary points, points equally spaced on the boundary before lensing will not lead to points equally spaced on the boundary after lensing. Indeed, the accuracy of the calculation increases when the final source boundary is best defined with the points equally spaced there. Starting with equally spaced points on the unlensed boundary creates the need for thousands of points before good lensed images are defined. A better method is to draw rays from the lens to the unlensed source boundary, using the intersection points to denote the boundaries of the unlensed source, and use these points in Equation 1.2.3 to calculate the position of the lensed image boundaries.

We used both numerical techniques to calculate the light curves presented here and find they agree very well. To calculate the light curve we moved the lens across the field of the source noting the lensing amplitude at many discrete points. The plot of the magnitude increases against the lens position (or time) designates the light curve. The abscissa of the light curves is given in ERU, and designates the distance of the lens from closest approach to the center of the unlensed source.

The numerical processes were carried out on a Leading Edge Home Computer using Microsoft FORTRAN, and an IBM 4341 main-frame using FORTRAN 77.

4.3) Light Curves for a Point and Circular Source

Figure 4.3.1 shows a sequence of light curves for a point lens acting on a point

source. This graph is the same as Paczynski (1986a) and is included for completeness and comparison with later light curves. From the standpoint of the observer there are several comments that can be made about the curves. First of all, the maximum lensing magnitude (more precisely, the magnitude of the unlensed source minus the magnitude of the source when it is at its brightest, hereafter ΔM_{max} , is a measure of the impact parameter in ERU. As seen in Equation 1.2.2, the ERU itself is a function of the mass of the lens, the distance to the lens, and the distance to the source.

The abscissa of Figure 4.3.1 is labelled in ERU units. Measured light curves would necessarily be in time units. Therefore, the direct correlation of a measured light curve to a theoretical one would necessarily give a correlation between ERU units and time. This correlation yields directly the relative velocity of the observer, lens, and source.

More precisely, this relative velocity can be defined in terms of an 'effective' lens velocity. If, relative to some rest frame, the lens and the source are at rest but the observer has some transverse (to the optic axis) velocity v_o, this can be seen to be equivalent to a lens velocity of $v_o(1 - D/d)$. Similarly, a source velocity v_s relative to an observer and lens at rest is equivalent to a lens velocity of $v_s(D/d)$. Therefore,

$$v_e = v_l + v_o(1 - D/d) + v_s(D/d), \tag{4.3.1}$$

where v_e is the effective, combined, transverse velocity of the lens, and v_l is the real

transverse velocity of the lens. The scalar v_e is then

$$v_e = (\mathbf{v}_e \cdot \mathbf{v}_e)^{1/2} = (v_l^2 + v_o^2(1 - D/d)^2 + v_s^2(D/d)^2 - 2v_l v_o(1 - D/d)\cos\theta_{lo}$$

$$-2v_l v_s(D/d)\cos\theta_{ls} - 2v_s v_o(1 - D/d)(D/d)\cos\theta_{so})^{1/2}, \qquad (4.3.2)$$

where θ represents the angle between the transverse velocity vectors.

Figure 4.3.2 shows a variety of half light curves for a single lens acting on a uniform circular source. Only half of each light curve is given, since these light curves are symmetric about ΔM_{max} . Figure 4.3.2a shows light curves that all have a ΔM_{max} of 1 magnitude, while those in Figures 4.3.2b and 4.3.2c have ΔM_{max} of 2 and 5 magnitudes respectively. ΔM_{max} occurs when b, the impact parameter, is smallest. A ΔM_{max} of 2 magnitudes means the brightness of the source is two magnitudes brighter than in the absence of lensing.

For a uniform circular source, there are two input parameters needed to generate a light curve. One of these is ΔM_{max} , the other is R, the radius of the source. Once R is specified, b is uniquely determined. The reverse proposition is not necessarily true: if ΔM_{max} and b are specified, R might not be uniquely determined. Indeed, there are several values of R that may fit.

From inspection of Figure 4.3.2, some conclusions may be drawn immediately. For a given magnitude of lensing, there is a source radius below which the shape of the entire light curve becomes, effectively, independent of source size. The curve is then equivalent to the corresponding curve shown in Figure 4.3.1, and is identical to that of lensing a point source. Alternatively, there is also a maximum source

radius above which it is impossible to obtain a given ΔM_{max} . Inspection of Figure 4.3.2 also shows a general rule: the larger the source radius, the broader the light curve.

We now wish to reverse the theoretical process and ask: what information could we recover from close scrutiny of a light curve? We will analyse the light curves correlating those parameters that can be measured from the light curve with those parameters generating them. Information that can be measured from the light curve are ΔM_{max} , parameters carrying information as to the intrinsic shape of the light curve, and parameters relating to the scale of the light curve abscissa.

A parameter relating to the scale of the abscissa is a chord across the light curve at small lensing magnitude, where the curve becomes like that of a point source. If the chord is drawn low enough, it will not be a strong function of light curve shape. One convenient such chord we will designate the '2-ERU line'. This chord is particularly convenient because its length is directly related to the ERU.

For a point source and any ΔM_{max} , the 2-ERU line lies $\approx$ 0.319 magnitudes above the baseline of the unlensed quasar light level. The same value is also a good approximation for some extended sources. If the observer notes the time between the two points on the graph where the magnitude brightening is 0.319 magnitudes, the time between the two points corresponds to an angular distance of lens motion of 2-ERU. So this length of time, divided by two, is the velocity of Equation 4.3.2 in units of ERU per time interval. We will refer to this velocity as just v. Corrections

to the 2-ERU line method of determining this 'proper motion' do occur at small ΔM_{max} and large R, and they will be discussed later.

One possible method for scrutinizing light curves such as those in Figure 4.3.2 in order to obtain lens and source information is described here. In some instances, the angular size of the source can be found quite accurately.

In lensing situations for which the lens becomes directly projected against the disk of the source, the central part of the light curve, around ΔM_{max} , becomes flattened. A convenient method of determining the degree of this flattening, and hence parameterizing the shape of the light curve, is to define a thickness parameter, h. The h we will use is defined as the distance between the inflection points of the light curve, as measured on the abscissa.

Using the inflection points to parameterize the light curve has several advantages. First, the information carried by the inflection points is invariant to the change in most of the other parameters, including ΔM_{max} , b, R, v, and the ERU. Second, inflection points are intrinsic features of a light curve; there is no *theoretical* ambiguity in their location.

Plots of R versus h for ΔM_{max} = 1, 2, and 5 appear in Figure 4.3.3. Two regimes can be seen, corresponding to when the lens passed directly in front of the disk of the source, and when it did not. Large sources had the lens pass directly between the source and the observer, resulting in a good correlation of h with R. Small sources show a less striking correlation. A sample interpretation to be made

is that for a lensing event with measured $\Delta M_{max} = 1$, and measured h value of 0.7, the source must have an angular extent of about 0.8 ERU. If the event had $\Delta M_{max} = 1$ and $h = 0.36$, then the source could have any range of angular extents, with $0 \leq R \leq 0.4$ ERU and $R = 0.65$ possible. The ambiguity between the first R range and the second distinct R value can be broken by noting the shape of the light curve. The light curve with the most flattened top corresponds to the higher R value.

Similarly, Figure 4.3.4 shows the correlation of b with h. The same two regimes are indicated. From inspection of the graph, we can tell that with $\Delta M_{max} = 1$ and $h = 0.7$, the lens must have passed almost 0.4 ERU of the center of the source.

Figure 4.3.5 shows a correlation between h^2 and $(R^2 - b^2)$. For all ΔM_{max} investigated, h^2 shows itself to be a direct measure of $(R^2 - b^2)$, when the later quantity is positive. The reason for this correlation is clear: the inflection points are accurate indicators of the times when the lens enters and leaves the boundary of the uniform source. Since the distance the lens traverses across the source is $2(R^2 - b^2)$, h is then a direct measure of the source length along the path of the lens.

If the lens did not cross the source boundary, $(R^2 - b^2)$ is negative, and h^2 is only a weak measure of source size. This situation is shown by the lower curves of Figure 4.3.5. From inspection of Figure 4.3.5a, we can see that when $\Delta M_{max} = 1$ and $h^2 = 0.5$, $(R^2 - b^2) = 0.5$, in agreement with the above mentioned values. This

means that the distance the lens traveled across the face of the source was 0.5 ERU.

For a circular uniform source, this situation is shown graphically in Figure 4.3.6. The graph was computer generated, and no part of the graph was 'scaled' to make the correlation between inflection point locations and source size more obvious. The dotted lines were added later to emphasize the effect.

A point that we will now address is the measuring of the thickness parameter, h. In observed light curves, h will be measured as a function of time. This is because observational light curves use time to designate the abscissa of the light curve instead of ERU. To determine h in ERU, one must divide this time by v, the extent (in time) of the 2-ERU line.

This procedure, however, has some internal error in it. The error comes about at large R from the flattening of the light curve. The flattening distorts the curve at the height of 0.319 magnitudes, the height at which the 2-ERU line is drawn.

As may be seen in Figure 4.3.2, larger sources have wider light curves at 0.319 magnitudes than do smaller sources. Therefore, light curves of larger sources will have v's measured by the above method lower than the actual values. To correct for this inaccuracy, one can refer to Figure 4.3.7. From this figure one can see there is a direct relation between the original h measurement and the actual h in ERU. We present only the mapping for the studied cases $\Delta M_{max} = 1$ and 2, since for $\Delta M_{max} = 5$ the correction is less than 0.1%.

Multiplying v by the actual h value, h_{ERU}, and dividing by the original value,

h_{ORIG}, as labelled in Figure 4.3.2, will give a v-value corrected for large source size. The actual thickness parameter, h_{ERU}, is the one we correlated with other variables.

4.4) Light Curves for Elliptical Sources

For an elliptical uniform source, there are 4 input variables needed to generate the light curve. They are ΔM_{max} , the maximum lensing magnitude; a_e, the major axis of the uniform source; b_e, the minor axis; and θ, the orientation angle of the major axis of the ellipse relative to the transverse velocity vector of the lens. Once these parameters are specified, the impact parameter of the lens is uniquely determined.

One method of scrutinizing the light curves - the method we will describe here - will utilize 3 parameters that can be measured from the light curve. These parameters are ΔM_{max} , v: the length of the 2-ERU line, and h: the abscissa distance between the inflection points. The parameter v continues to be an accurate measure of the relative velocity, but we can find no direct relation between h and a_e, b_e, or θ.

In h, however, we still retain an accurate measure of source length along the path of the lens, as shown in Figure 4.4.1. This figure also shows that light curves of uniform sources need not be symmetric about ΔM_{max} . Indeed, both curves shown here are somewhat asymmetric. As a general rule, the closer the lens passes tangent to a limb of a source, the more the light curve deviates from symmetry.

When the lens was far from the ellipse (on the order of a_e from the ellipse edge or more), the wings of the curve become symmetric, as even an ellipse mimics a point source when the lens is far from its boundary.

Figure 4.4.2 shows a typical lensing sequence of an ellipse as seen by the observer. This would be the appearance of the lensed ellipse if the observer could resolve it. The lensing scenario corresponds to that depicted by the lower path of Figure 4.4.1.

It is clear that lens and source information can be recovered from a light curve even if the source is not circular (but still uniform). Both source size and lens velocity can still be obtained. As long as the source boundary is simple, the inflection points give an accurate measurement of source length along the line of lens motion.

4.5) Discussion and Comments

We have found that, in theory, much can be learned from analysis of gravitational lensing light curves. We can derive information about both the lens and the source, although much of the information in the form obtained would be a mixture of both lens and source parameters.

One such datum derivable from analysis of the light curve is the relative motion between the observer, lens, and source, as derived in Equation 4.2.2. Light curve analysis recovers this parameter in units of ERU per time unit, and therefore involves the mass of the lens, the distance to the lens, the distance to the source, and the relative velocity in standard units.

If we envision a scenario wherein a star in a nearby galaxy microlenses a back-

ground quasar, we might assume that the distance to the galaxy and the quasar are known through their redshifts. This leaves the observer with a result that is a coupling of lens mass and velocity.

Another datum recoverable from light curve analysis is the size of the source, or a limit for it. Source size is recovered in ERU, so what is measured is really also a function of lens mass, lens distance, and source distance. As before, in the microlensing scenario, if we assume prior knowledge of the distance to the lens and the source, we are left with a coupling of lens mass and source size. If the lens did not pass in front of the source, we can determine that the source size parameter must be smaller than some value.

The third datum that can be measured from the light curve is the impact parameter. Once more, b is measured in ERU, so what is really measured is a function of b, lens mass, lens distance, and source distance.

We are thus left with the familiar problem of more unknown variables than measured parameters. In our imaginary microlensing scenario, the four unknowns are b, v, R, and m, where m is the mass of the lens. The three data convolve b and m, v and m, and R with m. If any of the parameters can be measured independently, the above relations can be used to solve for the other three. In fact, it should be useful to use estimates or constraints on data to find the corresponding estimate or constraint on the other parameters.

If we assume lenses of the order of Jupiter size masses, the angular scale we

would obtain information on is of the order of 10^{-7} arcseconds. Angular sources, if not perfect black bodies, would then yield 'equivalent uniform' source sizes with angular resolution on that scale. Similarly, the impact parameters would be calculated on the same scale.

Relative velocity would also be a function of the ERU. Proper motion would further convolve velocity with the duration of the event. If we further assume the relative velocity to be dominated by the proper motion of the galaxy that is host to the lens, and that the duration of the event is one year, we would know the relative proper motion of the galaxy to 10^{-6} arcsec/year or better.

If a library of lens events were compiled, we could use the distribution of impact parameters with time to estimate the number density of lensing objects along the line of sight. If we have an estimate for the mass of the lenses, we could then calculate mass density along the line of sight as well.

The opportunity to seek out, measure, and analyse candidate light curves has been available since the discovery of bright compact objects at cosmological distances. The photometric techniques are not new, and they are not fundamentally different from those used to measure variable stars. Indeed, it is possible that inspection of past light curves may lead to some gravitational lens interpretations, and the analysis outlined in this Chapter could be used on archival data. Future observers should be careful to obtain good time coverage of an event, so that accurate determinations of h and the 2-ERU line can be made.

Real measurements would probably not be so easy to interpret as the relatively 'simple' scenario covered here, although in principle the same information is recoverable. The main confounding factor would invariably be intrinsic quasar variability. This variability might swamp the gravitational lens - induced variability, making accurate data recovery impossible. Decoupling these two types of variation will be discussed in Chapter 7.

Even relatively small errors could impede the finding of the location of the inflection points crucial to the above analysis. This effect is particularly bad when the source is much smaller than the ERU, and the lens passes directly in front of the source. In this situation, a small error in the slope then could cause a large error in the location of the inflection points. If the error in the observational photometry is the only source of error, determinations of the lens and source parameters should be relatively straight-forward and accurate.

References

Bontz, R. J. 1979, *Ap. J.* **233**, 402.

Chang, K., and Refsdal, S. 1979, *Nature* **282**, 561.

Chang, K., and Refsdal, S. 1984, *A. Ap.* **132**, 168.

Liebes, S. Jr. 1964, *Phys. Rev.* **133B**, 835.

Maeder, A. 1973, *A. Ap.* **26**, 215.

Misner, C. W., Thorne, K., and Wheeler, J. A. 1973, Gravitation, San Francisco: Freeman.

Nottale, L. 1986, *A. Ap.* **157**, 383.

Paczynski, B. 1986a, *Ap. J.* **304**, 1.

Paczynski, B. 1986b, *Ap. J.* **301**, 503.

Refsdal, S. 1964, *M.N.R.A.S.* **128**, 295.

Figure Captions

Figure 4.2.1: Geometry of lensing for a point lens acting on a circular source. The quantity r is the distance from the lens to a given point on the source boundary, R is the radius of the source, b is the impact parameter, and ϕ is the azimuthal angle.

Figure 4.3.1: Light curves for a point lens acting on a point source. The abscissa coordinate x represents the positional coordinate for the lens as it moves parallel to the abscissa. At $x = 0$ one has the closest angular approach of the lens to the source. There should be a direct linear conversion from this position coordinate to the time base of a measured photometric light curve.

Figure 4.3.2: Half light curves for a point lens and an extended uniform circular source. The maximum lensing magnitude, $\Delta M_{max} = 1$, 2, and 5 are represented in plots a, b, and c, respectively. Each curve was generated from the input data of ΔM_{max} and R, the radius of the circular source. For the $\Delta M_{max} = 1$ plot, R is, for each curve, from left to right: 0.6, 0.0, 0.7, 0.8, 0.868. The $R = 0.0$ curve represents the curve for a point source and is included here for comparison. For $\Delta M_{max} = 2$ plot, we have, from left to right, the curves labelled by R = 0.23, 0.27, 0.30, 0.321. For the $\Delta M_{max} = 5$ plot, the lines correspond to $R = 0.014$, 0.016, 0.018, and 0.02 respectively. All R values are given in ERU.

Figure 4.3.3: Plots of R, the circular source radius, versus the thickness parameter, h, for $\Delta M_{max} = 1$, 2, and 5. For each plot, there appears two curves. The

upper curve represents cases where the lens passed directly over the source, so that h is a good measure of R. If the lens did not pass in front of the source the lower curve is applicable, and h becomes strictly a measure of impact parameter.

Figure 4.3.4: Plots of the impact parameter, b, versus the thickness parameter, h, for a circular uniform source. For each plot, two curves are again shown. For the upper curve the lens moved in front of the source, for the lower curve it did not. The $(h - b)$ ambiguity at certain b values can be resolved by noting the difference in the shape of the light curve.

Figure 4.3.5: Plots of $(R^2 - b^2)$ versus h^2 for a circular uniform source. When the lens passes in front of the source, there is a direct linear relation between the two parameters. When it does not, no linear dependance exists, and h is a measure of b alone.

Figure 4.3.6: Paths of the lens moving across a circular uniform source resulting in the light curves shown. Note how the inflection points of the light curve are an accurate measure of the points of the lens crossing into and leaving the source boundary.

Figure 4.3.7: Plots of h_{ERU}, the h that would be measured when the 2-ERU line really has a length of 2 ERU, versus h_{ORIG}, the h originally measured when the 2-ERU line is drawn at a height of 0.319 magnitudes on the light curve. For $\Delta M_{max} = 5$, h_{ORIG} is an accurate measure of h_{ERU} to better than 0.1%, and so this plot is not shown.

Figure 4.4.1: A construct similar to Figure 4.3.7, except applicable to an elliptical source. Note again how the inflection points of the curve are an accurate measure of the boundary of the uniform source.

Figure 4.4.2: A resolved lensing sequence for a point lens acting on an elliptical source. The lensing scenario given is depicted by the lower lens path of Figure 4.2.7. The x values of the lens are, from top to bottom, x = -1.0, -1/3, +1/3, and +1 ERU respectively.

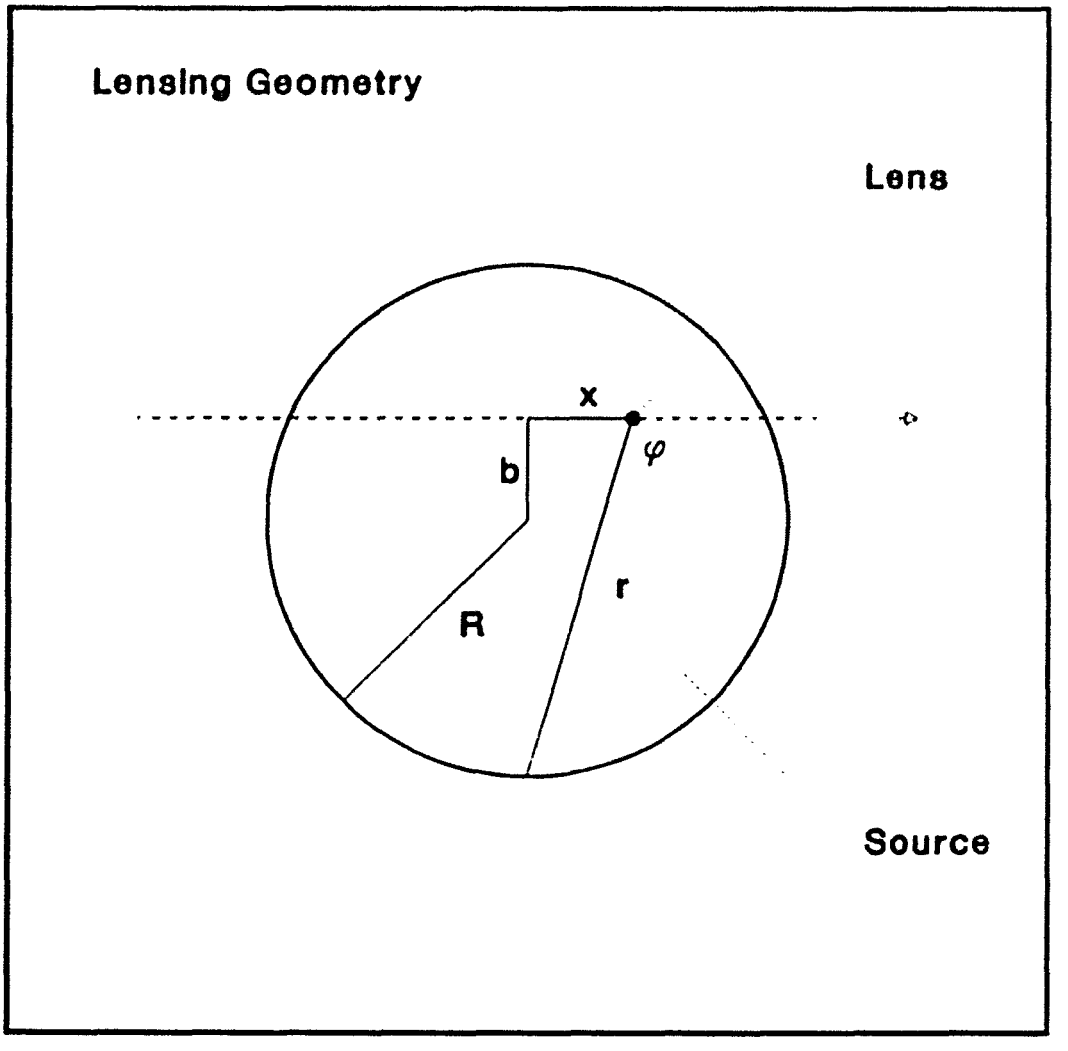

Figure 4.2.1

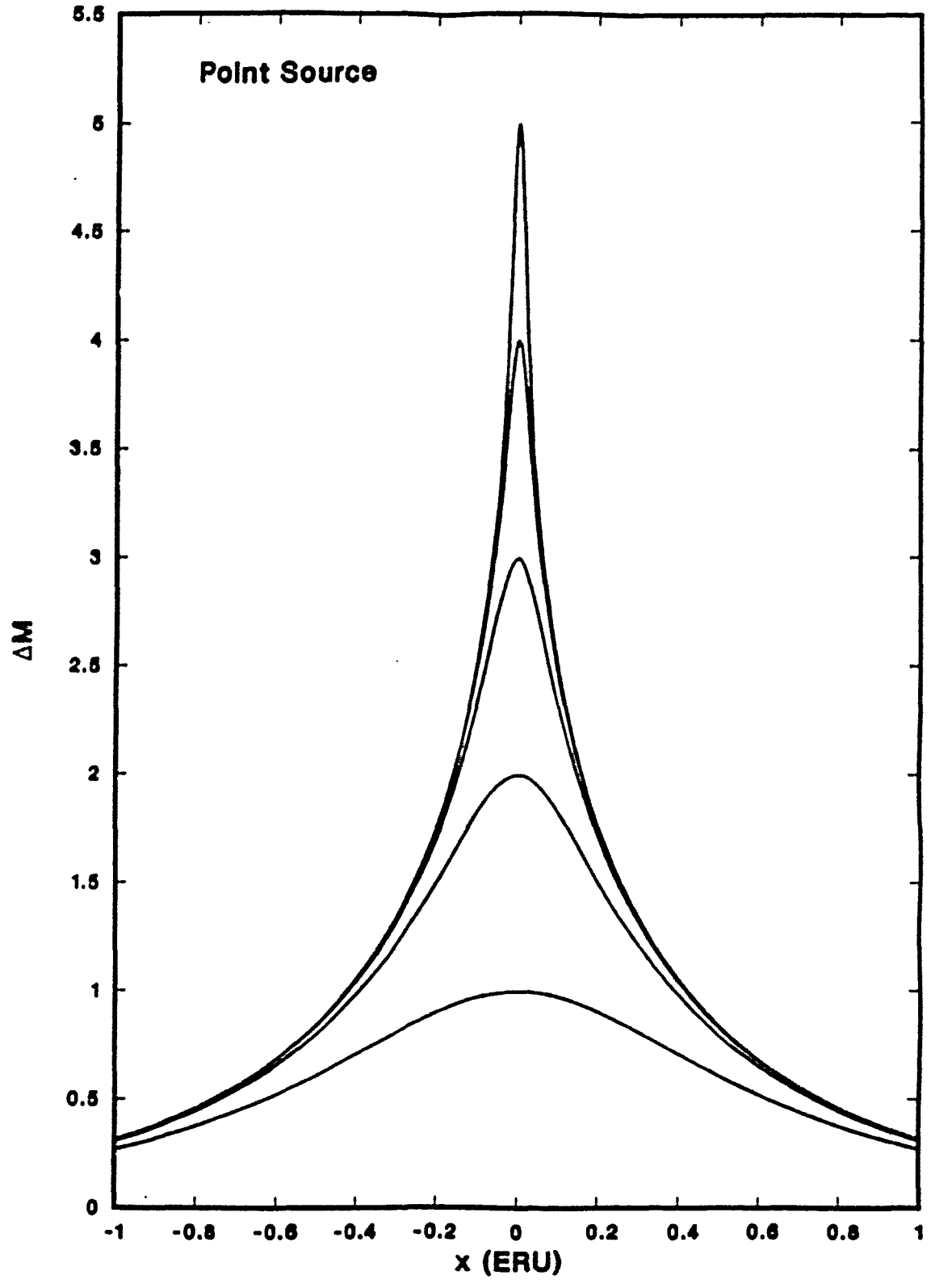
Point Source
ΔM
x (ERU)
5.5
5
4.5
4
3.5
3
2.5
2
1.5
1
0.5
0
-1
-0.8
-0.6
-0.4
-0.2
0
0.2
0.4
0.6
0.8
1

Figure 4.3.1

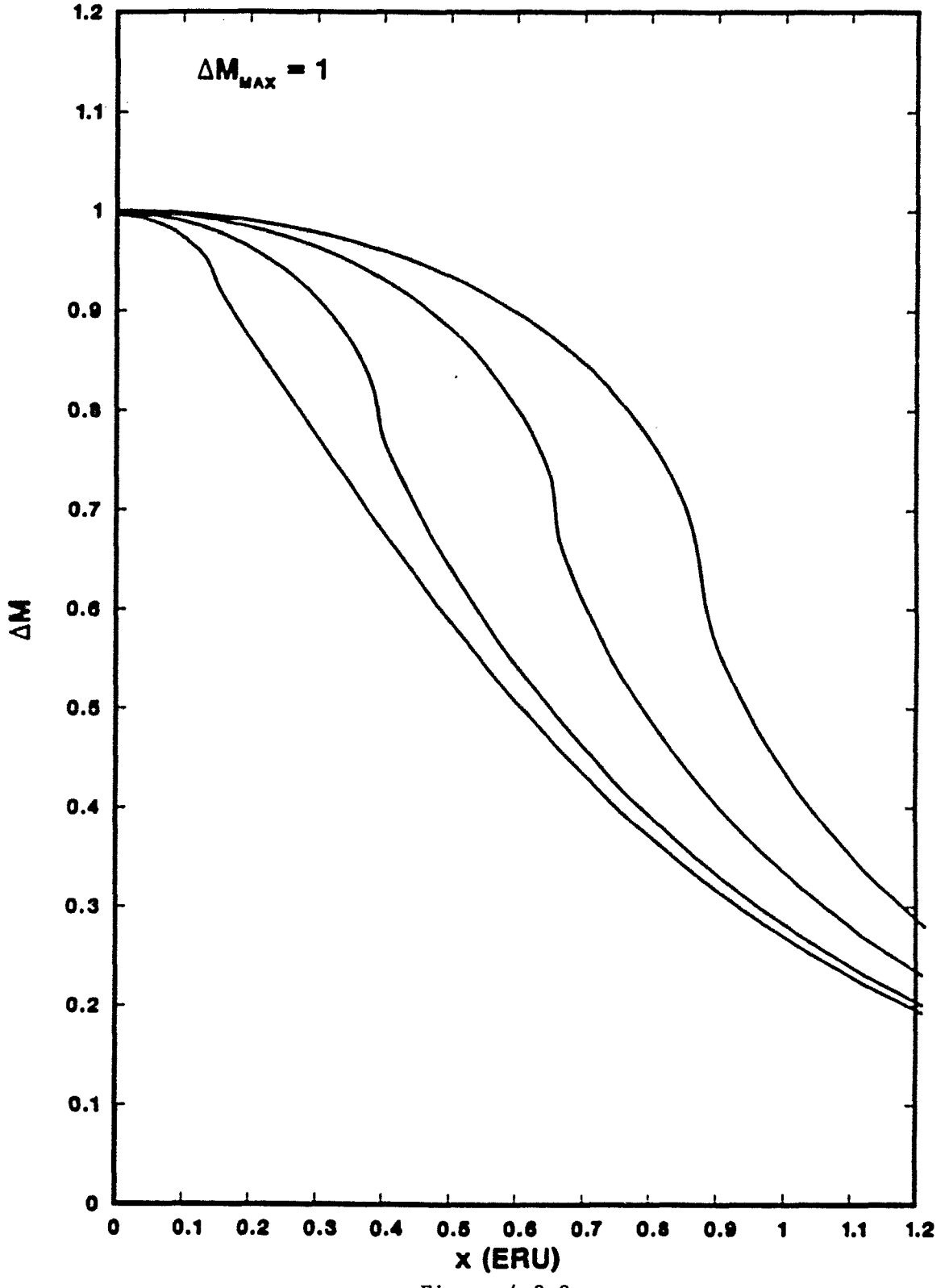

Figure 4.3.2a

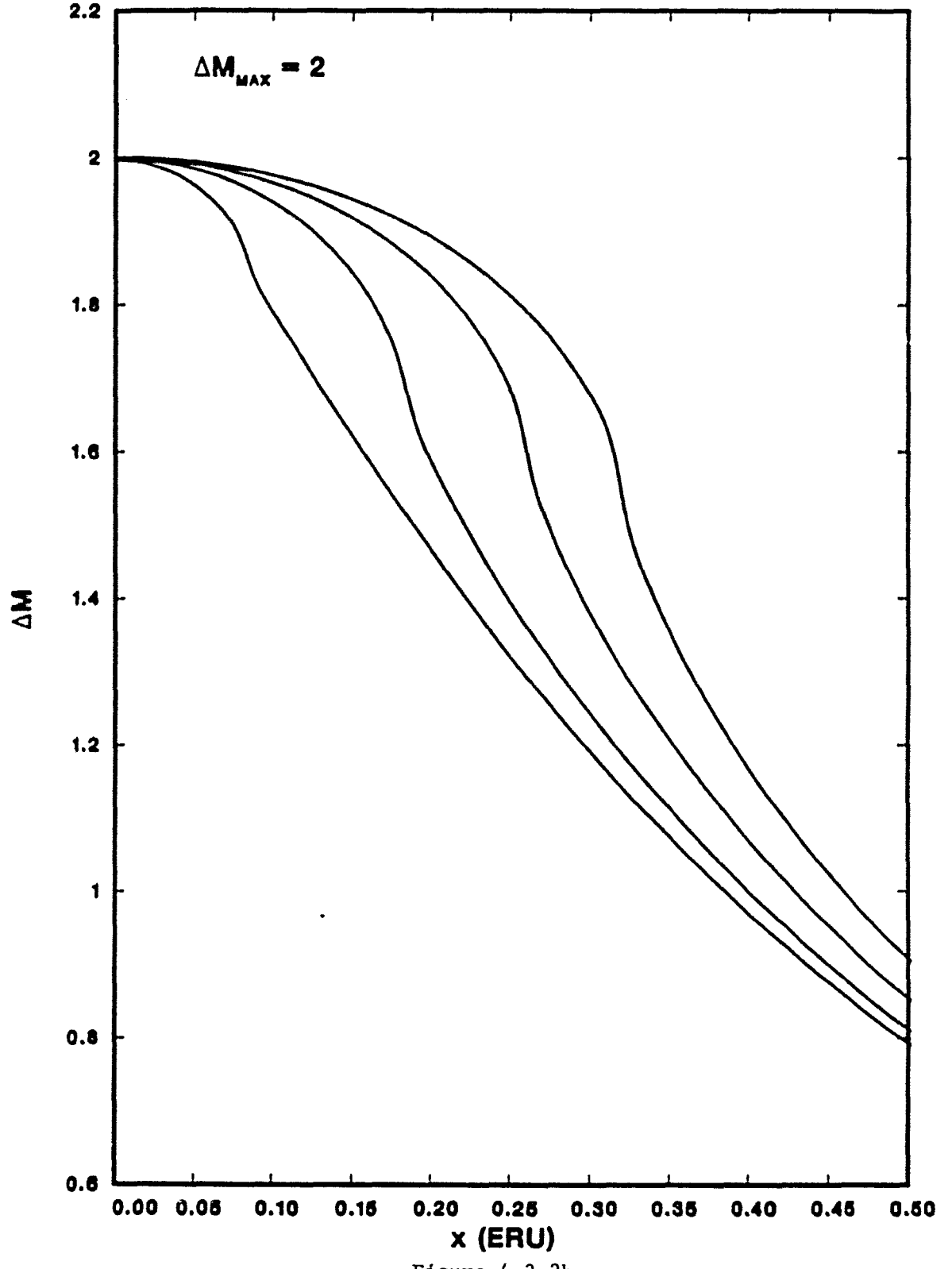
$\Delta M_{MAX} = 2$
2.2
2
1.8
1.6
1.4
1.2
1
0.8
0.6
ΔM
0.00 0.05 0.10 0.15 0.20 0.25 0.30 0.35 0.40 0.45 0.50
x (ERU)

Figure 4.3.2b

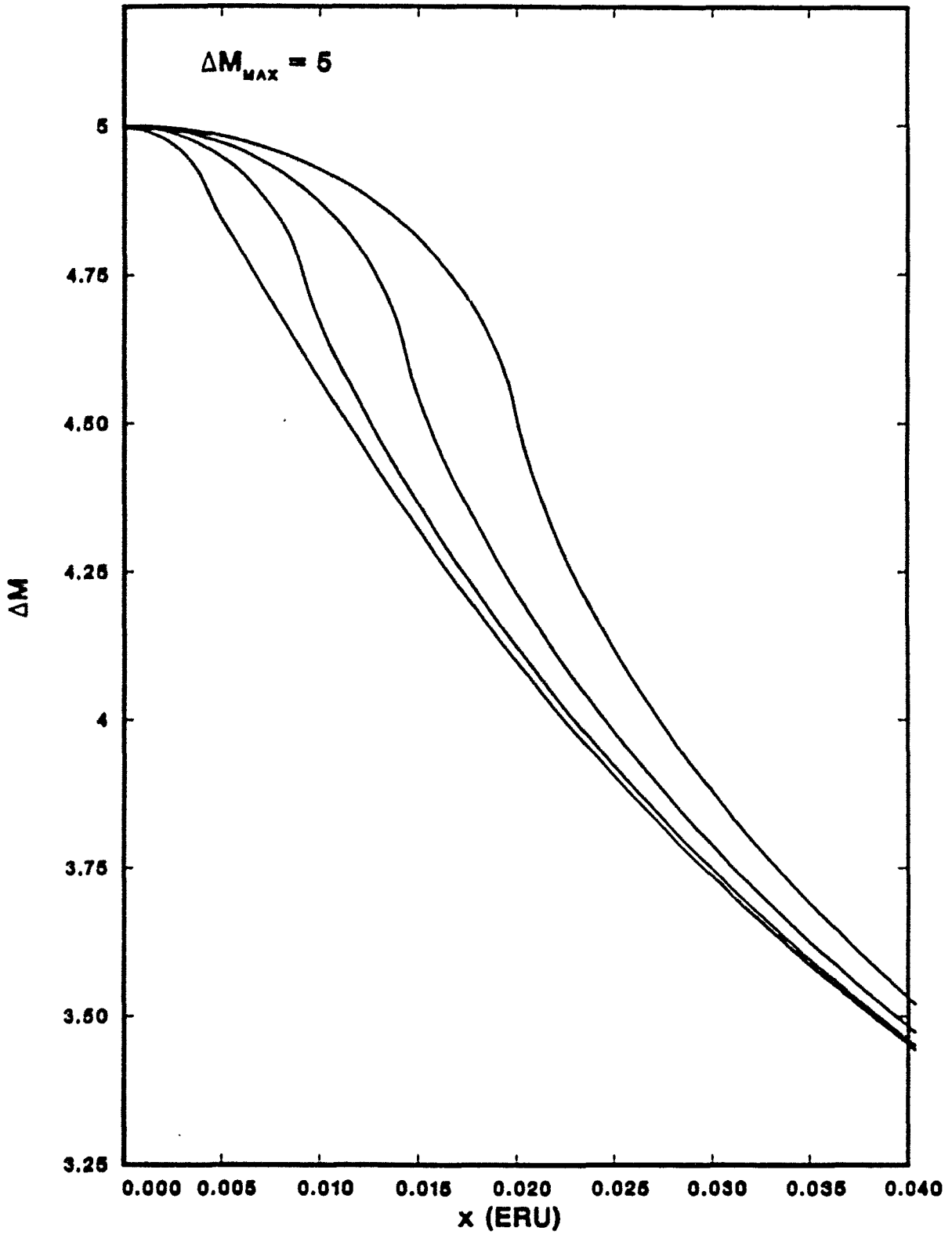
$\Delta M_{MAX} = 5$
5
4.75
4.50
4.25
4
3.75
3.50
3.25
ΔM
0.000
0.005
0.010
0.015
0.020
0.025
0.030
0.035
0.040
x (ERU)

Figure 4.3.2c

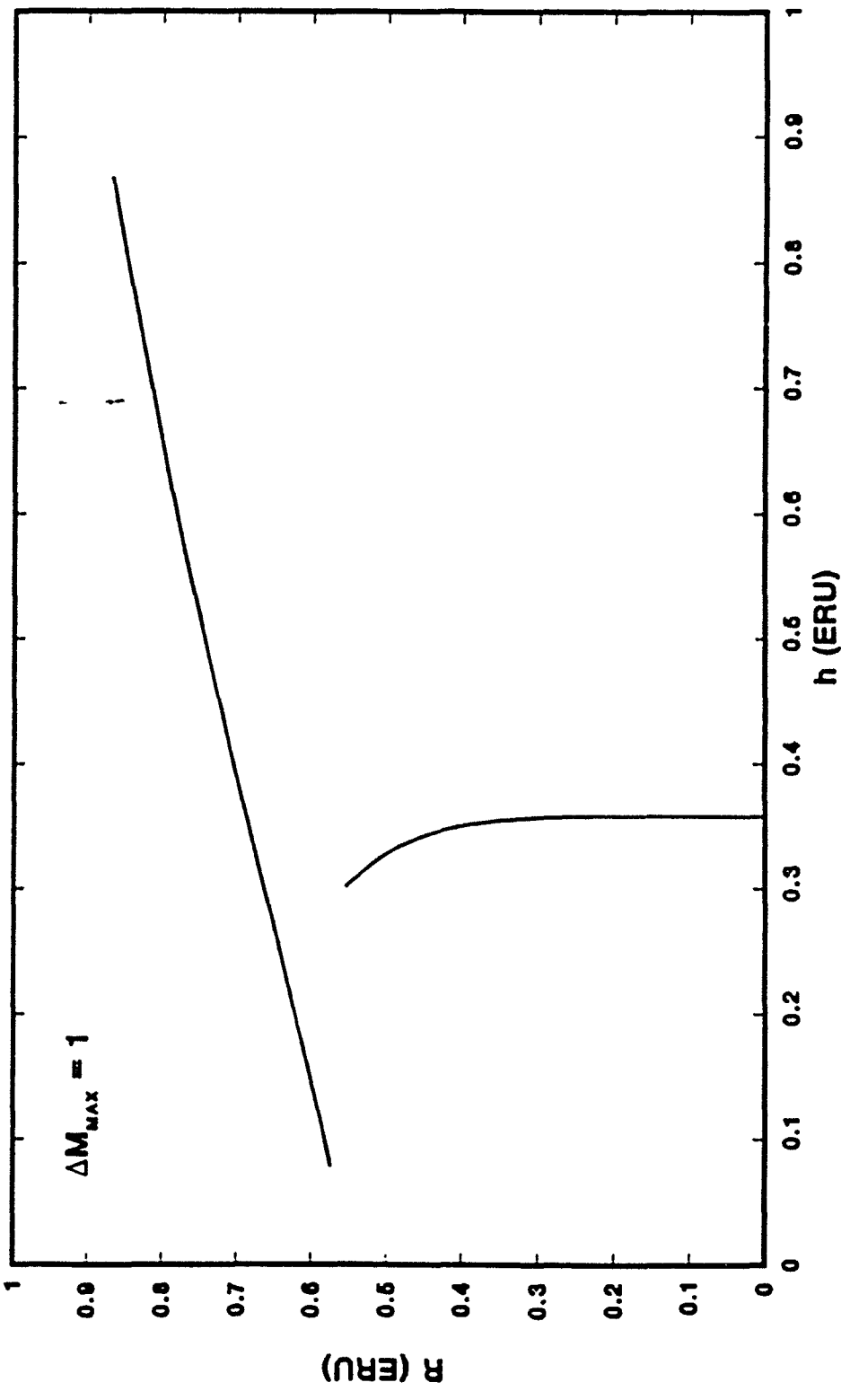

Figure 4.3.3a

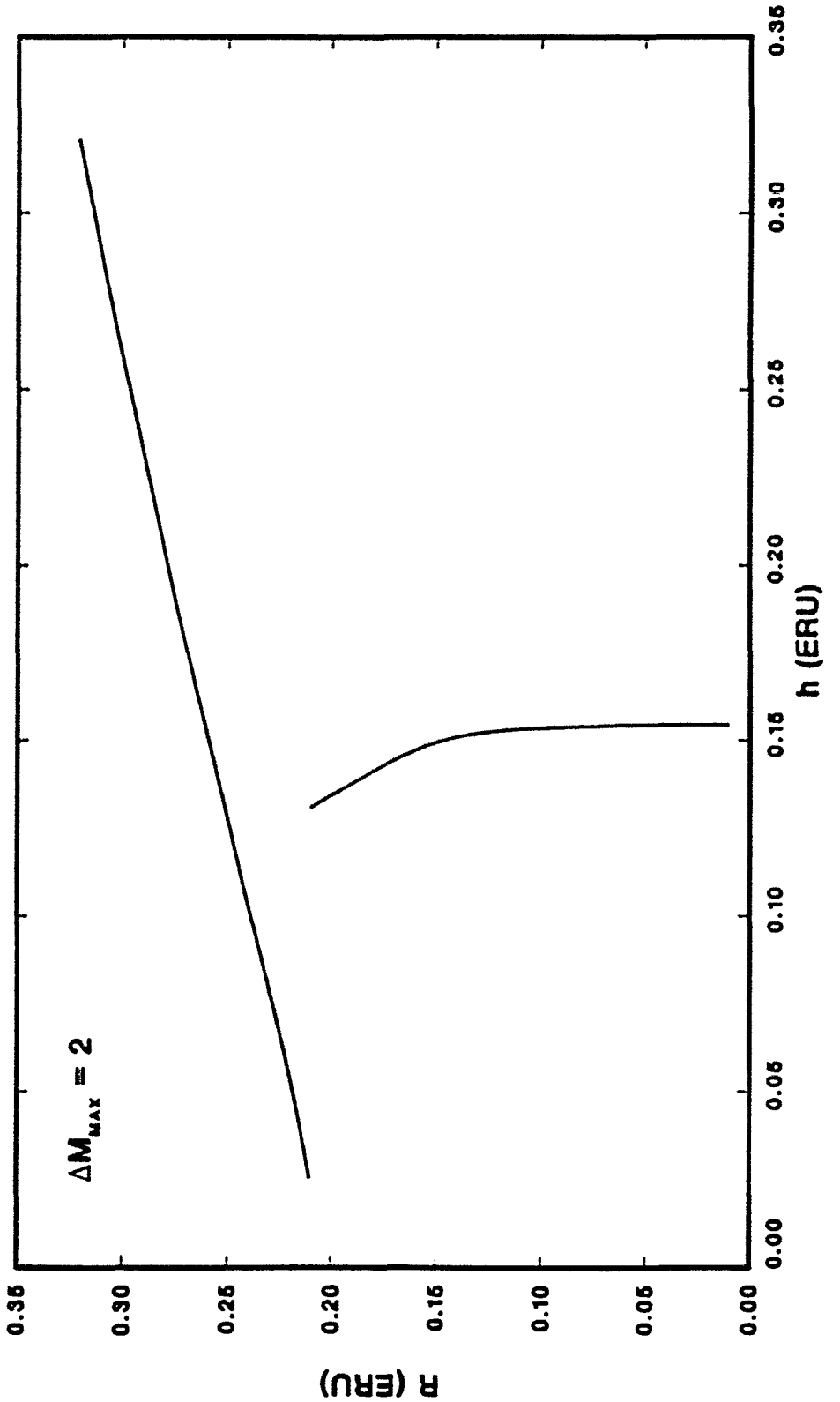

Figure 4.3.3b

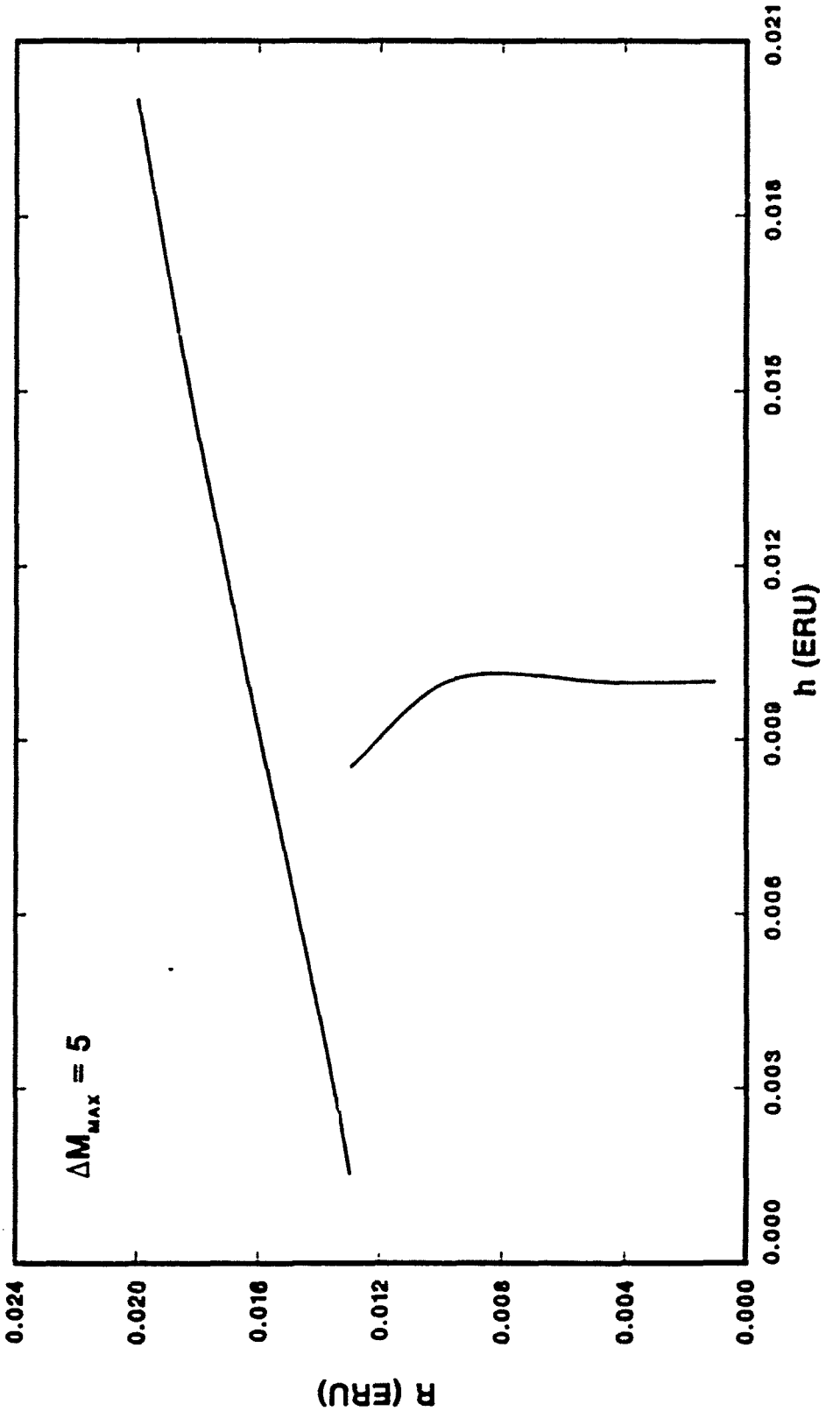
R (ERU)
0.024
0.020
0.016
0.012
0.008
0.004
0.000
0.000
0.003
0.006
0.009
0.012
0.015
0.018
0.021
h (ERU)
$\Delta M_{MAX} = 5$

Figure 4.3.3c

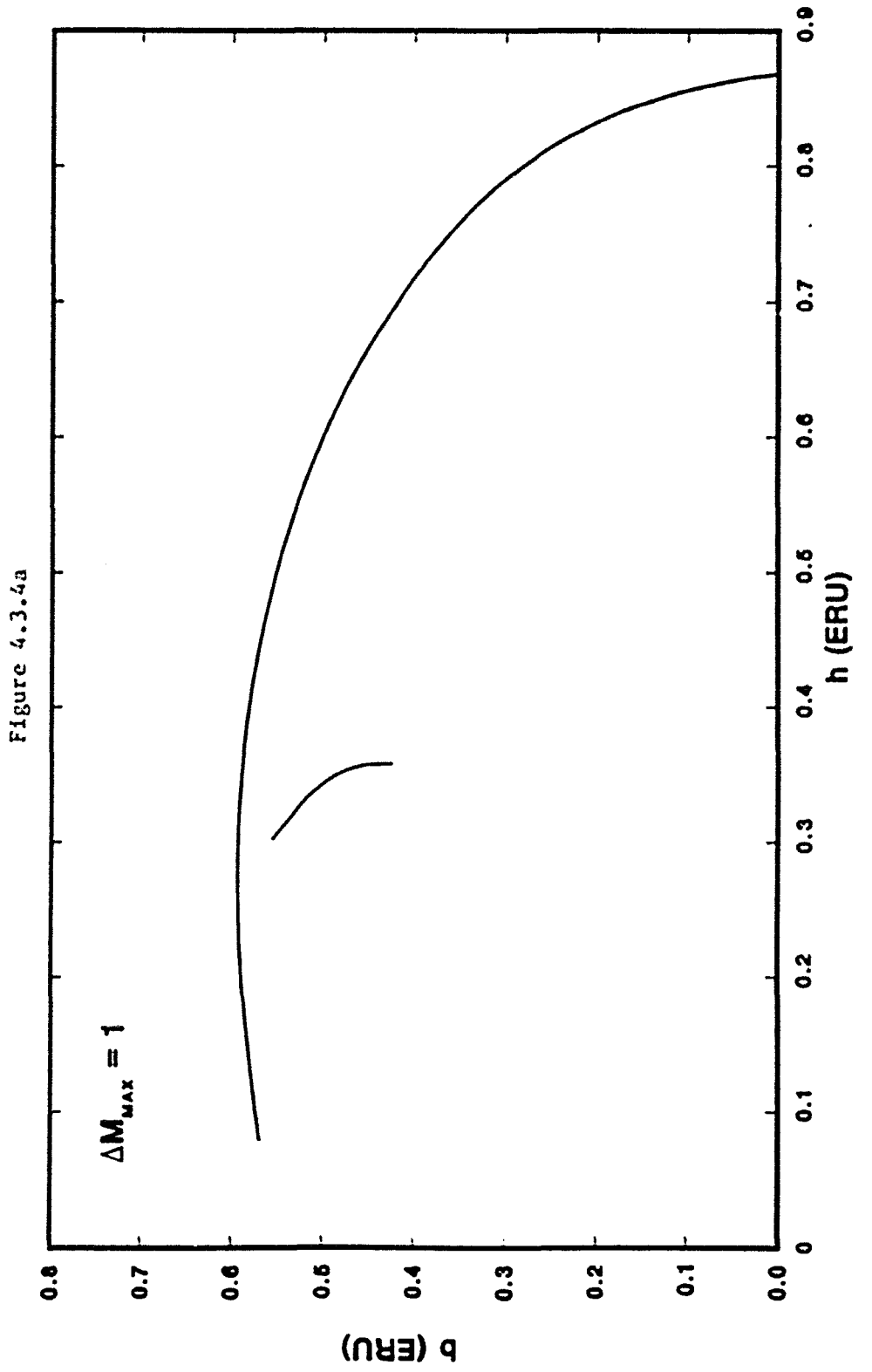

Figure 4.3.4a

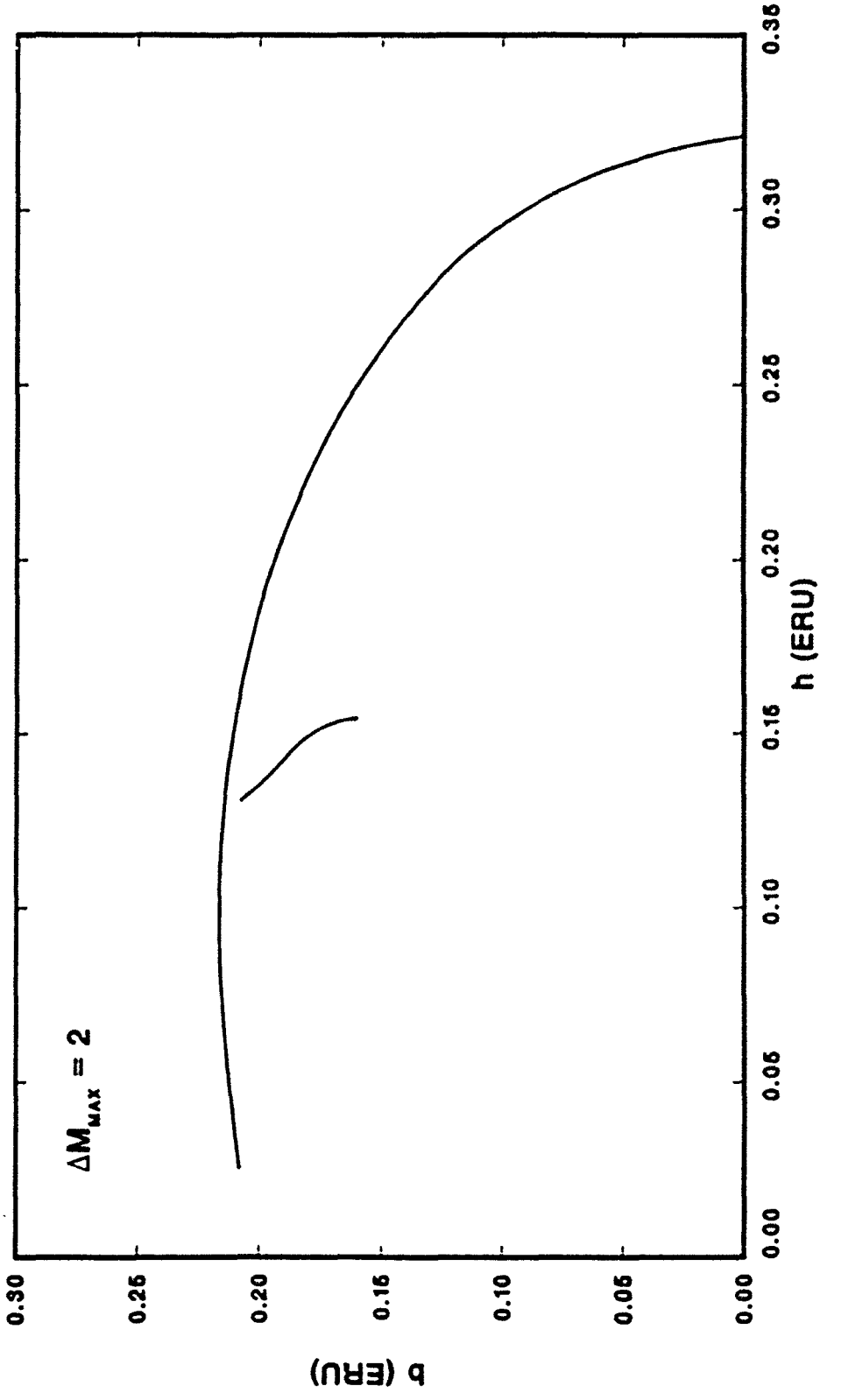
b (ERU)
0.30
0.25
0.20
0.15
0.10
0.05
0.00
h (ERU)
0.00
0.05
0.10
0.15
0.20
0.25
0.30
0.35
$\Delta M_{MAX} = 2$

Figure 4.3.4b

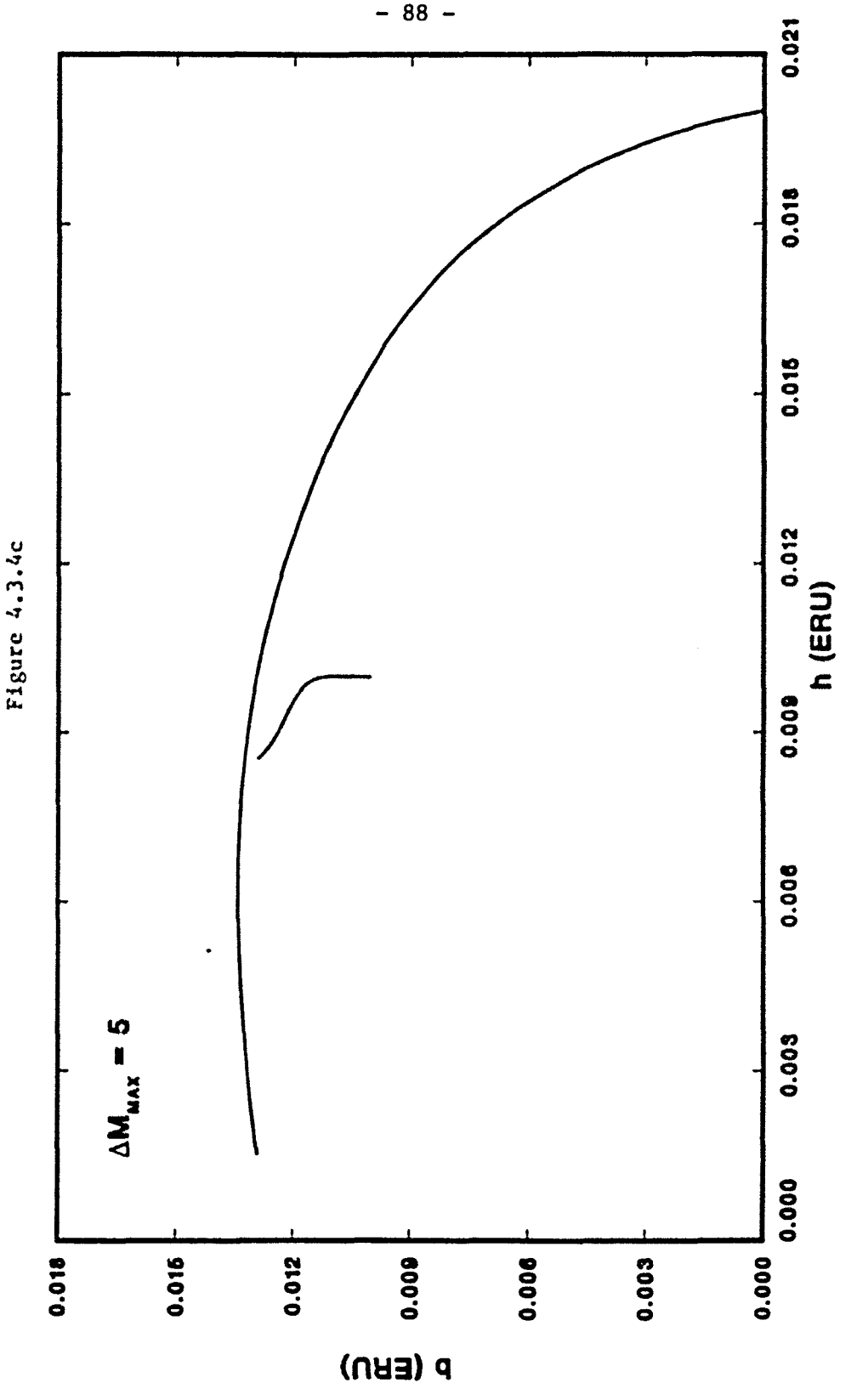
b (ERU)
0.018
0.015
0.012
0.009
0.006
0.003
0.000
h (ERU)
0.000
0.003
0.006
0.009
0.012
0.015
0.018
0.021
$\Delta M_{MAX} = 5$

Figure 4.3.4c

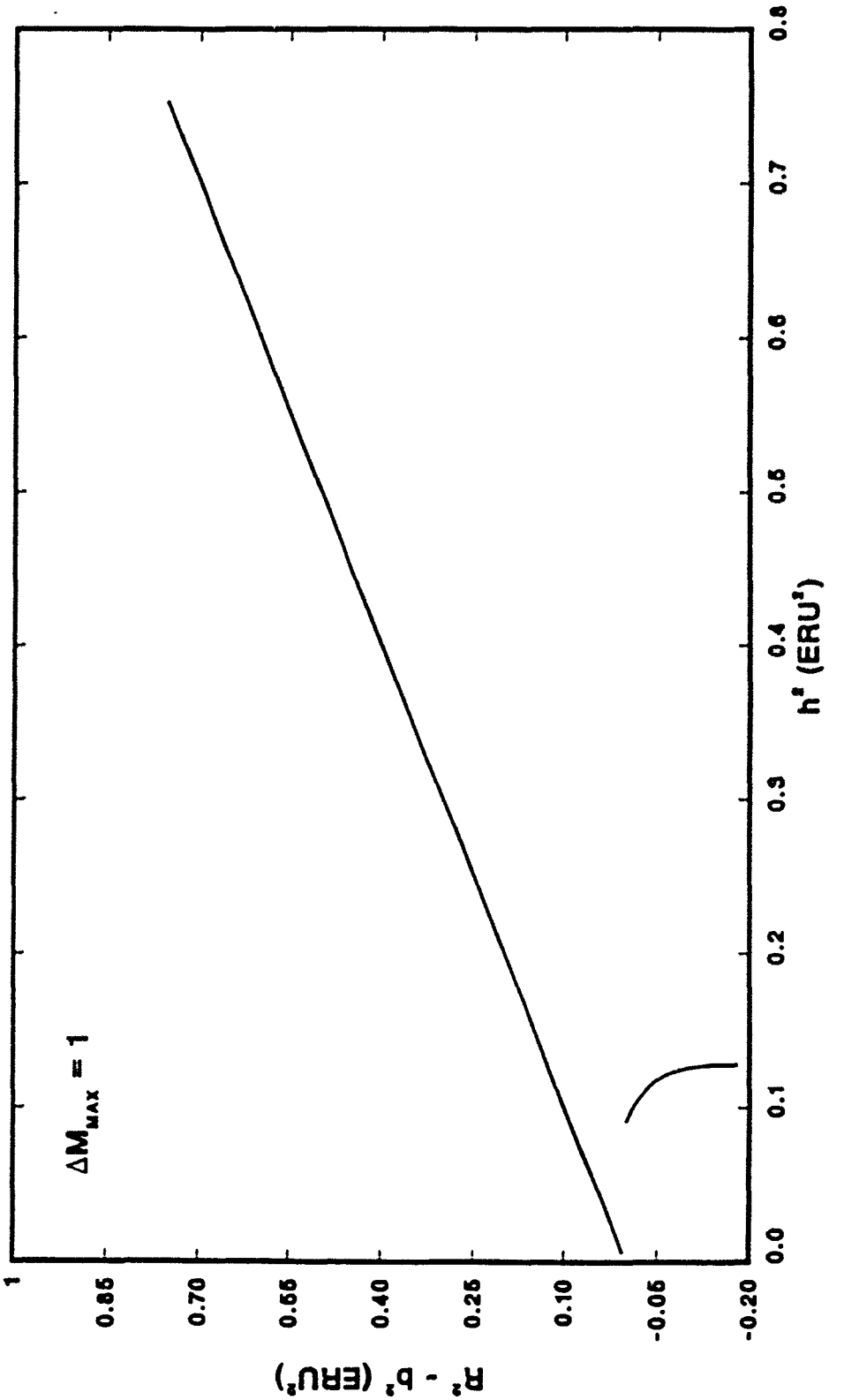
$R^2 - b^2$ (ERU^2)
1
0.85
0.70
0.55
0.40
0.25
0.10
-0.05
-0.20
$\Delta M_{MAX} = 1$
0.0
0.1
0.2
0.3
0.4
0.5
0.6
0.7
0.8
h^2 (ERU^2)

Figure 4.3.5a

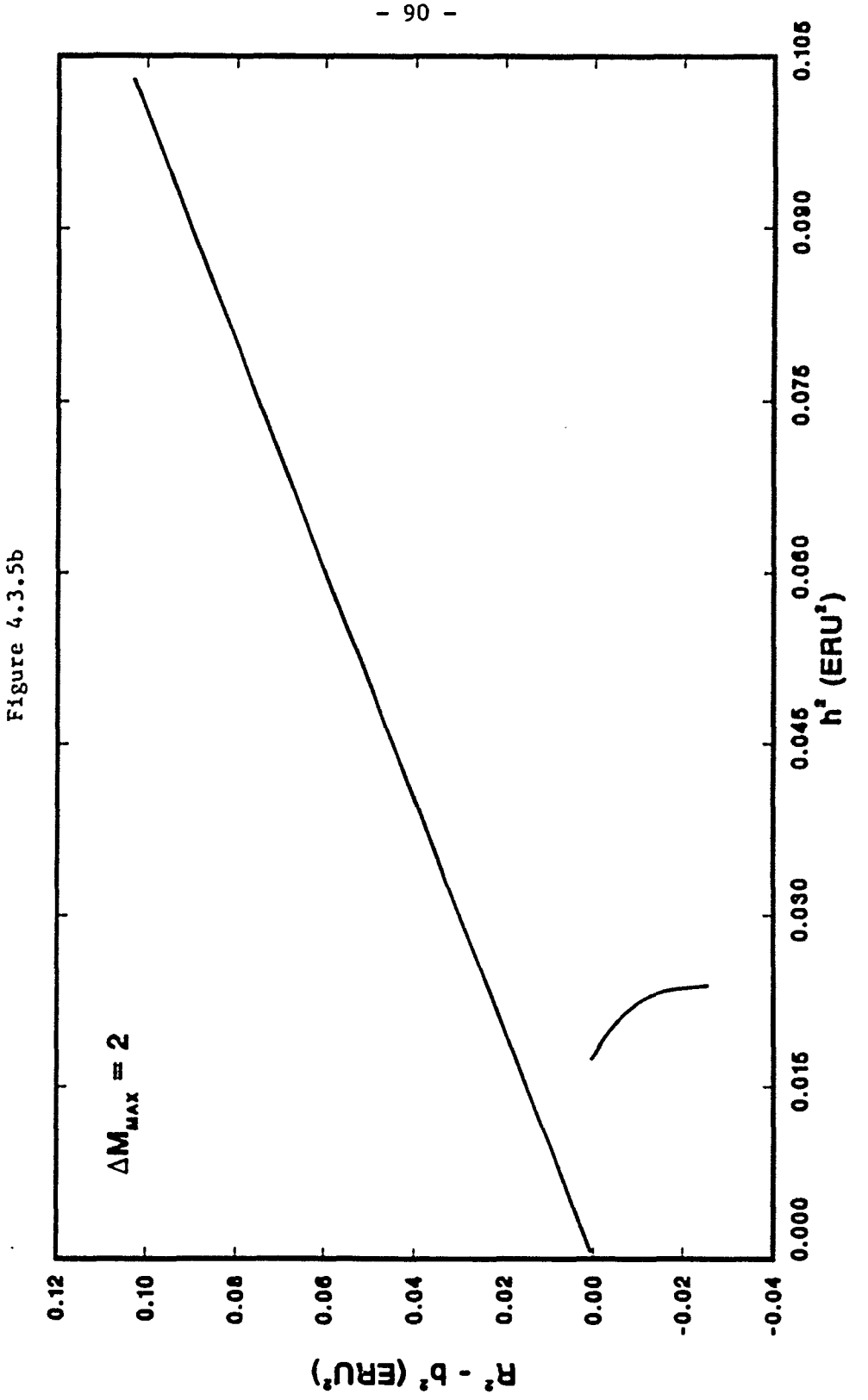
$R^2 - b^2$ (ERU^2)
0.12
0.10
0.08
0.06
0.04
0.02
0.00
-0.02
-0.04
0.000
0.015
0.030
0.045
0.060
0.075
0.090
0.105
h^2 (ERU^2)
$\Delta M_{MAX} = 2$

Figure 4.3.5b

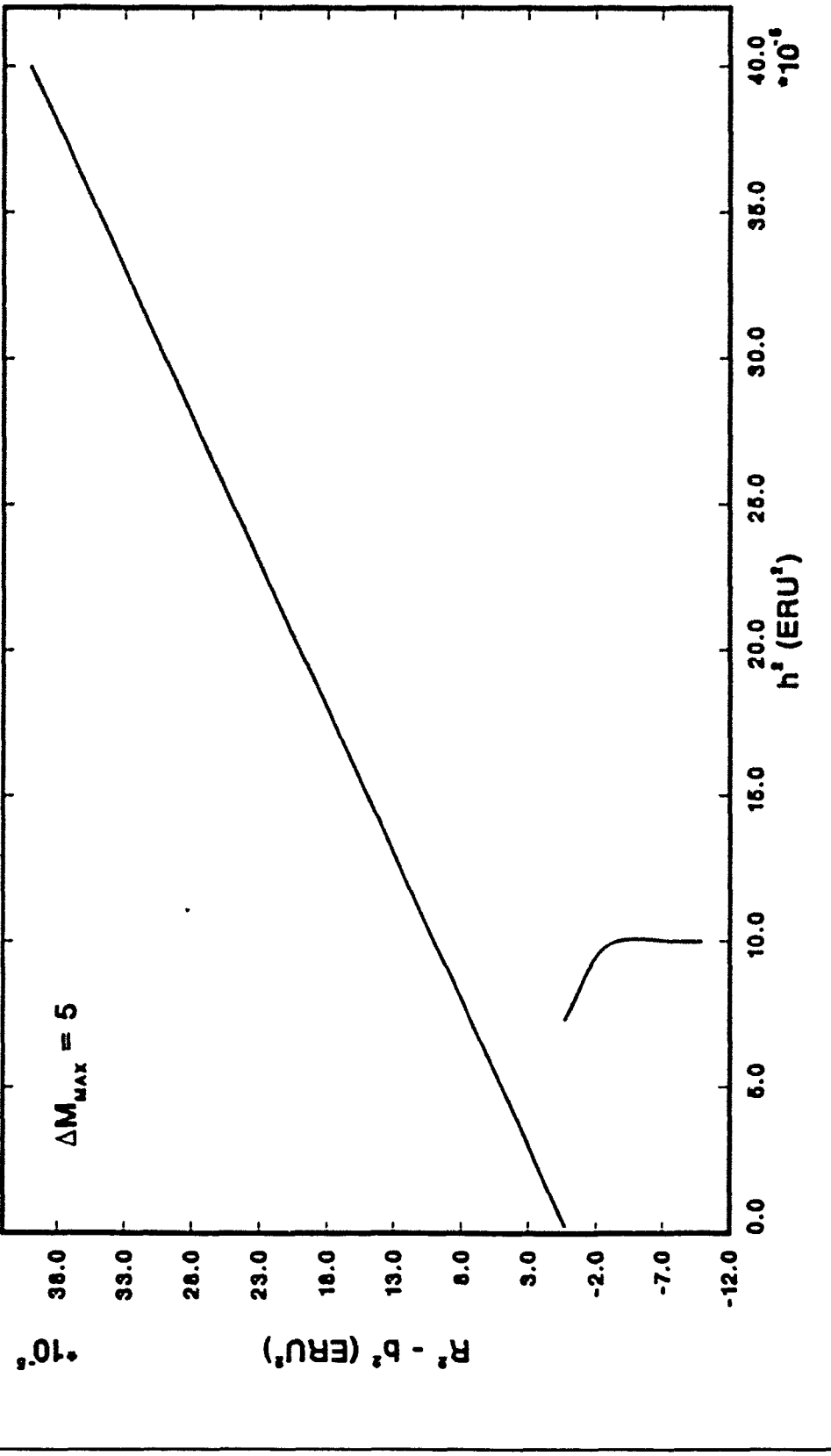
$\Delta M_{max} = 5$
$R^2 - b^2$ (ERU^2)
h^2 (ERU^2)
$\cdot 10^5$
38.0
33.0
28.0
23.0
18.0
13.0
8.0
3.0
-2.0
-7.0
-12.0
0.0
5.0
10.0
15.0
20.0
25.0
30.0
35.0
40.0

Figure 4.3.5c

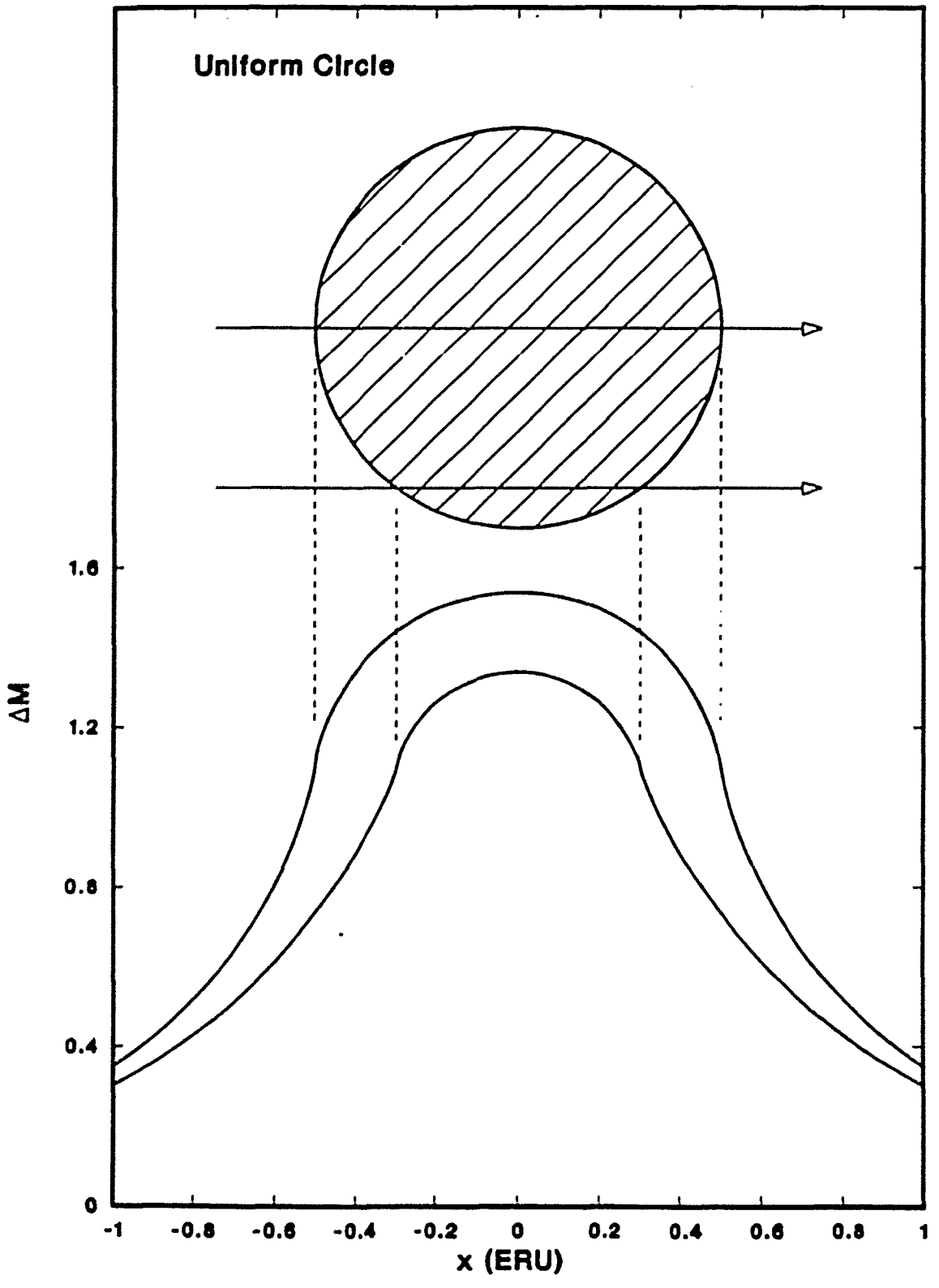

Figure 4.3.6

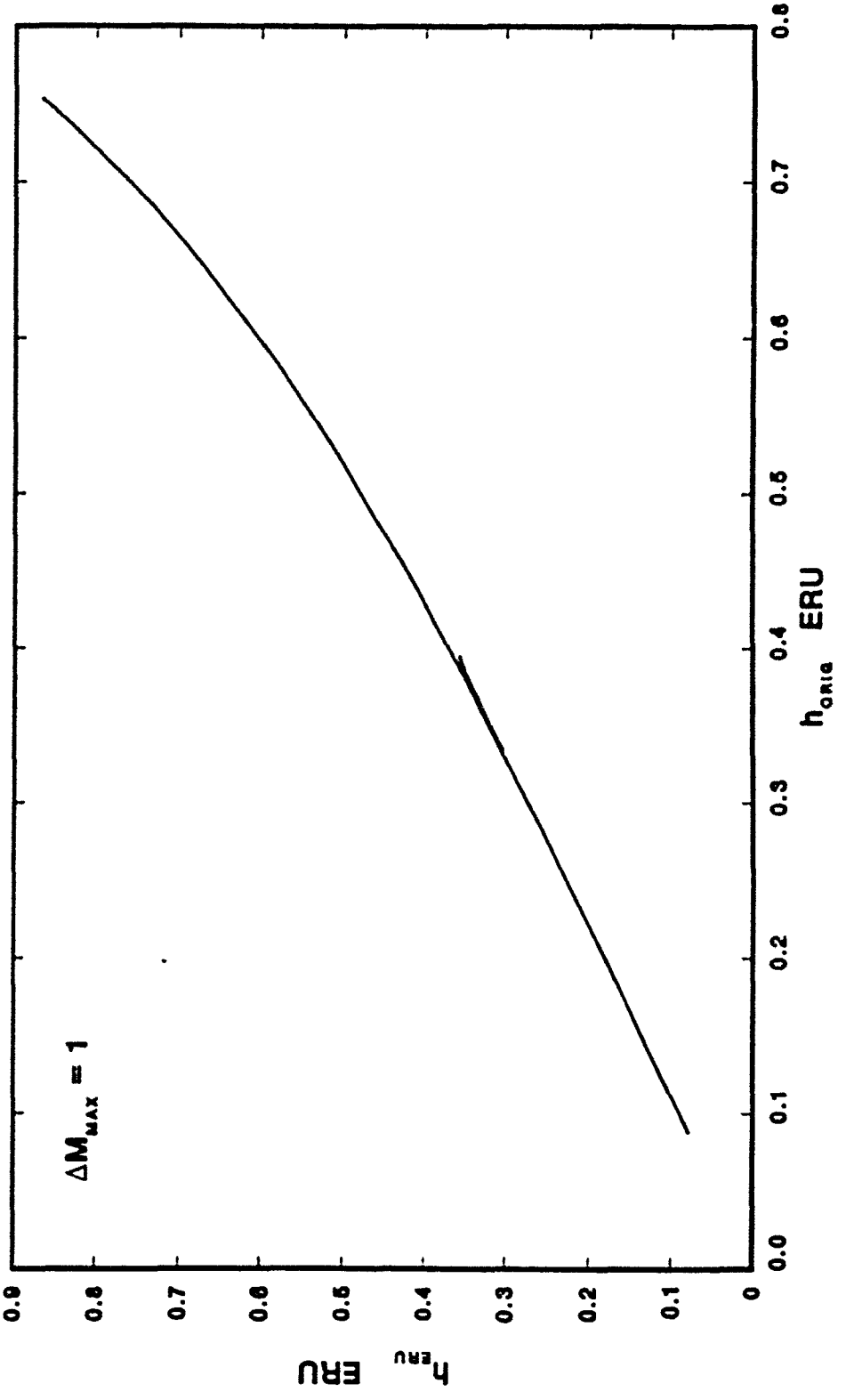

Figure 4.3.7a

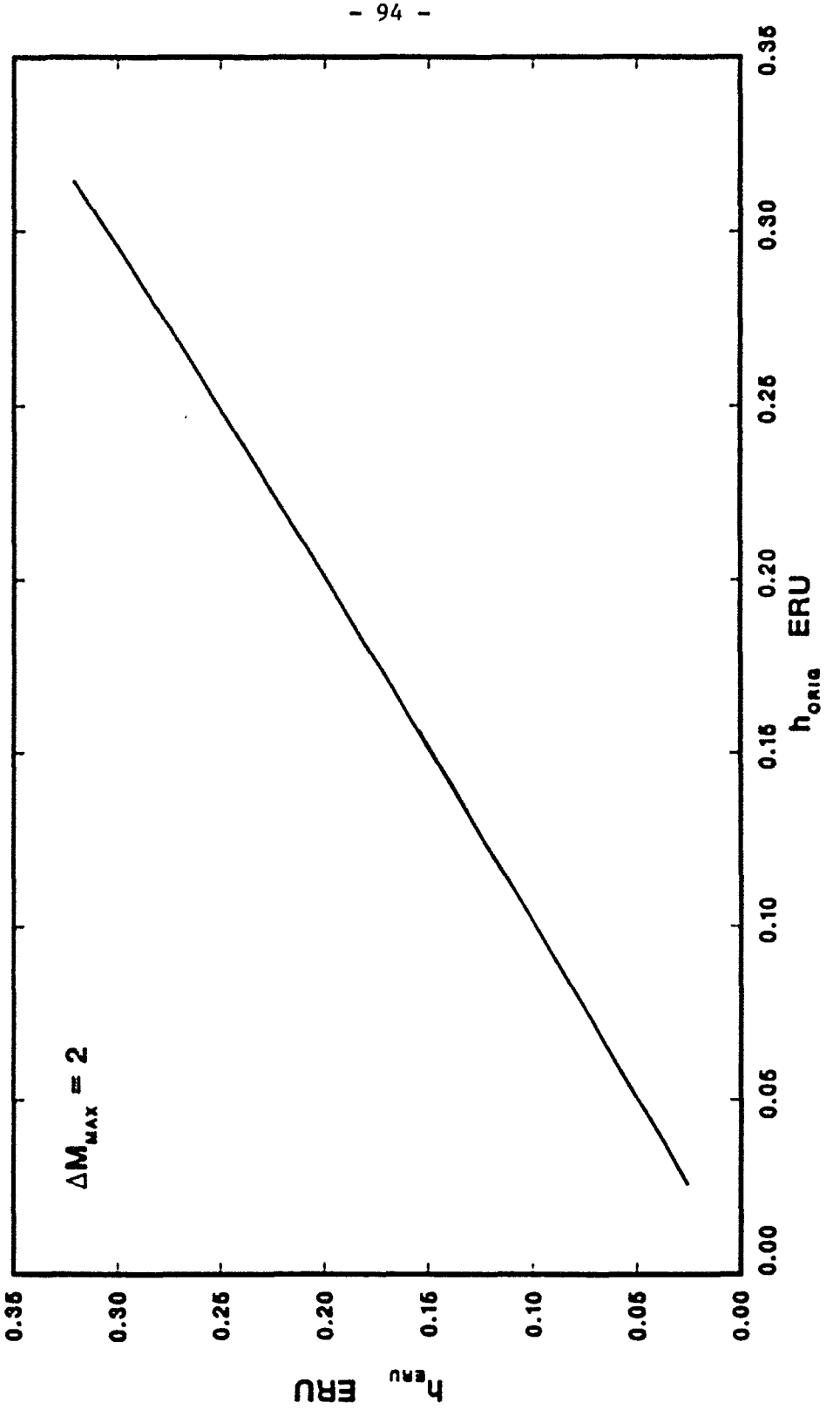

Figure 4.3.7b

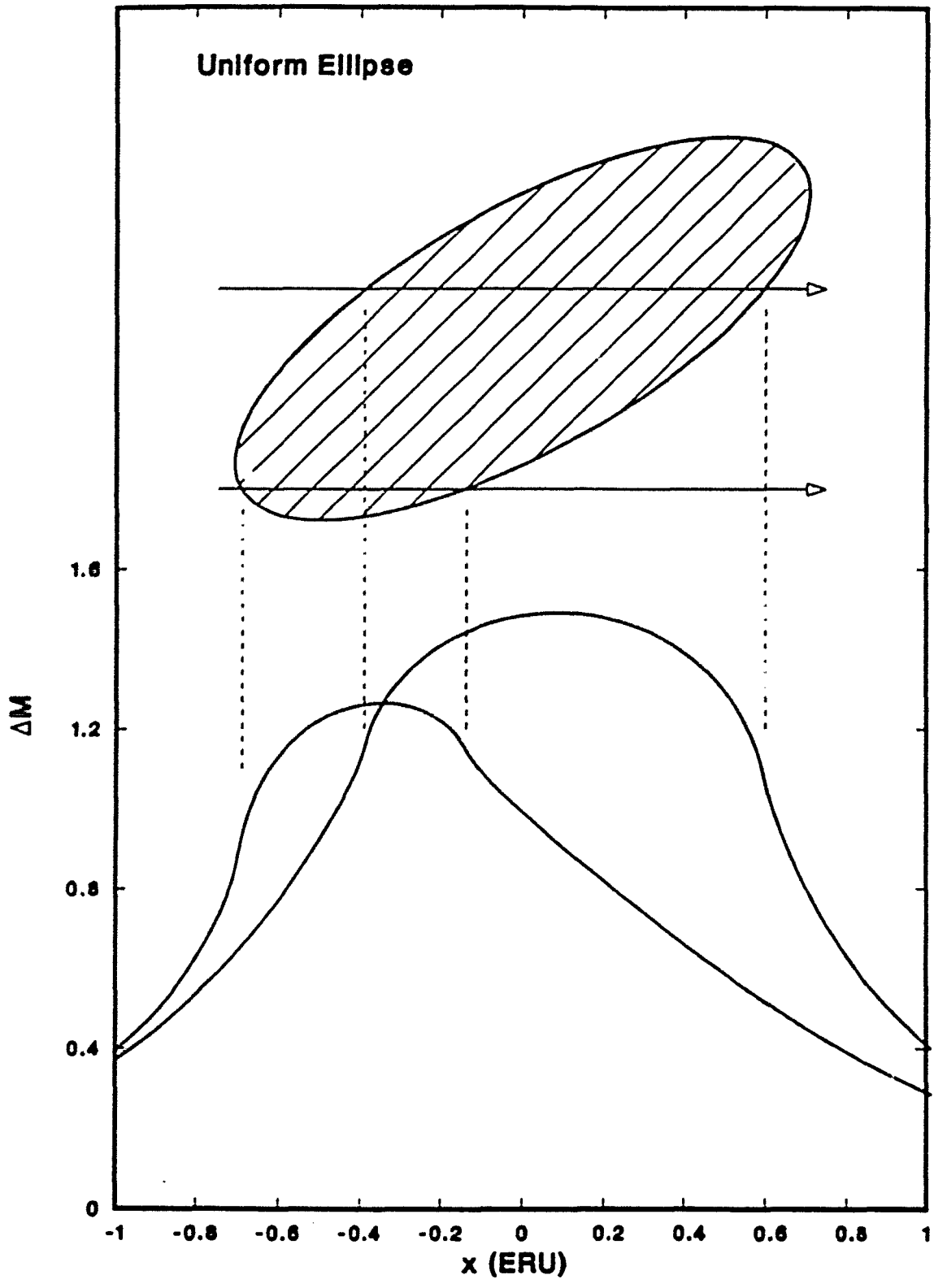

Figure 4.4.1

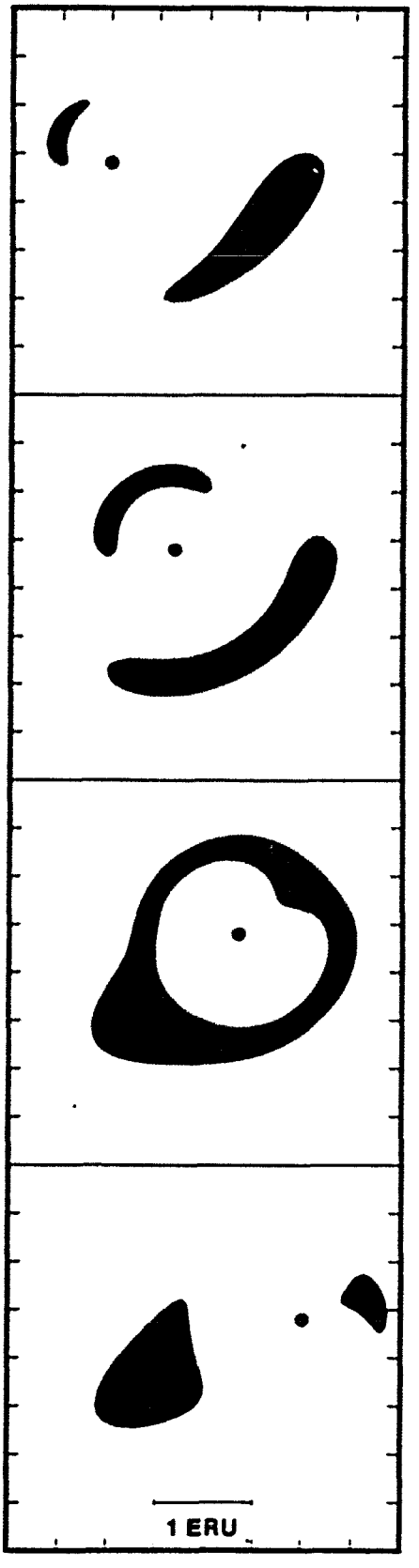

Figure 4.4.2

Chapter 5

Double Star Light Curves

5.1) Introduction

In this Chapter we will study the light curves that result from the relaxation of another of the LE requirements. Instead of a single star acting to lens a background source gravitationally, two stars will provide the effect.

In the previous chapters, we have shown that the single most likely microlensing event for most sources involves a single star as the lens. We did not include, however, the possibility of the superposition of stellar lenses, or that stars could be members of binaries, groups, or multiple systems. Although single stars are the most probable lenses to be encountered, we now consider the next most probable lens: that of two stars.

If the probability of a single star acting to amplify source light by a given amount is determined by the volume of the LE and is P, then the probability of two stars entering the same LE volume randomly is P^2. As an example we see that if the probability of lensing above some amplitude is 0.01, then the probability of this event, which involves a random superposition of two stars is 0.0001.

But the probability is significantly enhanced if one considers the incidence of binary systems. Heintz (1978) has shown that, at least in our galaxy, binaries or multiple star systems of wide separations make up a sizable fraction of the number of stellar systems, of the order of 20% or more. This fact greatly enhances the

probability of two stars entering the same LE at one time. Therefore double star light curves are not so unlikely a phenomenon, and it would be useful to know what they look like.

Studying double star light curves also serves other purposes. First, it represents the next most complicated lens after the single lens. It shows how light curve complexity can be changed by a change in the type of lens. This is in contrast to the last chapter, where we analyzed light curve changes due to a change in the source. Next, as we will see, double star light curves can provide some characteristic light curve shapes that could possibly identify the gravitational microlensing phenomenon even if single lens identifications fail.

In our study here, we will assume that all the LE conditions hold except the single lens condition. We will assume a point source, and that no other stars affect the source flux except the double system under consideration. We also assume that shear from nearby stars, galaxies, and clusters is negligible.

As before, the specific scenario we have in mind is microlensing, although the results are presented in units (ERU) which allow a generic interpretation. More specifically, two low mass stars in a nearby galaxy are thought to enter the LE of a background quasar (QSO, BL Lac, or any AGN) and significantly affect the observed flux. In the last section this formalism will also be applied to macrolensing.

Double star lensing was first studied by Barnothy (1968), who invoked it to explain the then mysterious pulsar phenomenon. Bartels (1981) derived many of

the analytical properties of the two point mass lens. Schneider and Weiss (SW 1986) have recently explored further many of the asymmetric properties of the two point mass lens. SW examined both analytical and numerical aspects of the two point mass lens acting on an extended source over a specific range of lens and source parameters. SW also calculated some light curves as an extended source underwent image creation events. They showed that the light curves for these systems were not just the simple linear addition of two single star light curves.

Section 5.2 describes the mathematical and numerical calculations involved in generating two star light curves. In section 5.3 we display typical two star light curves and discuss their features. Section 5.4 analyzes how the double star lens allows bright images to be separated by anomalously large amounts.

5.2) Fermat's Principle and Time Surfaces

The main mathematical principle used to calculate image location and intensity is Fermat's Principle: real images travel on paths for which the light travel time is a local extremum. For an example of the use of how Fermat's Principle on a more general scale, see Blandford and Narayan (1986).

If the lensing stars are considered to be confined to a plane between the observer and the source, we can assign a number to every point on the plane describing the light travel time from the source to the observer passing through the given point. If we then consider this number to be a fictitious height above the plane, we can draw a relative light travel time surface. When the surface shows a local minimum, for

example, the time it takes for light to reach the observer is at an extremum, and an image forms there. For the small, positive optical depths considered here, only minima and saddle points can occur.

Why can we consider both lenses to be in the same lens plane? In our microlensing paradigm, both stars are in the same galaxy. By Equation 1.2.1, we can calculate the focal length for a stellar lens at the radius of its ERU. We find this distance to be of the order of 1 Mpc. Since the sizes of typical galaxies are smaller than this, we see that the lens would deflect an image only a small amount (compared to its ERU) before it encounters the second star. We therefore find it a good approximation to consider the two stars to be in the same lensing plane.

Following discussions in Blandford and Narayan (1986), and Paczynski (1986a), we find that the equation for the relative light travel time near a double star lens of two equal masses is

$$\Sigma = r^2 - \ln(r_1 r_2), \tag{5.2.1}$$

where Σ is the relative light travel time, r is the projected distance in the lensing plane between the unlensed point source position (hereafter called the origin), and the point on the lensing plane at which Σ is being calculated. The quantity r_i is the distance from star i to the point on the lensing plane under consideration.

Images are formed when $\Sigma_x = \Sigma_y = 0$. Subscripts, here, denote spatial derivatives in the lensing plane. In practice, the image positions are found numerically

and the image amplitudes are found by the equation

$$A = 4 \mid \Sigma_{xx}\Sigma_{yy} - \Sigma_{xy}^2 \mid^{-1} . \qquad (5.2.2)$$

With no mass in the lensing plane, the time surface would consist simply of a paraboloid defined by the first term in Equation 5.2.1. The only critical point in this 'no mass' case is the minimum at the center. A single image at the unlensed source position would form there. The time delay surface depicting this situation is shown in Figure 5.2.1.

Stars placed in the lensing plane will distort the paraboloidal appearance of the time delay surface. This happens because photons passing close to a star suffer a general relativistic time delay (Einstein 1916). The closer a photon passes to a star, the larger the time delay. The effect of a star on the time surface is to create a logarithmic spike centered on the star's position. This can be seen by integrating the time delay along the photon path. Stellar spikes are represented by the second term(s) in Equation 5.2.1.

If we place the stars spike exactly in the middle of the paraboloid, the time delay surface displays a ring as its minimum. This situation is equivalent to placing the lens exactly collinear with the observer and the source. The ring that appears corresponds to the previously defined Einstein ring. The situation is depicted in Figure 5.2.2.

If, however, we place the stellar spike off center, the minimum is no longer a ring, but a single low point in the lensing plane. But now another point also occupies

a critical location: the saddle point on the far side of the logarithmic spike from the minimum. These two critical points represent the two images one would see if a point lens was placed off the axis connecting the observer to the source. This situation is shown in Figure 5.2.3.

In general, when a single lens acts, two images appear. One will always be a minimum point, and should correspond most closely to the original source image. As the lens is moved further from the optic axis, this minimum will move closer to the original source position, and the situation at the center will more closely resemble that shown in Figure 5.2.1.

If we now place a double star in the lensing plane, the time sheet displays two logarithmic spikes. If the lenses are close together, the two spikes appear side by side, as seen in Figure 5.2.4.

Typical double star lenses give three images. The particular three image scenario depicted in Figure 5.2.4 is somewhat reminiscent of the single star scenario of Figure 5.2.3. Two of the images correspond directly to the former geometry: the minimum at the bottom, and the saddle point opposite the minimum on the far side of the stellar spikes. A third image now becomes apparent, however. This image is between the stellar spikes, and is also a saddle point. This general image-lens geometry, consisting of a minimum, a saddle point between two stars, and a saddle point behind the combined spike of the two stars, will be referred to as configuration A.

Another three image geometry is possible. Each lens could have an individual saddle point behind it, opposite the minimum near the center of the time sheet. This general lens-image configuration is shown in Figure 5.2.5 and will be referred to as configuration B.

Only one distinct five-image geometry can occur. This is depicted in Figure 5.2.6. Here the two lenses are on opposite sides of the origin. Note that there are two minima and three saddle points. This arrangement will be called configuration C.

5.3) Light Curve Signatures

The most dramatic differences between double star light curves and single star ones occur when the two stars are separated by a distance of the order of an ERU. Here the ERU refers to that of the combined mass of the double star lens. If the two stars are much closer than an ERU, such as their separation being ERU/10 or less, they typically affect the source as would a single star of combined mass. The resulting light curve is usually identical to those in Figure 4.3.1.

If the two stars were separated by several ERU, 2 ERU or more, they affect the light curve mostly individually. Typical light curves resemble the linear addition of two light curves in Figure 4.3.1.

Light curves were generated by a Monte Carlo technique in which the position, mass, and direction of motion were randomly chosen for each star in the lensing plane. The mass of each star in the binary was chosen, with uniform distribution,

randomly between zero and one, and their sum was normalized to one ERU.

Each star was placed randomly within a circle of one ERU radius of the point source at the center. The positions were chosen in a uniform fashion, and no preference was given for placements in relative proximity to the source or the other star.

For some of the simulations, the stars were taken to be a bound system traversing the field of the source, while for other simulations each star was given the same magnitude of velocity but a random direction in the lensing plane. The bound systems always moved in a given (yet arbitrary) direction and at a given (yet normalizable) transverse speed.

In the unbound systems, each star moved in a uniformly random transverse direction. Each star also moved with a random velocity. Each velocity was chosen uniformly between zero and one, and was normalized to a given value after the simulation was complete.

After the selection of the initial parameters of the system, time was run-off in the simulation until the center of mass was one ERU from the origin. The simulation was then run 'in reverse' until the center of mass of the system was one ERU from the center. Since gravitational lensing light curves are time-symmetric, time running forward or backward is only a relative effect and has no entropic interpretation. The lenses were then allowed to move again until the center of mass was again one ERU from the origin.

We have set the time base of the light curves to 50 years, but this time can be reset by the analysis in Chapters 2 and 3. The time base derives from a combined-mass lens of one solar mass at a distance of $5x10^8$ pc moving transversely at 500 km/sec in front of a point source at 10^9 pc.

The light curves presented in Figure 5.3.1 are typical of all the light curves generated. Since the Monte Carlo technique was not expected to sample a realistic pool of double star possibilities, the approximate statistics listed are not to be taken too seriously. We hope to obtain an idea of the kinds of light curves which are possible and typical in double star lensing, and what are not.

Inspection of Figure 5.3.1 shows that double star light curves can be surprisingly complex when compared to the simple linear addition of two single star light curves. Figure 5.3.1a shows a typical light curve, which is, however, practically identical to a single star light curve. Roughly 35% of the light curves generated were of this character. This type of light curve has a single, symmetric peak, and occurs when the stars are too close to affect the source flux individually. Light curves such as Figure 5.3.1a sustain a single configuration, either A or B, for the duration of the graph shown.

Figure 5.3.1b is another typical light curve from a double star event. No images were created or annihilated during this event, yet the slopes on the sides of the peak are asymmetrical, both close to the peak and far from it. Light curves such as these depict an image configuration that would, typically, start in configuration

B, change to configuration A, and then return to configuration B again. From this type of curve we learn that one cannot rule out microlensing for single peaks solely from a lack of symmetry of the light curve.

Figure 5.3.1c shows another typical light curve. Again, there were no image creation-annihilation events. Each peak was usually *not* caused by each star individually moving closest to the source in turn, but rather by both stars acting together in a more complex way. Light curves like those in Figures 5.3.1b and 5.3.1c, also comprised about 35% of those seen in the simulations. Here, as before, the typical image configuration through this event moves from an initial configuration of B to A, and then returns to B again.

Double star light curves can exhibit numerous peaks. These additional peaks occur when a pair of images is created or destroyed. As there can be only 3 or 5 images, images are created and destroyed in pairs. In the language of other authors (SW, for example), image number changes when the source has crossed a 'critical line'. As the star placements change, the critical lines move about, themselves being created and destroyed. We therefore feel it is clearer not to keep track of critical lines, but rather to concentrate on the number and configurations of images. We noted that at no time did an image ever change from a saddle point to a minimum or vice-versa.

The unusual hump in Figure 5.3.1d is a single image creation- annihilation event. This is the most common light curve we found which involves image creation. For

a brief period there were 5 microimages of the source instead of 3. The image geometry started in configuration B, then became configuration C, then went back to B again. Figure 5.3.1e is a similar curve demonstrating that an additional peak can occur during the creation-annihilation interval. Light curves with a single image creation event occurred roughly 25% of the time.

Light curves such as shown in Figure 5.3.1f, although somewhat rare, are typical of two image creation events. These type light curves were found only about 5% of the time. Here the images started in configuration B and the first image creation event changed the images into configuration C. Two images then annihilated causing configuration A. Later two images were created again in configuration C and two images then annihilated to restore the initial configuration B. In short, this was a BCACB event.

Figure 5.3.1g was one of the few curves (out of hundreds generated) wherein 3 separate image creation-annihilation episodes were found. The amazing complexity and novelty of the curve commended its inclusion here. Light curves this complex were found less that 1% of the time. Such a curve is not likely to be seen, but demonstrates the range of the complexity which the double star lens can generate. A scenario that would generate such a curve is BCACACB.

There are several interesting features about the image movements. Most of these features are generic to lensing near critical lines and are reviewed elsewhere (see, for example, Bourassa and Kantowski 1975, Hogan and Narayan 1984). When

images are near each other, as when two of them are created or annihilated together, they appear relatively bright, usually dominating the light of all the other images combined. Images created together are *not* annihilated together. Either one of the created images will merge with another previously existing image, or two previously existing images will merge.

The maximum lensing amplitude is dependent on the angular size of the source. As shown in Peacock (1982), Nityananda and Ostriker (1984), and Chang (1984), the maximum lensing amplitude is inversely related to the source size. The effect of considering extended sources is that the height and sharpness of the peaks of the light curves in Figure 5.3.1 will be diminished, and the events of fastest amplitude change spread out in time (SW).

Two-point mass lensing is not the only way to create complicated light curves. Chang and Refsdal (1979) have shown that complicated light curves can be generated by a single star and a non-negligible shear term. Alternatively, Paczynski (1986a) has shown that complicated light curves may be expected at high optical depth of single stars. Kayser, Refsdal, and Stabell (1986) have shown that one can expect complicated structures for various couplings of shear, optical depth, and source size. Each of these scenarios has its own light curve signatures.

We consider an important aspect of the light curves in Figure 5.3.1 to be that they are prototypical signatures of microlensing. The features of these light curves might be easier to distinguish from those due to intrinsic quasar luminosity changes

than would be possible for the single star case (see Chapter 7 for discussion of this point).

5.4) Large Separation Image Geometries

An interesting gravitational lens effect came to light during the development of the foregoing simulations. It involved the transition from configuration A to B (and also from B to A). When the lenses were far from the origin, the images usually situated themselves in configuration B. But sometimes they would leave (enter) the field of the origin in configuration A. We therefore found that sometimes, when the lenses were close together and moving together, that the transition from A to B would occur far from the origin. A transition from A to B is usually accompanied by an increase in lensing amplitude, or at least a drop off slower than would be expected if either configuration held throughout the event. Many times a transition from A to B is also accompanied by an image creation event such as ACB.

A common assumption in gravitational lensing is that images of comparable brightnesses can occur only when a single lens is close to the origin. The two bright images then created would be separated by very nearly 2 ERU. But now we find that a double lens can create images of comparable brightnesses with image separation much greater than 2 ERU. The separation of the images is theoretically unlimited. We will refer to this situation as 'lensing outside the Einstein ring.'

One effect that derives from lensing outside the Einstein ring is that image separation can now be somewhat divorced from the mass of the lens. This can

allow large image separations to be created by lenses of lesser mass. This may turn out to be relevant, not only in our microlensing paradigm, but in a macrolensing one as well.

The statistical probability of lensing outside the Einstein ring is actually very small, the more distant the separation of the images, the smaller is the probability. The configuration of the lenses has to be nearly exact. It is not the purpose of this section, however, to estimate this probability, as it depends critically on the number density of objects, their tendency to congregate in pairs, and the strength of the selection bias favoring distant images. We merely wish to show that these effects are possible and to predict observational consequences of such a scenario.

For a single point lens, we always have two images. If we reduce the angular separation of the lens from the unlensed source position to a fraction of an ERU, we get two images of comparable brightness. As we now move the lens far from the origin, we get two images of increasingly different brightness. The magnitude difference between the images is shown as a function of image separation by the upper curve in Figure 5.4.1. One image is the relatively undistorted quasar image (hereafter referred to as the 'original' source image), while the other is seen closer to the lens, but on the far side of the original image (hereafter referred to as the 'far' image). The situation is as described in the previous section and is shown graphically in Figure 5.2.3.

If we have a double lens, we typically get three images instead of two. Assume

the lens to start close to the origin in configuration A. If we now increase the angular separation from the lens to the origin, we again begin to find a situation quite similar to the one point mass lens case: one image is near the origin and is relatively unaffected by the lens, while now the combined brightness of the images in configuration A have approximately the same brightness as the far image in the single lens case.

At a certain distance, however, unlike the single lens case, and only for specific arrangements of the two masses, the far image conglomeration will become anomalously bright. This is shown by the lower, more complicated curve in Figure 5.4.1. This may cause the set of images far from the original image to be of magnitude comparable to or brighter than the original image.

The far images, near the lensing masses, can never consist of only a single image (in the absence of strong, superimposed, high- shear, microlensing effects; Chang and Refsdal 1984). On the contrary, sufficient resolution of this region should show two or four images, with mean separation of the same order as the separation of the double lens. All images in this close image group would be on the opposite side of the lensing masses (if the lenses are visible) from the original image. The magnitude difference between and among these two or four images may, however, be very great, and it depends on the exact angular placement of the lens and the source.

These results were generated numerically and found to be consistent with the

analytical treatment of SW. This effect is strongly influenced by the angular size of the source. If the source size became of the order of the lens separation or larger, we would not expect strong amplifications, thus negating the effect.

One macrolensing system in which this effect might prove to be important is the unusual candidate gravitational lens system Hazard 1146+111 B,C. Paczynski (1986b) suggested that this system, with candidate images separated by 157 arcseconds, is created by a massive black hole lens of the order of $10^{15}\ M_{\odot}$. Recent observations have failed to confirm this hypothesis (Lawrence, Readhead, and Moffet 1986), and there is now some doubt that this system can be explained by gravitational lensing.

With the double star effect, however, the mass of the lens can be reduced to the range of $10^{8} - 10^{12}\ M_{\odot}$. The double lens makes some predictions that can be tested. One of the images of Hazard 1146+111 B, C must be multiple: consisting of either two or four images with separation(s) of the order of 0.001 arcsecond. All of these images would be on the same side of the lens, and on the opposite side of the lens from the original quasar image. One of the images would *not* be expected to show extended structure, as the double lens would image only small regions.

References

Barnothy, J. M. 1968, *A. J.* **73**, S164.

Bartels, G. G. 1981, Thesis, Hamburg University.

Blandford, R., and Narayan, R. 1986, *Ap. J.* **310**, 568.

Bourassa, R. R., and Kantowski, R. 1975, *Ap. J.* **195**, 13.

Chang, K. 1984, *A. Ap.* **130**, 157.

Chang, K. and Refsdal, S. 1979, *Nature* **282**, 561.

Chang, K. and Refsdal, S. 1984, *A. Ap.* **132**, 168.

Einstein, A. 1916, *Ann. Phys.* **49**, 769.

Heintz, W. D. 1978, Double Stars, Reidel.

Hogan, C., and Narayan, R. 1984, *M.N.R.A.S.* **211**, 575.

Kayser, R., Refsdal, S., and Stabell, R. 1986, *A. Ap.* **166**, 36.

Lawrence, C. R., Readhead, A. C. S., and Moffet, A. T. 1986, *A. J.* **92**, 1235.

Nityananda, R. and Ostriker, J. P. 1984, *J. Ap. A.* **5**, 235.

Paczynski, B. 1986a, *Ap. J.* **301**, 503.

Paczynski, B. 1986b, *Nature* **321**, 419.

Peacock, J. A. 1982, *M. N. R. A. S.* **199**, 987.

Schneider, P., and Weiss, A. 1986, *A. Ap.* **164**, 237.

Figure Captions

Figure 5.2.1: The time delay surface for a lensing plane of no mass. The x and y axes represent axes in the lensing plane. The z axis represents the relative time to travel from the source to the observer while passing a given point in the lensing plane. The minimum at the center shows that the path of minimum travel time from source to observer is a straight line.

Figure 5.2.2: The time surface for perfect observer-lens-source alignment. The surface shows a minimum as a circle around the logarithmic spike of the lens. This circle is the Einstein ring, and the radius of the circle is, by definition 1 ERU.

Figure 5.2.3: The time surface for a single lens not on the optic axis. Note that here there are only two images, one near the original unlensed quasar position, and one on the opposite side of the lens spike.

Figure 5.2.4: A time surface for a double lens. The three critical points on the surface correspond to the image locations by Fermat's Principle. One image is the minimum at the bottom of the time surface, another is a saddle point of the far side of the lens spikes from the minimum image, while the third is between the logarithmic spikes. This geometry defines configuration A.

Figure 5.2.5: The other three-image time surface possible for a double lens. One image corresponds to the minimum near the center, while again the other two are saddle points. Here each stellar spike creates a source image on the opposite side of the spike from the minimum. This configuration is labelled B.

Figure 5.2.6: The five image geometry time surface is shown. Here there are two minima evident and three saddle points. This image configuration is labelled C.

Figure 5.3.1: Microlensing light curves for double star lenses. The magnitude of brightening is plotted against time in years. The graphs represent prototypical double star lensing events.

Figure 5.4.1: The magnitude difference between two image groups as a function of the angular distance between them. The top curve results from a single mass lens while the bottom curve depicts a double star lens with projected separation of 0.44 ERU. Note that the double star case allows large separations with comparable magnitude differences.

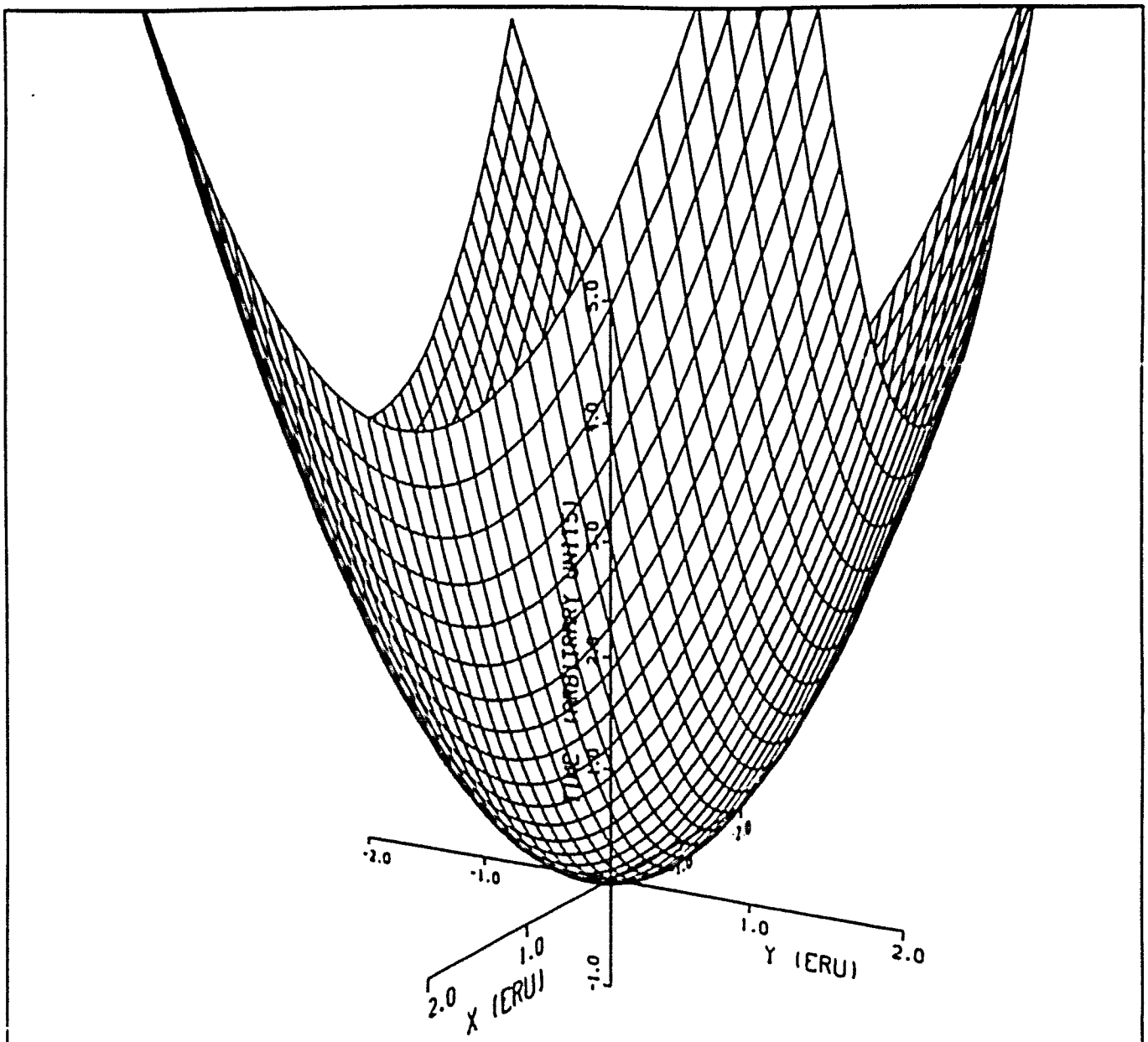

Figure 5.2.1

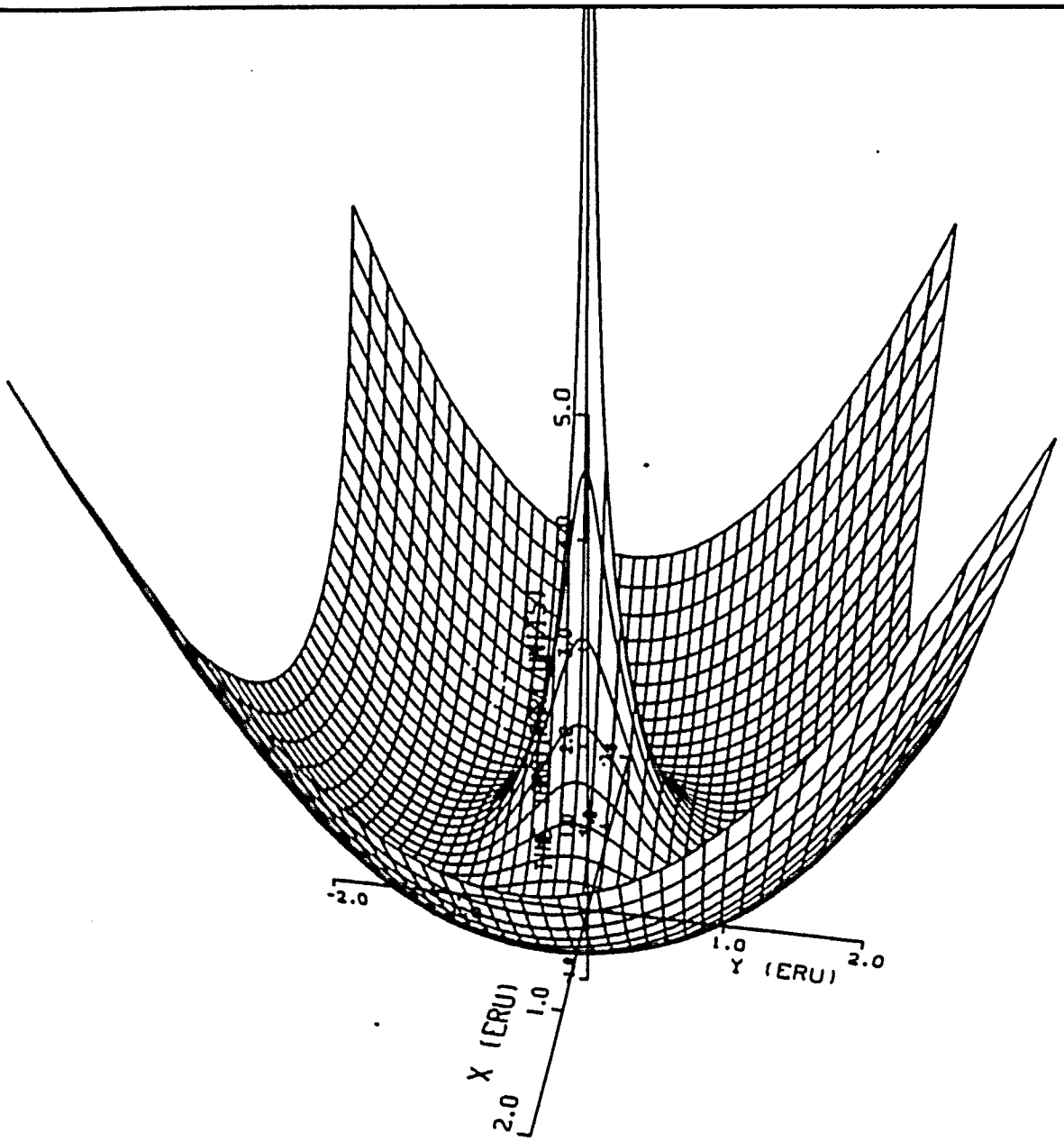

Figure 5.2.2

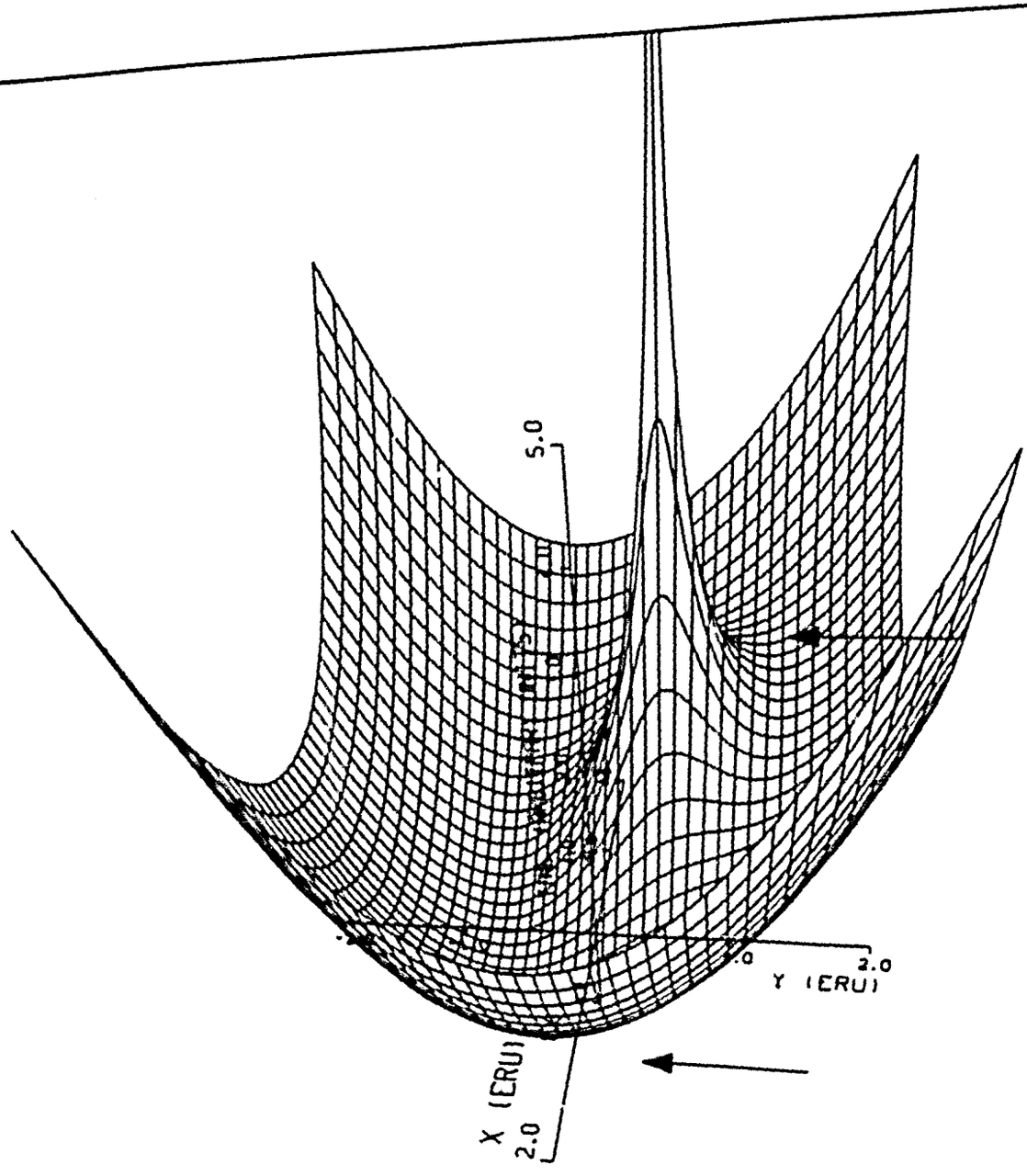

Figure 5.2.3

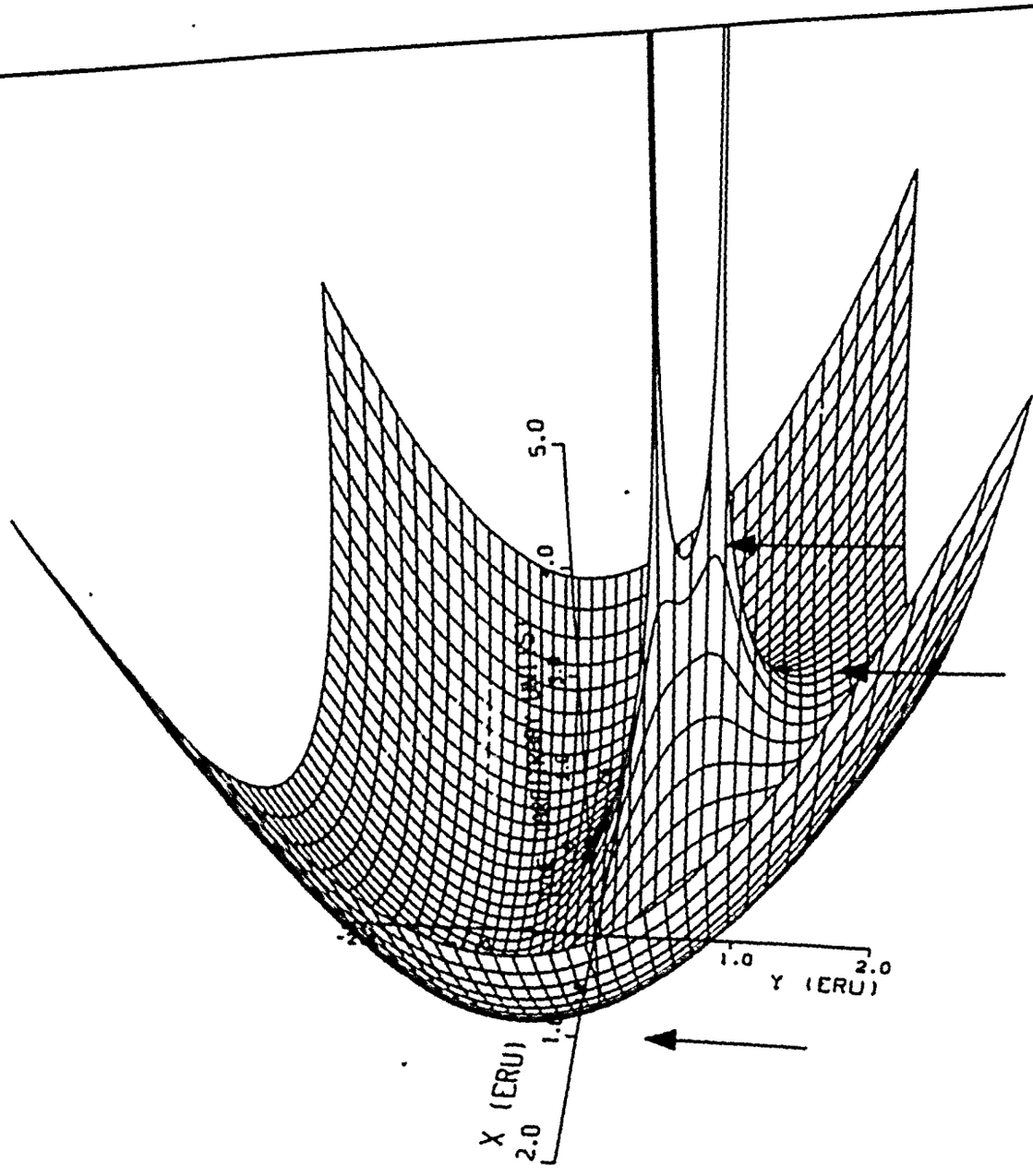

Figure 5.2.4

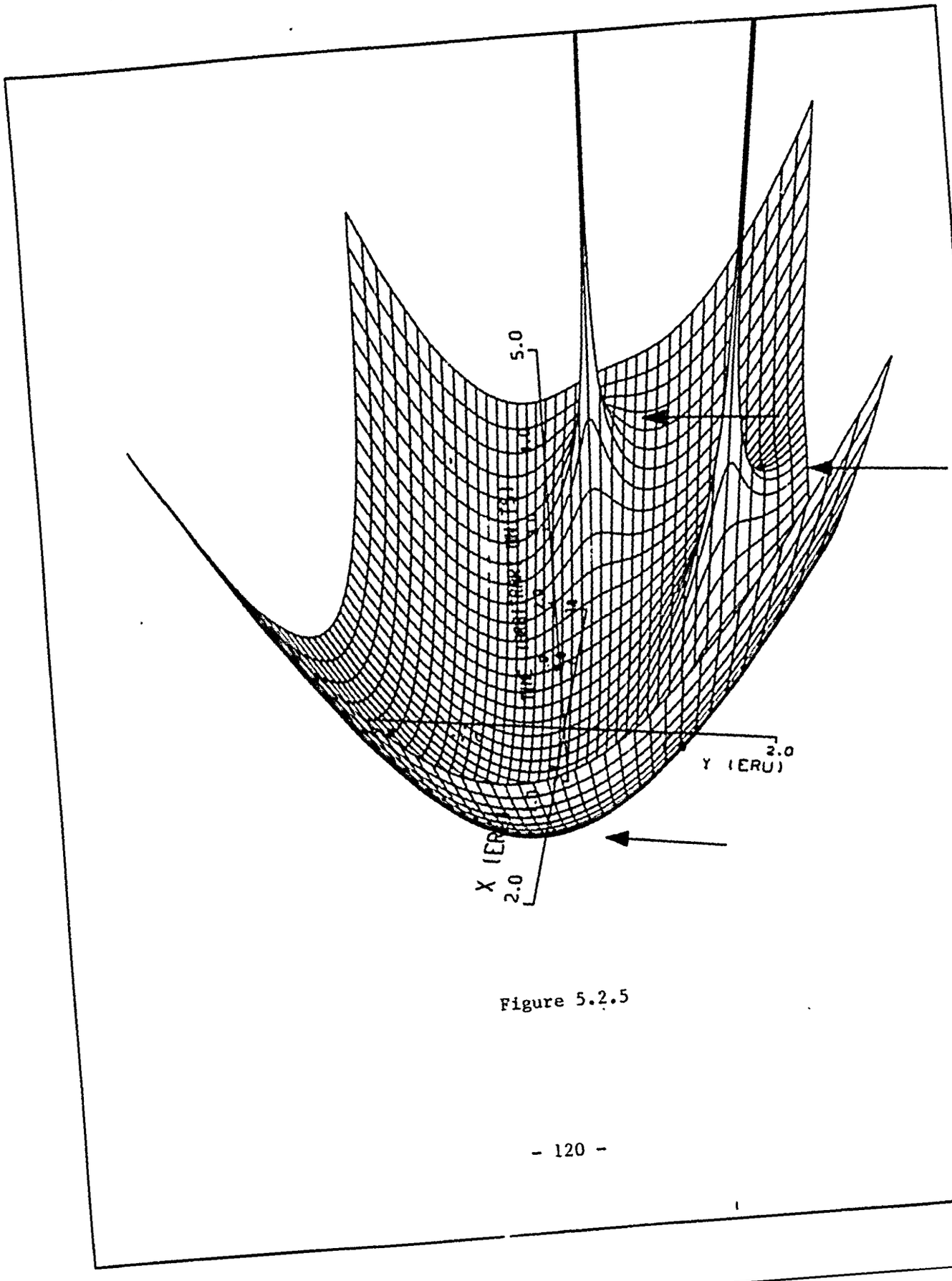

Figure 5.2.5

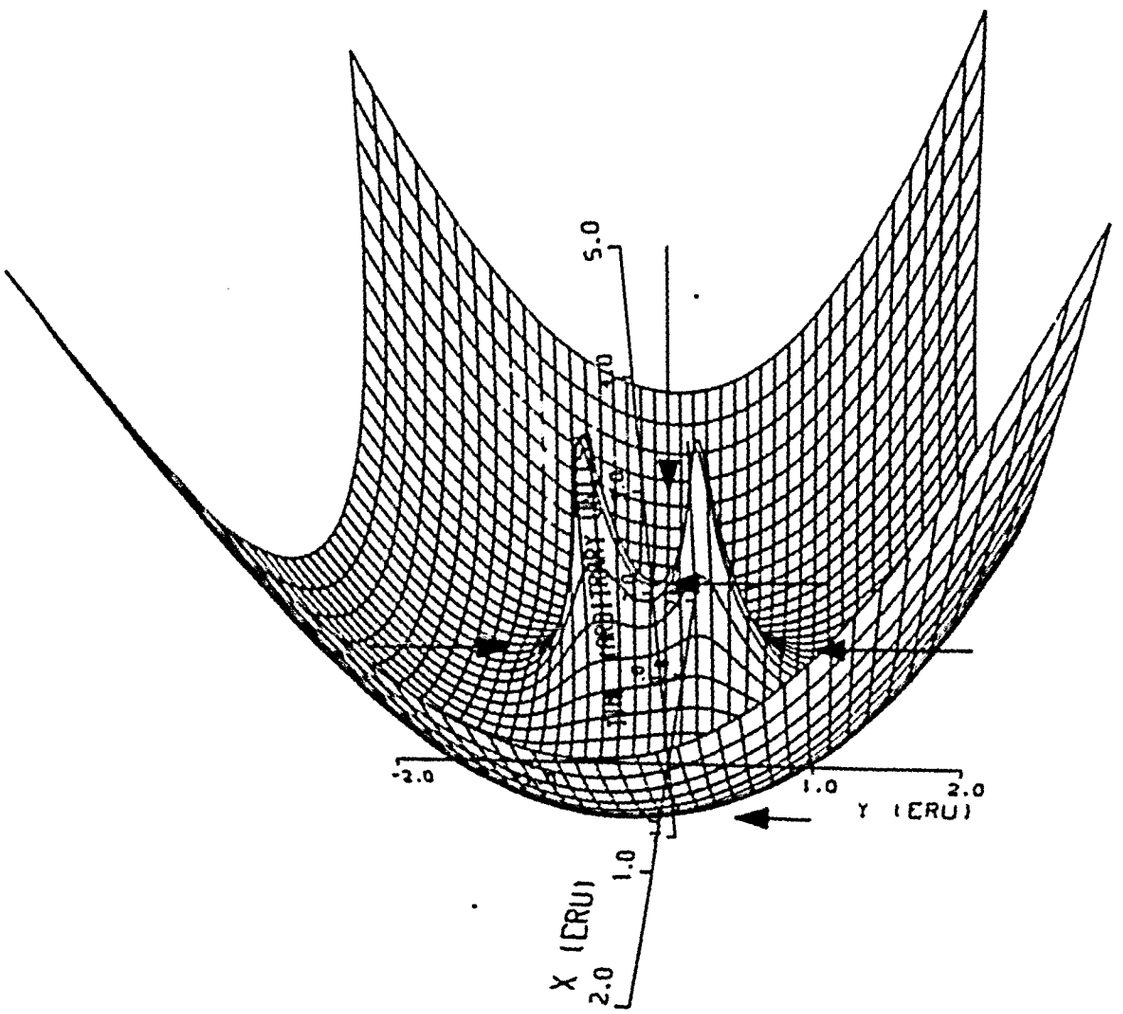

Figure 5.2.6

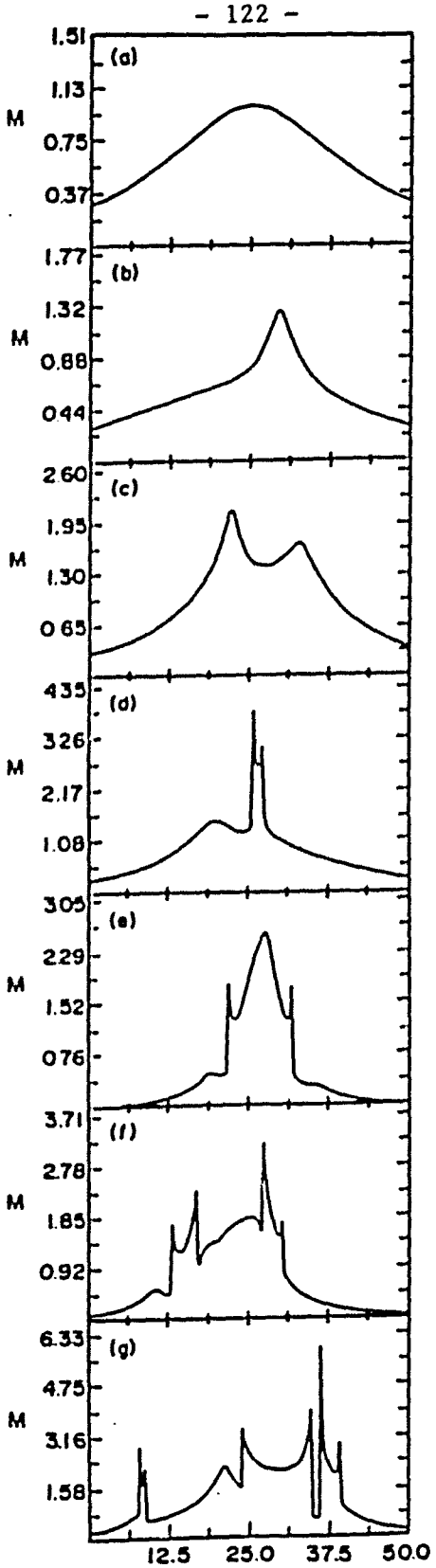
(a)
1.51
1.13
0.75
0.37
M
(b)
1.77
1.32
0.88
0.44
M
(c)
2.60
1.95
1.30
0.65
M
(d)
4.35
3.26
2.17
1.08
M
(e)
3.05
2.29
1.52
0.76
M
(f)
3.71
2.78
1.85
0.92
M
(g)
6.33
4.75
3.16
1.58
M
12.5
25.0
37.5
50.0
TIME IN YEARS

Figure 5.3.1

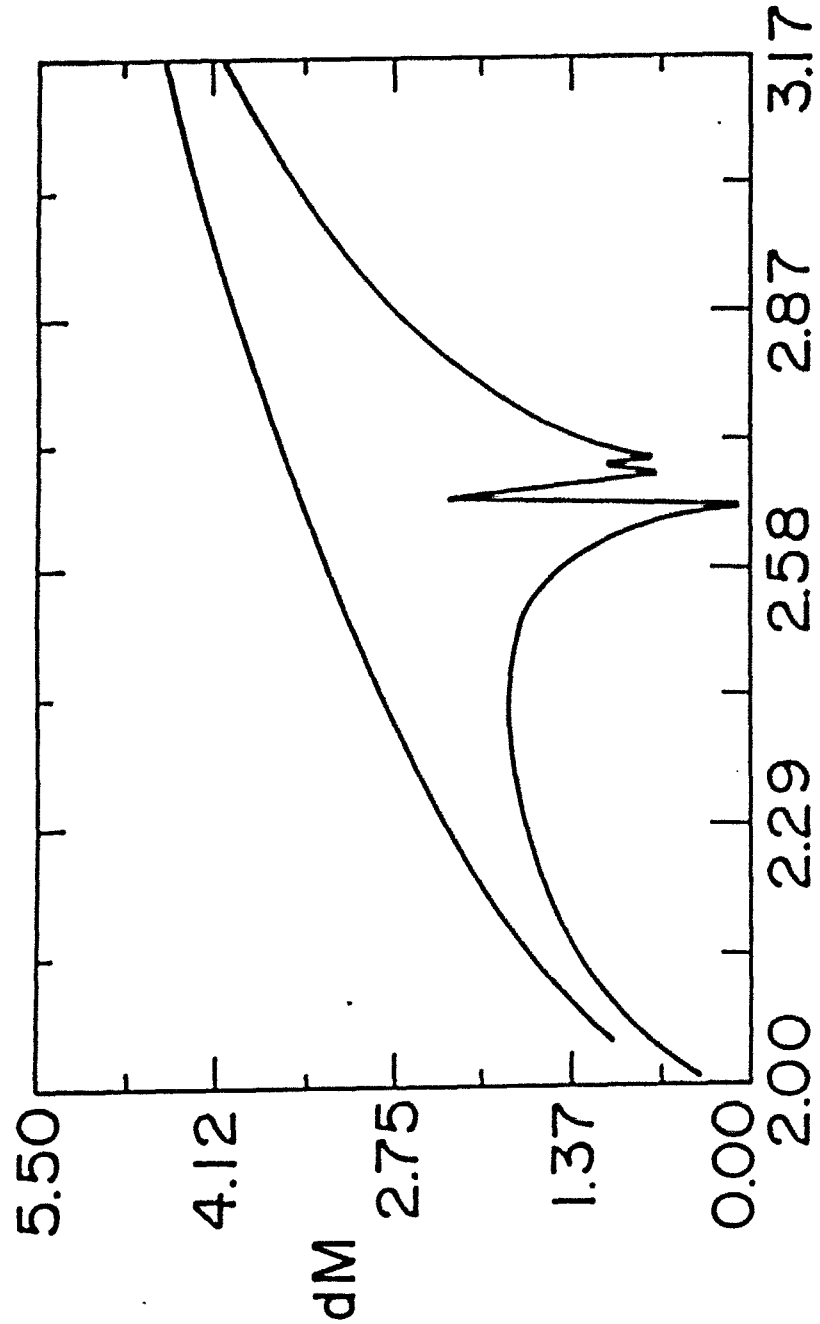
5.50
4.12
2.75
1.37
0.00
dM
2.00
2.29
2.58
2.87
3.17
IMAGE SEPARATION (ERU)

Figure 5.4.1

Chapter 6

Spectroscopic Effects

6.1) Quasar Broad Line Regions

The microlensing analysis of the previous chapters concerned itself with the lensing of AGN continuum radiation. This was because such radiation is thought to be emitted from one of the smallest regions of the AGN, and hence the point source approximation would best apply. In this Chapter we will discuss a region thought to be much larger: that directly outside the 'continuum region'. The point source approximation is usually not valid here, as hypothesized sizes for this region run from less than a tenth of a parsec to greater than a parsec. We will therefore expand our analysis to include the main distinguishing feature of this region: broad emission lines. The region itself is frequently referred to as the broad emission line region, or just BLR. For a good review of AGN properties, see Wiita (1985) or Weedman (1986), and references therein; much of the current discussion is based on these reviews.

There are many theories of the structure of the BLR region, and no general consensus of its physical composition has come forward. Most of these theories involve the motion of many small mass clouds. Each of these clouds is supposed to be small; small enough to be considered a point source in the gravitational lensing sense, being only 1 AU or so in extent. With about 10^{10} clouds of about $10^{-9}M_{\odot}$, the whole BLR region is thought to contain between 1 and 100 $M_{\odot}$.

The major kinematic feature which BLR theories strive to explain is the shape of the BLR spectral emission lines. The lines are seen to have logarithmic shapes away from their peaks, with widths that imply motions of the order of 10^4 km/sec. Most theories use the macroscopic motion of the clouds to explain these velocities. The Doppler shifting of the clouds causes an cumulative emission line that is much broader than the temperature of the individual clouds would imply. It is for this reason that each cloud is modeled as emitting a single frequency in contributing to the overall spectral line.

We wish to discuss these regions with regard to the effects that gravitational lenses can have on them. We will consider a standard paradigm: a stellar lens of 0.01 $M_\odot$ in a galaxy at 10^8 pc acts to lens a BLR in a quasar much further in the distance than the lens. Specifically, we will assume distances in the lens plane to be 10 times that of distances in the source plane. The exact distance to the source is then a function of cosmology. For a flat Euclidean universe, the quasar would be found at a distance of 10^9 pc.

Distances intrinsic to the BLR will be given in two convenient units. The first is that of parsecs (pc) in the source plane, while the second will be the Einstein ring unit (ERU) of the lens. The parsec is an accepted unit of QSO analysis. The ERU is angular (see Equation 1.2.2) and given to make our analysis of the problem more general. This generality allows our analysis to be applied to a wider range of lensing scenarios than the specific lensing paradigm cited above. The conversion

factor between the two systems of units in our current paradigm is 230 ERU/pc.

In the following analysis, we will see that, if some dynamic theories of cloud movements are correct and if some specific parameters of their movements fall in a given region, microlensing effects may be evident. Such effects were hypothesized briefly and in a qualitative manner by Canizares (1982) and Weedman (1986). In other theories, and in some regimes of the former theories, no microlensing effects are to be expected. When microlensing effects are evident, they act to change the shape of the spectral emission line.

6.2) Theories and Predictions

In the following analysis we will concentrate on five basic models of the movements of the BLR clouds. These models are 1) random motions, 2) constant acceleration, radial outflow, 3) constant velocity, radial outflow, 4) gravitational infall, and 5) Keplerian disks. We will predict and discuss possible characteristic emission line changes of the BLR region due to gravitational lensing for each of these scenarios.

All of the following models were calculated numerically. For each model, typically 10^6 clouds were placed randomly. For models involving acceleration, the time of movement for a cloud to go from starting point to finishing point was calculated first. The clouds were then placed by assuming a uniformly random time for each in this interval, and then calculating its resulting position and velocity. All regions of the QSO were assumed to remain optically thin.

The numerical simulations were run on both an IBM 4341 mainframe and an

Leading Edge PC with similar results. The graphs presented have been smoothed with polynomial interpolation techniques.

6.2.1) Random Motions

The first model we will consider is that of random cloud movements. Models involving random cloud movements have been discussed by others including Capriotti, Foltz, and Byard (CFB, 1980) and Osterbrock (1978). In generating the BLR spectral lines with this model, several assumptions were made. All clouds were considered to have the same brightness. The position of each was assumed to be random and uniform inside a sphere of radius r_{max} = 1 pc. Velocities were assumed random, following a Gaussian distribution for which the dispersion velocity was 2000 km/sec.

A typical BLR emission line generated with these assumptions is shown in Figure 6.2.1. The ordinate has been scaled to an arbitrary luminosity. For present purposes, its exact maximum value is not important, since it is strictly a function of the number and brightness of the individual clouds. Similarly the abscissa is scale invariant; we could have scaled the cloud velocities to any dispersion.

The shape of the spectral line was not greatly altered by the placement of a foreground lens anywhere in the field. When r_{max} was placed at 1 pc, no lensing effects were evident. Even when r_{max} was reduced to 0.1 pc, as depicted by the Figure 6.2.1, gravitational distortions of the emission line increased but were still very small, of the order of 1%. This slight effect is visible as an enhancement of

the central peak of the spectral line. Figure 6.2.1 shows a emission line generated with the above model. The numerical error in the luminosity was about 0.02 of the normalized luminosity units used in the graph.

6.2.2) Constant Acceleration Radial Outflow

Some of the leading theories of BLR structure involve radial outflow. Blumenthal and Mathews (1975) consider theories of outflow generated by radiative emission from the continuum region, and show that such a theory can successfully account for the logarithmic shape of the spectral lines away from the peak. Another theory predicts that the outflow is caused by a radial wind of particles emitted by the continuum region (Weymann et al. 1982). Both of these models hypothesize the acceleration of the clouds in a radial direction, away from the continuum region. Many dynamical variations of these themes that have been considered (CFB).

The calculations below will involve the following assumptions that are part of many of the outflow theories. We will assume spherical symmetry about the origin of the BLR. We will not include the luminosity of the continuum region at the center of the BLR in the lensing calculations. The clouds will be created at a characteristic radius r_{min}. They start with zero velocity and maintain constant luminosity. They will undergo constant acceleration until they reach r_{max}, where they will abruptly become dark. All clouds are assumed identical to each other.

We found that the lens can affect the shape of the spectral line under certain conditions. A typical lens distortion of a fiducial BLR spectral emission is depicted

in Figure 6.2.2. Here r_{max} was assigned to be 1 pc and r_{min} was equal to 10^{-3} pc (0.23 ERU). The lens was placed 1 ERU from the center of the BLR.

Inspection of Figure 6.2.2 shows the center of the spectral line increased, while the rest of the spectral line remained essentially unchanged. This is the typical effect of a single gravitational lens in an accelerated outflow model. The lens affects the center of the spectral line the most strongly because small redshifts predominantly originate in the central region of the BLR, which also has the highest concentration of source points. Here the numerical error in the luminosity calculation was less than 0.01 of the normalized luminosity units.

The line distortion effect is extremely sensitive to the value of r_{min}, for a given r_{max}. The smaller is r_{min}, the greater is the lens effect. Current theories do not usually speculate on the value of r_{min}. Wiita (1987) suggests that its size can be as small as several Schwarzschild radii of the central black hole. This would put the value of r_{min} at roughly 10^{-5} pc (0.0023 ERU) for a 10^7 $M_\odot$ black hole. Weymann et al. (1982) consider scenarios with r_{max} between 0.15 and 0.96 pc, while r_{min} is of the order of 0.03 pc (6.8 ERU), but state these assumed values of r_{min} are only an assumption. If Weymann et al. (1982) are correct in this assumption, no lens distortion of the BLR spectral line is to be expected.

The lens effect is also sensitive to the value of r_{max}. For a given r_{min}, the greatest lens effects arise from the smallest r_{max}.

For the BLR line distortion to take place, r_{min} must be of the order of a few

ERU or smaller, and the lens must occupy a region extending from the center of the BLR to within a few ERU outside of the projected r_{min}. If the lens is outside this region, it will not distort the spectral line significantly. As we are dealing with a single lens, the lens can never act to de-amplify portions of the spectral line, only to amplify it. Also, the lens will always affect both sides of the spectral line by the same amount. This follows from the assumption of spherical symmetry.

6.2.3) Constant Velocity Radial Outflow

The other type of radial outflow which will be considered is that of constant velocity of the clouds (see CFB). In this model the clouds are created and given a specific velocity (10^4 km/sec or so) at r_{min} and allowed them to coast out to r_{max} where they turn off. Here the clouds do not maintain constant brightness as they leave the center, but rather the brightness drops off inversely with distance from the center. This decrease in cloud luminosity is necessary to create the observed logarithmic shapes of the wings of the spectral lines.

The lens affects the constant velocity model qualitatively much the same as for the constant acceleration model. A sample line distortion is shown in Figure 6.2.3 for the same lens and source parameters that generated Figure 6.2.2. As before, the lensing effects are extremely sensitive to the assumed value of r_{min} and the location of the lens with respect to the BLR center. Again the observed distortion of the spectral lines that can be generated is that of an increase in the strength of the central part of the line.

6.2.4) Gravitational Infall

Probably the most interesting effects were generated with a gravitational infall model. This model, discussed in CFB, involves clouds falling radially from some radius r_{max}. The model closely resembles one discussed by Kwan and Carroll (1982), with the clouds following parabolic orbits about the central region . We did not allow the clouds to get any closer than r_{min}. The clouds, maintaining constant luminosity over their trajectory, were dropped from rest at a radius of r_{max} and allowed to fall to a radius of r_{min}, where they abruptly turned off. The mass of the central object was that necessary to cause a velocity of 10^4 km/sec at r_{min}.

The gravitational lens effects were typically greatest on the wings of the lines, rather than near the center. The lens effects were sensitive to the values of both r_{max} and r_{min}, particularly r_{max}. For r_{max} of 1 pc, and r_{min} of 10^{-3} pc, the lens effect could be quite dramatic. For a lens perfectly centered, the maximum lens effect produced wings of the line typically increased by several times their original luminosity, while the center changed much less than this, of the order of 10% or less.

Dramatically different lens effects were generated depending on where the lens was located. If the lens was superimposed on the central region of the BLR, the wings were amplified greatly, as shown in Figure 6.2.4. If the lens was several ERU away from the central region, its effects were weaker but concentrated on the central region, as shown in Figure 6.2.5. When the lens was between these two regions, the

portion of the line between the wings and the center was most greatly enhanced, as is shown in Figure 6.2.6.

Were a lens to move across a BLR region of this character and dimension, the first effects noticeable would be an enhancement of the central part of the emission line. As the lens moved toward the center, the line distortion would increase and move outward from the center of the line. Finally, as the lens approached the center, the wings of the line would be the most enhanced by the gravitational distortion. Then, as the lens exited the BLR region, the whole procedure would reverse. Equivalently, in time order, we would see Figures 6.2.5, 6.2.6, 6.2.4, 6.2.6, and back to 6.2.5 again. The time scale for these observations is the same as those discussed in Chapter 3.

The emission line generated with this analysis does not have a logarithmic profile (as discussed by CFB). To generate a profile of this type, one must demand that cloud brightness drop off as the square of its distance from the center. Our attempts to model the BLR in this way with the numerical methods outlined above proved too time consuming for the computers being used. We hypothesize that dimming clouds far from the center would only strengthen the effects outlined above, which predominantly result from the lensing of the central region.

The numerical error of the gravitational infall simulation was greater than in all of the other simulations. The error was greatest near the wings of the lines, where there were the fewest clouds, and also behind the lens, where small numerical

errors in cloud placement were greatly amplified by the lens. The error in lensed luminosity was on the order of the (additional) lensed luminosity itself. Away from the lens and the error was comparatively small, less than 1% of the (additional) lensed luminosity.

6.2.5) Keplerian Disks

There are many theoretical disk models currently considered as possible progenitors of the emission lines generated in the BLR. Some of these theories have been put forward by Osterbrock (1978), CFB and others. The main problem with the disk models is that they usually fail to reproduce the observed shape of the spectral lines. Without specific assumptions, many of these models would create spectral lines with two peaks or non-logarithmic wing profiles. Thus some of these models are somewhat ad-hoc.

In this section we will concentrate on a model similar to the original one put forth by Osterbrock (1978). We will assume a Keplerian disk with r_{max} (outer radius) of 0.1 pc. Again, r_{min} will be assumed to be $r_{max}/1000$. The exact value of r_{min} is not so important as it was in previous models, as we will consider neither the density of clouds nor their brightness to be enhanced in the central region.

The disk will involve Keplerian revolution of clouds around the center in circular orbits, the clouds being too small to block each other (the disk is assumed to be optically thin). The height of the disk will be assumed to be 2/5 the value of r_{max}.

A typical simulation yielded the spectral line shown in Figure 6.2.7. In this

simulation, we also made the following assumptions. The disk is seen tilted 45 degrees to our line of sight. The velocity of rotation was $2 x 10^4$ km/sec at r_{min}. The value of r_{max} was 0.2 pc and r_{min} was $r_{max}/1000$.

Superimposed on the circular motion is random motion 2/5 that of the cloud velocities at r_{min}. The random motion was assumed Gaussian in nature.

Line distortion effects are again most evident in the center of the line, but for first time in any of our simulations, the distortions were typically not symmetric. In Figure 6.2.7, the lens was 0.7 ERU from the center and superimposed on a region away from the projected axes of the projected ellipse. Here the lens affected one side of the spectral line, near the center, stronger than the other side. These distortions were typically small, showing the most asymmetry when the lens was closest to the central region.

The reason for the distortion asymmetry in the lensed emission line derives from the fact that the lens is superimposed on a region with bulk motion with respect to the observer. The lens acts to amplify the light from the region of bulk motion more than the rest of the BLR, and hence creates an abnormally high contribution from this region toward the complete spectral line. This abnormal contribution results in the observed line asymmetry.

The lens distortions of Keplerian disks can act to change the central redshift of the BLR line, but only to a small degree. For the simulation described above, the lens could cause the center of the line to 'sway' of the order of hundreds of km/sec

to either side, but not more. Figure 6.2.8 depicts the same scenario described above but with the exception that the lens was projected onto the opposite side of the BLR region. Close inspection of the two graphs will show the redshift change of the magnitude described.

The numerical error in the luminosity was on the order of 0.01 in the given luminosity units. The error in the 'sway' of the line was less than 10 km/sec.

This line shift may be important in identifying QSO's with multiple macroimages. Were microlensing effects strong, they could cause a difference in the redshifts between images by as much as 0.01. One might then not rule out close QSO's with a redshift discrepancy in this range, but consider them candidates for both macrolensing and microlensing. These candidates should then be monitored to see if their redshifts change in the way indicated here.

When r_{max} was of the order of or larger than 1 pc. the lens effects were small, of the order of 1% or less.

6.3) Discussion

The analysis in this chapter is aimed at opening a new window through which gravitational lensing may be detected. The gravitational distortion of spectral lines in the BLR may give us a tool to explore many popular phenomena in astrophysics. Information on the size, make-up, geometry, and dynamics of the BLR region may be recoverable. Similarly, BLR lensing may tell us about dynamics, number, and mass density of the lenses involved.

The analysis invokes several assumptions. The weakest assumptions probably involve the estimation of the angular sizes of the lenses' ERU compared to the QSO's BLR region. A change in any of a number of parameters will result in a change of the relative sizes of the regions. These changes could involve parameters such as the mass of the lens, the distances to the lens and the source, the actual size of the BLR region, and the cosmology of the universe. Change in these assumptions would not necessarily negate the above analysis, but would result in a different realization of parameter space than the paradigm investigated here.

Another important assumption which the analysis incorporates is the assumed size of the inner radius where the BLR starts: r_{min}. Most of the spectral distortion effects come from the lensing of this inner region because it usually houses the highest density of clouds. As the current models do not typically make strong predictions on the value of r_{min}, its assumed value is uncertain by several orders of magnitude. Nonetheless, if r_{min} is large compared to the ERU and a reasonable fraction of r_{max}, no distortions of BLR emission lines are to be expected.

Yet another assumption that is important to the accuracy of our analysis is that of the spherical symmetry of the BLR region. Any large geometric asymmetries or asymmetries in the brightness distribution may end up as asymmetries in the shape of the spectral line. These asymmetries are sure to affect the way a lens would distort a BLR line.

It is important to realize that in many scenarios of BLR structure, these line

distortion effects are not improbable to measure, relative to continuum enhancement effects. The probability of spectral line distortion is usually equal to the probability of amplification of the inner continuum region and in some cases can even slightly exceed it. That the BLR region maps spatial regions onto a spectral line can *help* in distinguishing regions that are gravitationally amplified from those that are not.

The above analysis is predictive in at least two aspects. First, one can compare those QSO's that are candidates for gravitational lensing with those which are not, looking for comparative differences in the shapes of their broad emission lines. One might investigate the shapes of the transient emission lines of the current BL Lac's that are thought to be lensed (Nottale 1986, Ostriker and Vietri 1985). One might also investigate those currently known macrolensed systems for anomalous line shapes, as they are also prime candidates for microlensing. We speculate that amplifications due to critical lines, common at higher optical depths, would not significantly affect the shape of the spectral lines differently than the single stars investigated here, at low optical depths, but this needs further investigation.

Secondly, one might look for time variability of the broad line phenomenon to see if it conforms to any of the models with the analysis outlined above. The time scale for change in these lines should match the timescales discussed in Chapters 2 and 3. One would expect not only changes, but a specific pattern in the changes to characterize specific microlensing scenarios.

References

Blumenthal, G. R., and Mathews, W. G. 1975, *Ap. J.* **198**, 517.

Canizares, C. R. (1982), *Ap. J.* **263**, 508.

Capriotti, E., Foltz, C., and Byard, P. 1980, *Ap. J.* **241**, 903.

Kwan, J., and Carroll, T. J. 1982, *Ap. J.* **261**, 25.

Nottale, L. 1986, *A. Ap.* **157**, 383.

Osterbrock, D. E. 1978, *Proc. Natl. Acad. Sci.* **75**, 540.

Ostriker, J. P., and Vietri, M. 1985, *Nature* **318**, 446.

Weedman, D. W. 1986, Quasar astronomy, Cambridge: Cambridge U. Press.

Weymann, R. J., Scott, J. S., Schiano, A. V. R., and Christiansen, W. A. 1982, *Ap. J.* **262**, 497.

Wiita, P. J. 1985, *Phys. Rep.* **123**, 117.

Wiita, P. J. 1987, Private Communication.

Figure Captions

Figure 6.2.1: The broad emission line profile generated from random (Gaussian) cloud motions. See the text for a more complete description of cloud motions and microlensing paradigm assumed. The dispersion of the velocity distribution is 2000 km/sec. The effects of a lens 0.1 ERU away from the BLR center do not strongly affect the shape of the line. Only a small (1%) effect of the brightening of the central peak is noticeable. The region was assumed to be 0.1 pc in radius.

Figure 6.2.2: Constant radial acceleration outflow model of BLR emission line generation. A lens 1 ERU distant from the BLR center increases the emission from the central peak. The excess emission due to gravitational lensing is denoted on the graph by the hatched area. The parameters that define the size of the BLR region are $r_{max} = 1$ pc, $r_{min} = 10^{-3}$ pc.

Figure 6.2.3: Constant radial velocity outflow model of BLR emission line generation. A lens 1 ERU distant from the BLR center increases the emission from the central peak. The size of the BLR region is the same as that in the constant acceleration model above.

Figure 6.2.4: Radial gravitational infall model of BLR emission line generation. The region was modeled with $r_{max} = 1$ pc and $r_{min} = 10^{-3}$ pc. A lens 2.3 ERU distant from the center of the region creates the line distortion shown. Note that the lens primarily affects the peak of the line.

Figure 6.2.5: Radial gravitational infall model of BLR emission line genera-

tion. The BLR parameters are the same as before, but here a lens is 0.11 ERU from the region center. Note that the lens effects are greatest in the wings of the line.

Figure 6.2.6: Radial gravitational infall model of BLR emission line generation. Again the BLR parameters are the same as before, except that the lens is 0.68 ERU from the region center. Note that the lens effects are most prominent between the peak and the wings.

Figure 6.2.7: Keplerian disk model of BLR emission line generation. Here the disk is tilted 45 degrees to the line of sight, and has $r_{max} = 0.1$ pc and $r_{min} = 10^{-4}$ pc, and a height of 0.04 pc. Part of the cloud motion is turbulent: a (Gaussian) random distribution with a dispersion velocity of of 2000 km/sec. The rest of the cloud motion is ordered: a circular Keplerian orbit about the BLR center, with $v = 2x10^4$ km/sec at r_{min}. Here the lens was placed 0.7 ERU from the center and situated so that it would affect one side of the line differently from the other. This effect is not large, but a slight bias of the line toward smaller redshifts is discernable.

Figure 6.2.8: Keplerian disk model of BLR emission line generation. The BLR model is the same as in the one used to generate Figure 6.2.7, except that the lens is superimposed on the opposite side of the BLR disk region. This causes the line to tilt in the opposite direction from the previous line, resulting in a redshift difference between the two of the order of hundreds of km/sec.

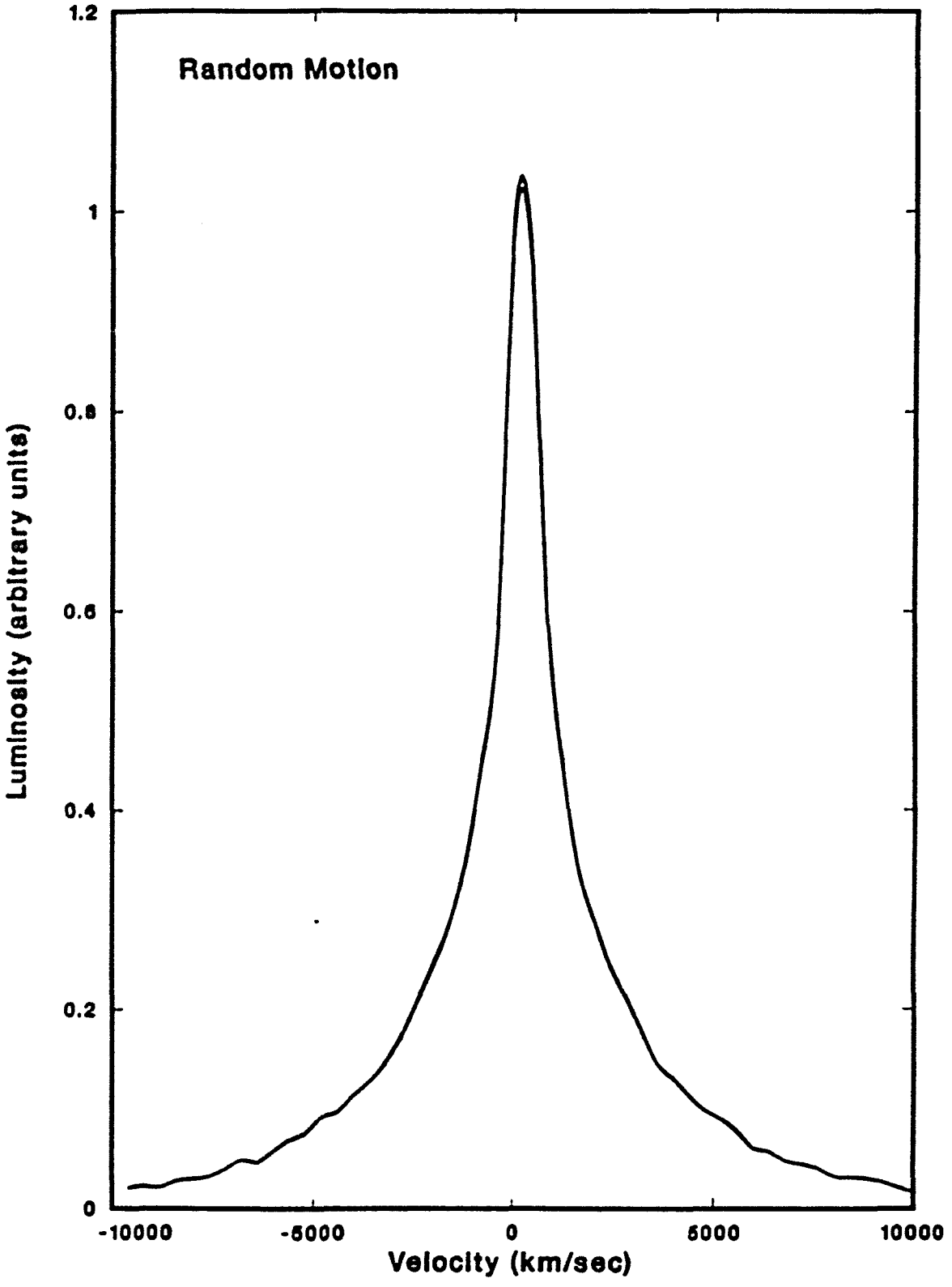
Random Motion
Luminosity (arbitrary units)
1.2
1
0.8
0.6
0.4
0.2
0
-10000
-5000
0
5000
10000
Velocity (km/sec)

Figure 6.2.1

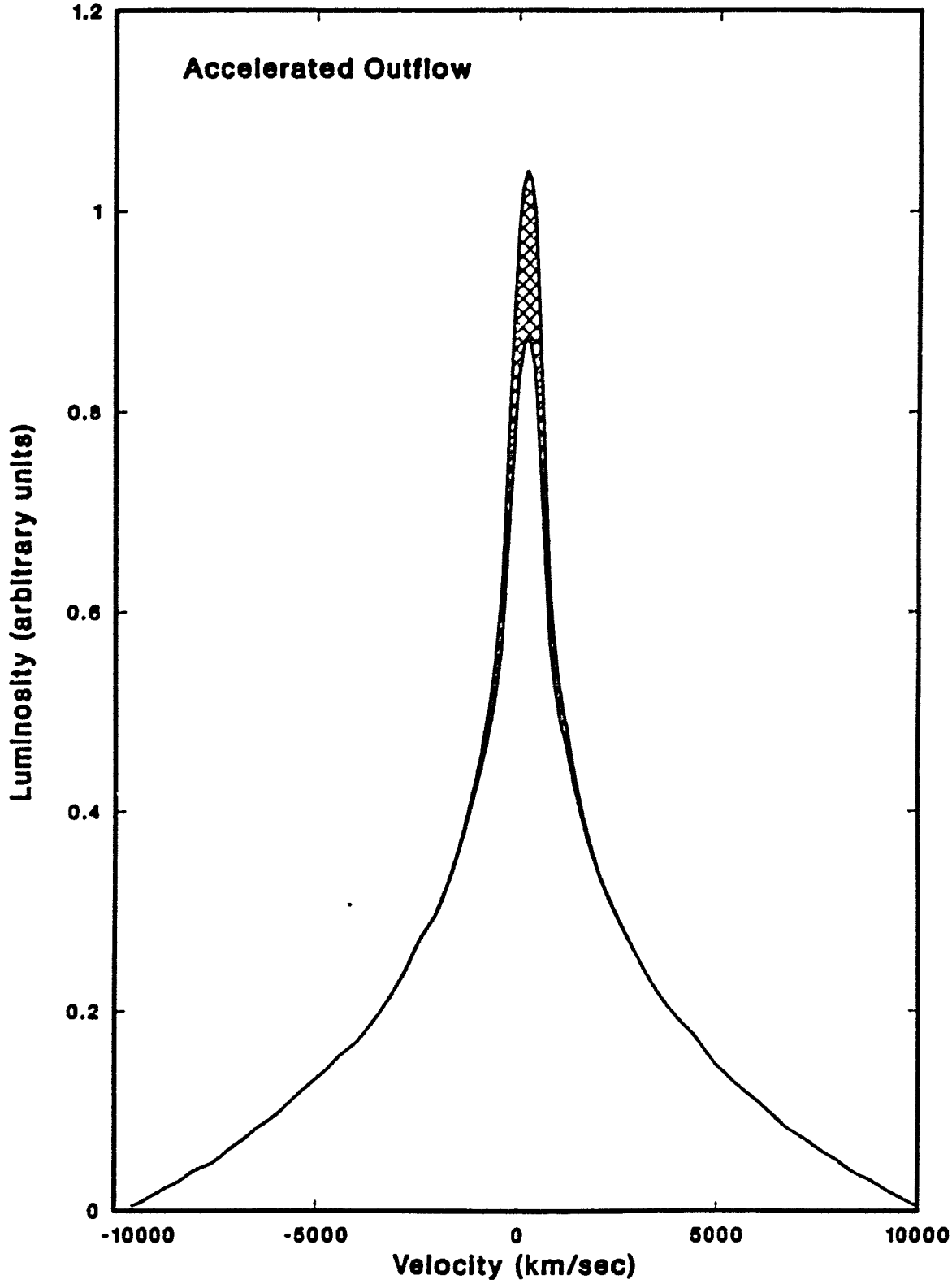
Accelerated Outflow
Luminosity (arbitrary units)
1.2
1
0.8
0.6
0.4
0.2
0
-10000
-5000
0
5000
10000
Velocity (km/sec)

Figure 6.2.2

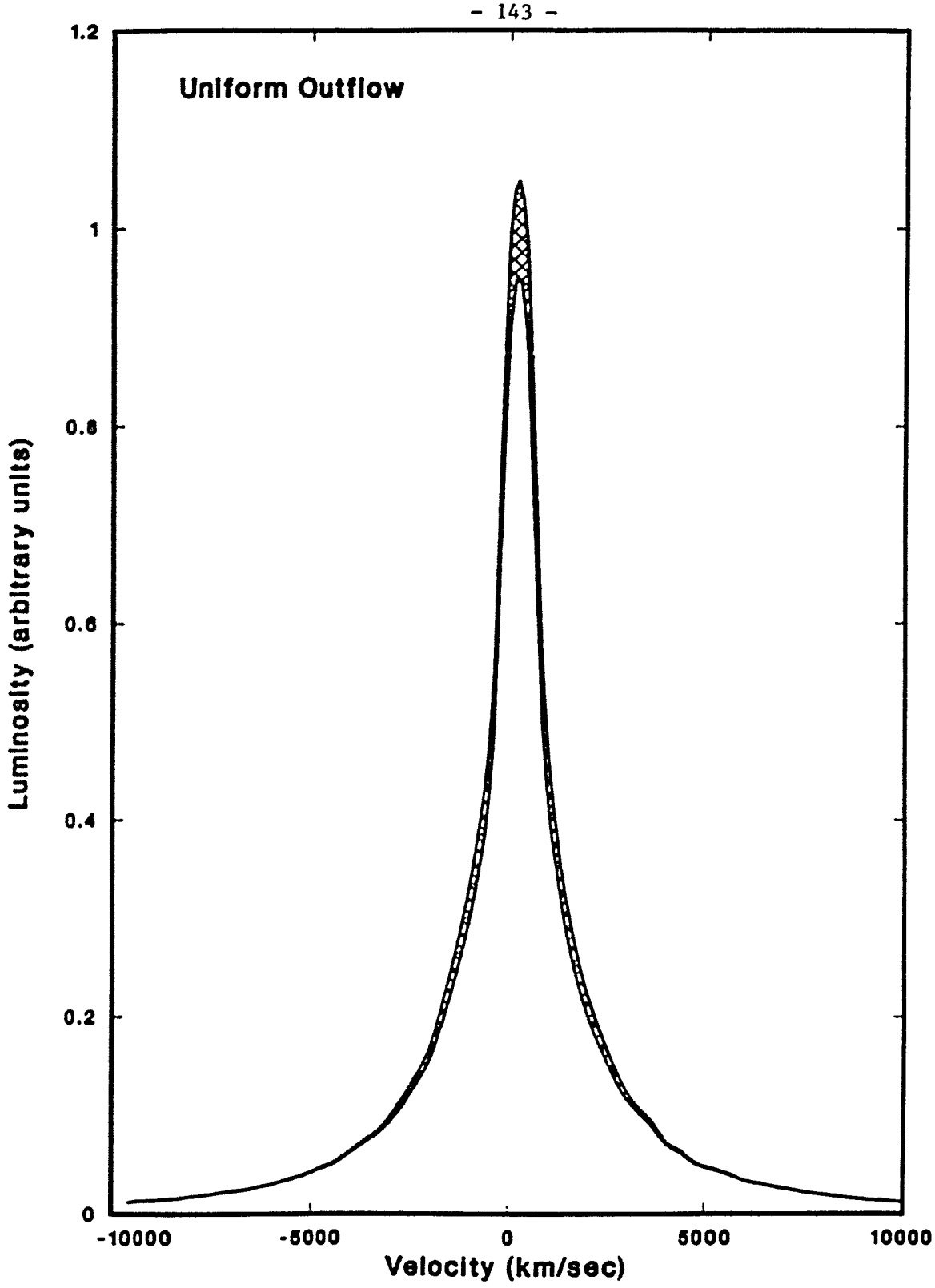
Uniform Outflow
Luminosity (arbitrary units)
1.2
1
0.8
0.6
0.4
0.2
0
-10000
-5000
0
5000
10000
Velocity (km/sec)

Figure 6.2.3

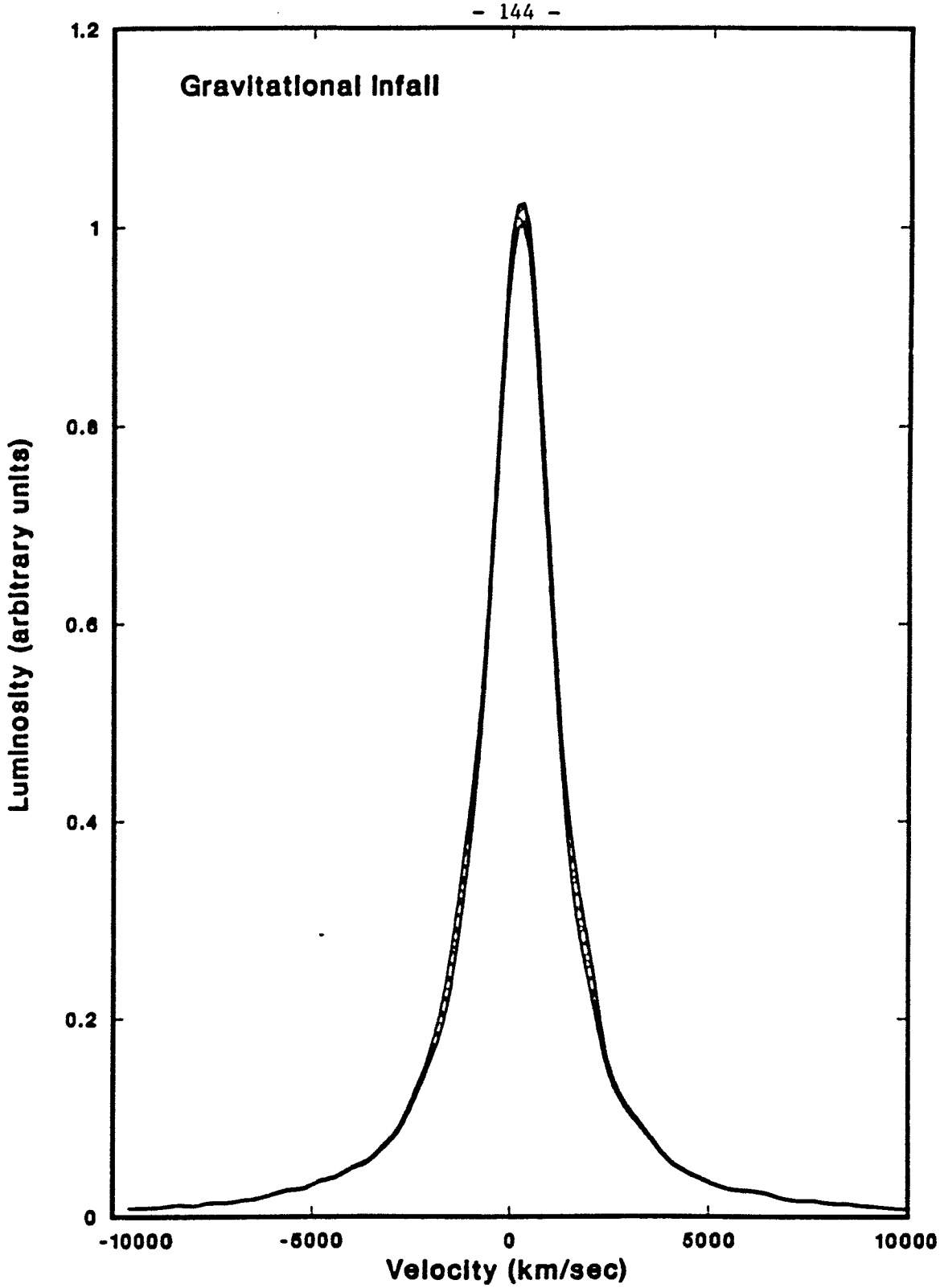
Gravitational Infall
Luminosity (arbitrary units)
1.2
1
0.8
0.6
0.4
0.2
0
-10000
-5000
0
5000
10000
Velocity (km/sec)

Figure 6.2.4

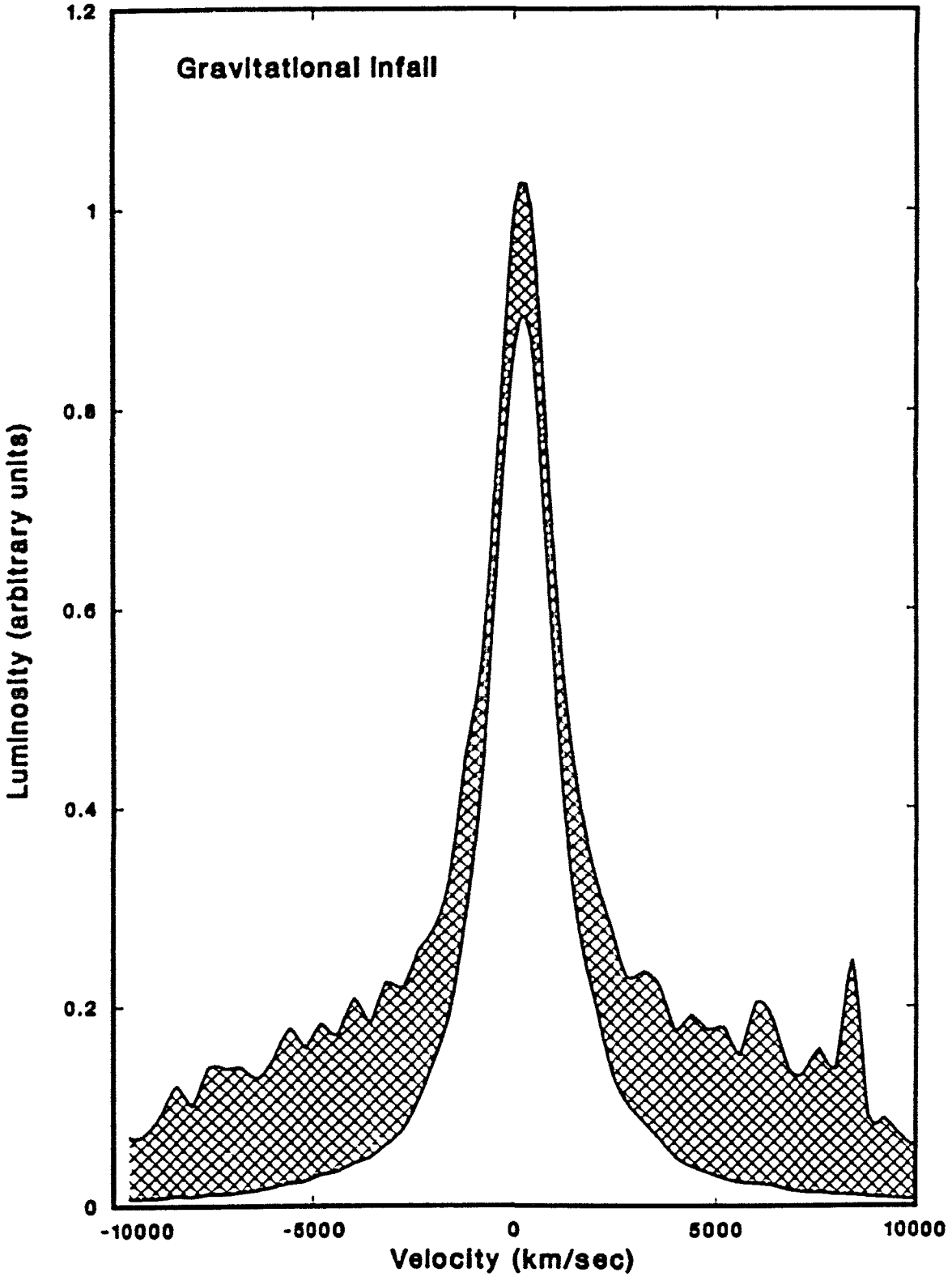
Gravitational Infall
Luminosity (arbitrary units)
1.2
1
0.8
0.6
0.4
0.2
0
-10000
-5000
0
5000
10000
Velocity (km/sec)

Figure 6.2.5

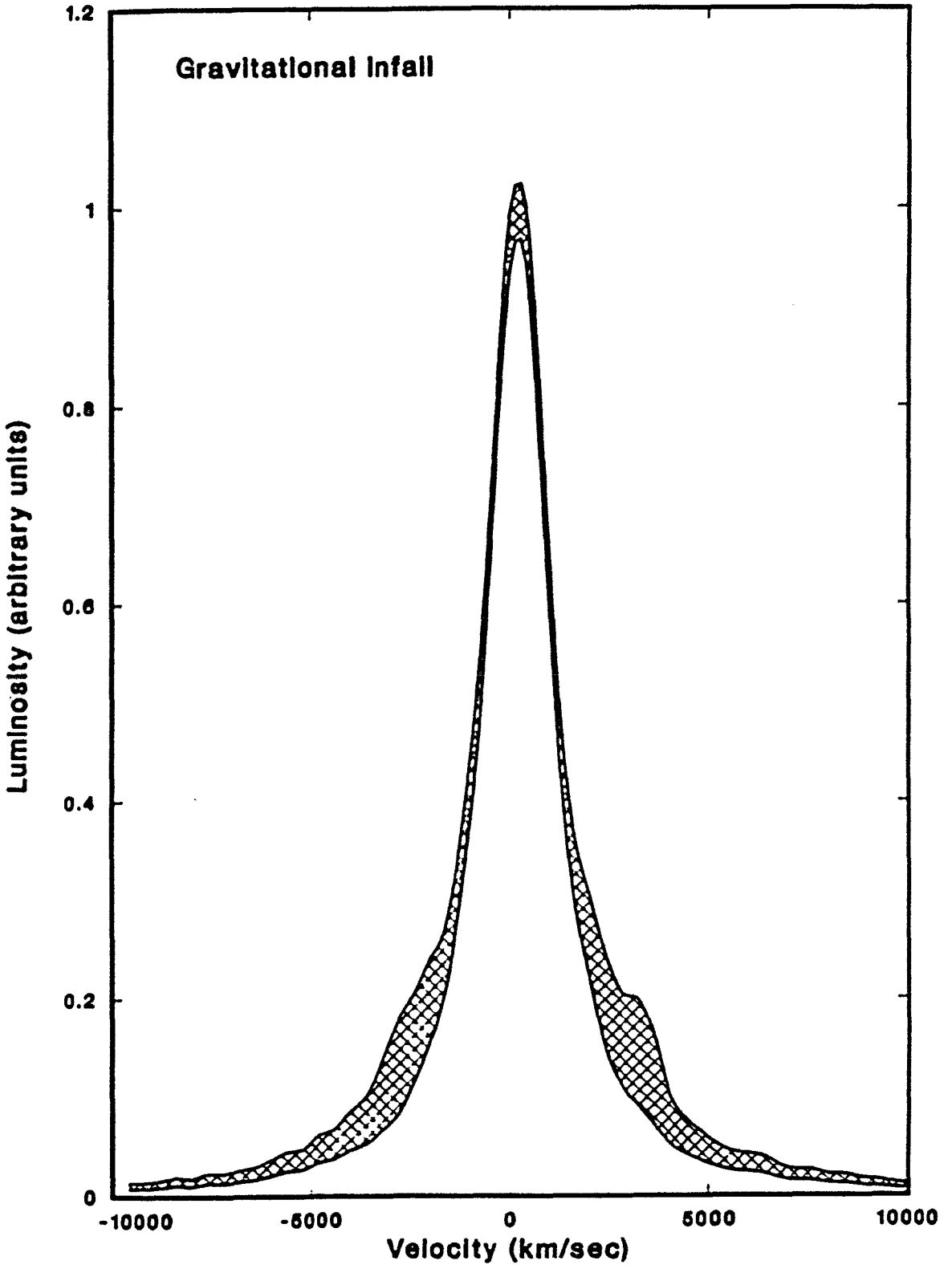
Gravitational Infall
Luminosity (arbitrary units)
1.2
1
0.8
0.6
0.4
0.2
0
-10000
-5000
0
5000
10000
Velocity (km/sec)

Figure 6.2.6

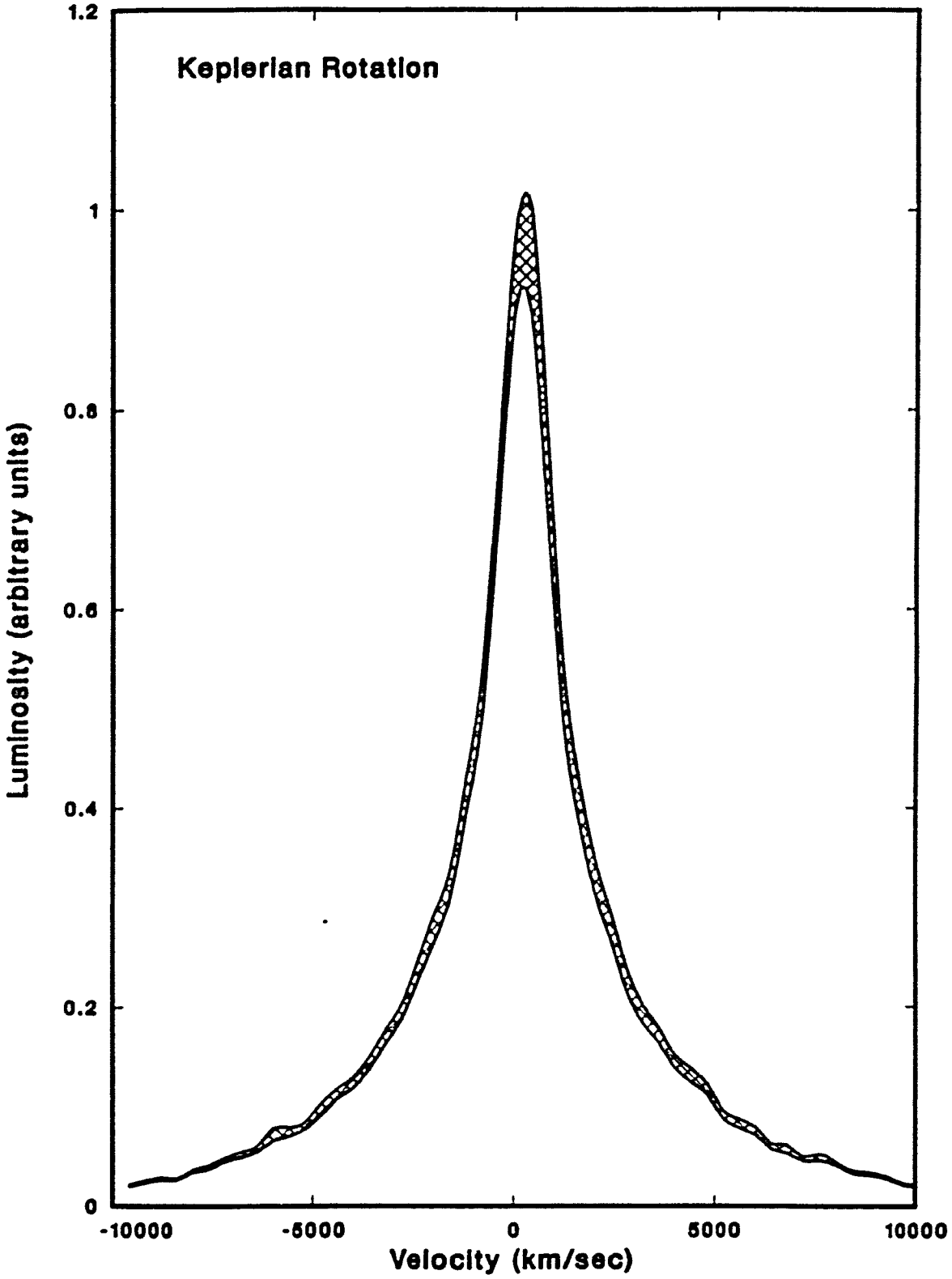
Keplerian Rotation
Luminosity (arbitrary units)
1.2
1
0.8
0.6
0.4
0.2
0
-10000
-5000
0
5000
10000
Velocity (km/sec)

Figure 6.2.7

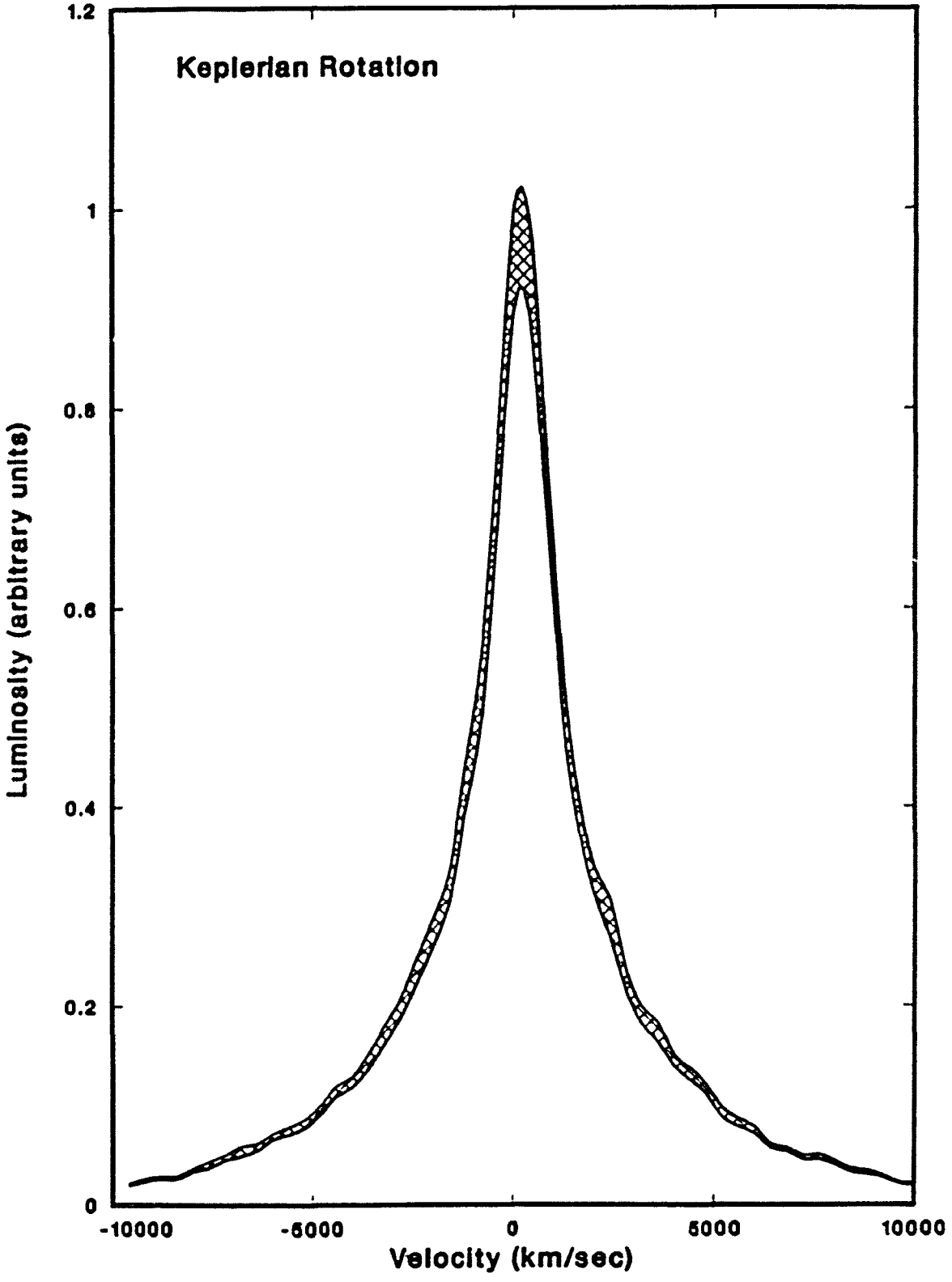
Keplerian Rotation
Luminosity (arbitrary units)
1.2
1
0.8
0.6
0.4
0.2
0
-10000
-5000
0
5000
10000
Velocity (km/sec)

Figure 6.2.8

Chapter 7

Microlensing Diagnostics and the Realistic Observer

7.1) Individual Diagnostics

There are many possible methods an observer can hope to use to detect microlensing. In the first section of this Chapter we will briefly discuss each technique that has come to our attention. Most of these methods did not originate with us, and so much of this section is a review. In the second section we will discuss the possibility of using one or more of these methods in a manner that could isolate microlensing effects. Finally, in the third section, we discuss possible realistic observing programs that may be used to measure these effects. All of the methods discussed will involve a standard microlensing paradigm: a star (or stars) in a galaxy acts to amplify gravitationally the background light from a distant AGN.

The best studied effects involving microlensing involve the prediction of photometric variations for a high optical depth of lenses ($\tau > 0.4$). Some notable works include Paczynski (1986a), and Schneider and Weiss (1987). High optical depth light curves can be quite complex. When the optical depth is near to or greater than one, the amplification can be very high, but few easily discernable structures are obvious in the light curve.

The study of microlensing in the lower end of the high optical depth range ($0.1 < \tau < 0.4$) does reveal recognizable features (Paczynski 1986a). Light curves at these optical depths tend to show image creation and annihilation peaks which

are more easily identifiable.

Some of the aforesaid authors have also studied negative optical depth. Negative optical depth is said to occur when the uniform mass density in the lens plane is high enough so that $\tau_{uniform} > 1$. When one considers a strong uniform component, such as weakly interacting massive particles (Press and Spergel 1985) or massive neutrinos (Bond, Efstathiou, and Silk 1980), one must define two optical depths: one due to the compact objects and one due to the uniform component. As shown by Paczynski (1986a), negative optical depth lensing can also have distinguishing light curve signatures when $\tau_{compact}/(1 - \tau_{uniform})$ is small. A significant feature of these analyses is the prediction of deamplification of source flux (Chang and Refsdal 1984).

In Chapter 3, we have assumed that $\tau_{uniform}$ is much less than unity. Even if the uniform component is the dominant matter in galaxies this is usually a valid assumption. This can be seen by noting that the optical depths quoted in Table 3.1.1 were computed using the dynamical mass of galaxies, not the visible mass. Under the uniform matter assumption column 3 would then list $\tau_{uniform}$ instead of $\tau_{compact}$. In these cases $\tau_{compact}$ would be lower than the values listed in this table.

Incorporating the shear effects of the host galaxy into microlensing effects has also been looked at in some detail. Chang and Refsdal (1979, 1984) computed light curves for a single star in the presence of high shear effects. Kayser, Refsdal, and Stabell (1986) have computed light curves at high optical depths and shear.

Other photometric effects involve low optical depth and shear scenarios ($0 < \tau < 0.1$). Such analysis goes back to Liebes (1964) and Refsdal (1964a). As discussed in Chapter 5, double star systems would create interesting light curve signatures that could help to identify microlensing. Single star systems, studied for example in Chapter 4, provide the simplest light curves and contain a great amount of recoverable information.

Another feature that might identify microlensing is a polarization signature. Schneider and Wagoner (1987) have predicted a microlensing-induced polarization signature on distant supernovae. The effect is based on the expansion of the supernova image behind the field of the lens.

Some AGN are known to emit polarized light. One might expect that microlensing of these AGN would result in not only a amplification signature but a polarization signature as well. To the best of our knowledge, no published work has appeared on this subject.

Schneider and Wagoner (1987) also raise an interesting point about the time scale of observations required to detect the microlensing of supernovae. Supernovae provide a smaller time base over which a detection signature could occur. A supernova goes from the realm of a point source to an extended source over about a month, whereas lensing events which rely on the relative motions of stars have a time base of years.

Yet another indicator of microlensing might be a diffraction effect at radio wave-

lengths (Deguchi and Watson 1986). When the observed radiation from a point source has a wavelength in the radio region, one would expect stellar lensing to create diffraction rings. A specific light curve signature might again be expected as the observer passes through successive diffraction maxima and minima.

Spectral line changes induced by microlensing may result from many theories of cloud movements in the broad line regions (BLR) of AGN. This effect was discussed in detail in Chapter 6.

Saslaw, Narasimha, and Chitre (1985) estimate that it may become possible in the near future to discern 'gravity rings' around local stars with VLBI and future planned high resolution radio instrumentation. If the angular scale of brightness change behind a nearby stellar lens is less than both the angular scale of the ERU and the angular scale of resolution of an imaging device, one expects the lens to induce ring-like distortions (gravity rings) in the measurements of this background image. Gravity rings, caused by local stars, may be found on the images of galaxies, galactic nebulae, or even meandering isophotes of the background sky.

Paczynski (1986b) has calculated the time distortion effects microlensing would have on time-singular background events. In some ways this effect is analogous to the work of Saslaw, Narasimha, and Chitre (1985), in that it deals with time resolution in a similar manner to their work with spatial resolution. Here if the *time* scale of brightness change behind a stellar lens(es) is less than both the time delay between microimages and the time scale of resolution of the detection device,

one expects the lens(es) to produce time-like distortions in the measurements of this background image. For certain stellar distributions in other galaxies, Paczynski makes predictions on the effects of different microlensing optical depths on a time-singular recurrent gamma-ray event behind them.

7.2) Cumulative Diagnostics

A major problem in the detection of microlensing variations of background AGN is distinguishing them from intrinsic AGN variations. There is a danger that a single diagnostic may be identified as intrinsic variability. This section will describe methods specifically formulated to distinguish the two types of variations.

The first method was originally discussed by Gott (1981). Gott suggested that the simultaneous observation of multiple macroimages of the same AGN could help separate the two types of variability. Specifically, if the time delay between images is known, one can compare the images and assume that intrinsic AGN variations occur in all images, while microlensing effects occur in each image individually. The subtraction of one image brightness from another (including the time delay) should therefore isolate microlensing variations (more accurately: isolate those effects that occur along the line-of-sight) and cancel intrinsic effects.

One problem with this analysis is that the optical depth to at least one of the images must be high (Gott 1981). The rapid variations at high optical depth would therefore make it difficult, in practice, to find the time delay and recover information about the source or lenses.

Another clever method was suggested in Greiger, Stabell, and Refsdal (1986). They suggested that multiple observers might be of use in distinguishing between the two sources of variability. If several observers were separated by 0.1 AU of more, they should all measure the same intrinsic variations but observe different microlensing variations. Microlensing effects would make themselves known through a relative time delay in the variability measured by the different observers. This would be caused by the slightly different alignments among observers, lens, and source.

One problem with this method stems from not having the ability to create such a multiple observer scenario easily. We understand that this group is currently investigating the possibility of using a Voyager spacecraft to help make these measurements (Refsdal 1986). Another confounding factor is that one needs short events on which to measure short time delays; AGN do not usually vary on a time scale much shorter than hours.

A less fancy method of distinguishing intrinsic variability from microlensing variability involves monitoring both the BLR emission lines and the continuum simultaneously. Since the center of the BLR is usually the larger contributor to line changes, and since the center of the BLR is hypothesized to be coincident with the continuum region, an observer might expect to see microlensing -induced variations occur in both the lines and the BLR at the same time. Intrinsic changes in AGN brightness might be expected to be seen first in the continuum region, and later

propagate through the BLR (see, for example, Ulrich et al. 1984). The time scale for continuum variations to propagate outward through to the BLR is of the order of days to weeks.

A mostly subjective method for discerning microlensing variations is to inspect AGN light curves for microlensing signatures. If candidates for low optical depth microlensing are investigated, one should have a good idea, from the record of theoretical research, what microlensing light curve signatures are to be expected. A major confounding factor with this method is observer bias. It is possible that any light curve with a hump would look like a microlensing event to an observer eager enough for discovery.

Finally, if we could combine all the cumulative diagnostics at once, we may get a single reliable diagnostic. Unfortunately, only a single event has been put forward to date, and this event was the result of a single diagnostic (Nottale 1986).

7.3) Towards a Realistic Observing Program

Armed with the preceding analysis on detection methods and variability indicators, what observational program might one embark upon in order to measure microlensing? In this section we briefly outline a few possible observing programs that might result in a microlensing detection. The first part of this section focuses on preferentially detect lensing at high optical depth, while the second part of the section is geared toward finding microlensing events at low optical depth.

7.3.1) Detection of High Optical Depth Events

Our first suggested observing program is based on the analysis of Gott (1981) discussed above. Observers should keep a close watch on the variability of each macroimage of a multiply-imaged AGN. Searches should be made for variations in one image that are repeated, after some time delay, in another image. Such variations would be indicators of intrinsic variations. Refsdal (1964b) has indicated that the measurement of such a time delay could give a measurement of the Hubble constant.

Once events were seen to be repeated from image to image, and the time delay between images found, analysis of the discrepancies between the variations could be made in terms of line-of-sight effects. One such line-of-sight effect is microlensing. Discrepancies between images might be great and highly variable, as the optical depth along the light paths could be near unity.

Observations of the first candidate gravitational (macro-) lens system 0957 + 561 A,B have been made since the discovery of the object. Schild and Cholfin (1986) have claimed measuring a time delay of 1.03 years between the two known images, but this claim is based only the repetition of a few photometric events and has not yet been independently verified. Their observational program, however, can be considered a model for future programs looking for high optical depth events.

If the two images cannot be completely resolved, one might look for repeated structures in their combined light curve. These repetitions could be the intrinsic

variations of the AGN occurring sequentially in each of the unresolved images. The light curve could then be processed to eliminate these intrinsic variations, leaving only the sum of the line-of-sight variations, from which microlensing effects might be identified.

7.3.2) Detection of Low Optical Depth Events

It is our view that microlensing variations in AGN are the exception rather than the rule. The rule is intrinsic variability. Unfortunately, most AGN studied are highly variable. This does not mean, however, that most AGN are highly variable. In fact, studies indicate that more than half are not (Wiita 1985, Hamuy and Maza 1987). Observers have historically found the highly variable AGN more interesting, and hence studied them more intensely. We therefore feel there is a need to compile a list of *stable* AGN: ones with little intrinsic variation. These AGN may, by definition, be less likely to undergo intrinsic variations, but, as a class, equally likely to undergo microlensing variations.

Finding stable AGN does not require much telescope time. In fact, it may not indicate the need for *any* telescope time. This is because quiet AGN can probably be found in the same surveys that located the highly variable ones. What is needed is a search of archival records and the compilation of a list.

Once such a list is compiled, some analysis can be done immediately. A statistical analysis should be carried out to find whether stable AGN inhabit any preferred position with respect to foreground galaxies. One might expect that AGN angu-

larly close to galaxies, or those containing strong metal lines indicative of being seen through a galaxy, to have higher variability than those angularly distant from galaxies. One could then attribute excess variability, if found, to effects including microlensing, peculiar to the foreground galaxies,.

Another list that would be useful is a subset of the prior list: one that isolates those AGN angularly close to foreground galaxies. A list that includes close AGN-galaxy angular associations has already been compiled for other purposes (Monk et al. 1986). This list has over 100 members. A supplementary list, possibly including thousands of AGN would be even more useful statistically.

Next, one might want to fragment our hypothetical list even further by including only those AGN behind galaxies that are likely to have high transverse velocities. If we are to observe transient events, the higher the relative observer-lens-source speed, the shorter the duration of these events will be, and the less observing time is necessary. Those galaxies that are thought to be in clusters, or have anomalously high redshifts are excellent candidates, as they are likely to have high transverse velocities.

If we assume that our motion with respect to the microwave background is peculiar, one might suspect that galaxies outside our local supercluster would not share this peculiar motion. These galaxies would then be likely to exhibit high relative transverse motions. Therefore, AGN behind more distant foreground galaxies would be the better candidates for successful observation.

The next step would be to observe the galaxies on a final list on a regular basis. One would then regularly inspect the light curves for signature indicative of microlensing. To define a more precise observing program, we must first make some generalizations and assumptions. We first assume, from the analysis in Chapter 3, that (conservatively) a given AGN on this list would undergo a microlens variation greater than 0.3 magnitudes to be 'observable'. Next we generalize all microlensing variations (based on the assumptions in Chapter 3) to say that a given quasar would be expected to undergo an observable microlensing event every 1000 years. We further assume that this variation would last of the order of a few years, and that of the order of 100 photometric observations are needed to define the light curve sufficiently to be able to identify it as microlensing. We can now estimate the time needed in our observing program.

If our list contains 100 candidate AGN, then observing each member of the list once a week for 10 years should 'catch' an observable lensing event. Alternatively, if a list can be made containing 1000 AGN candidates, then a one year observing program of each AGN, once a week, would be warranted to record at least one event. During the observational period, those AGN that are known to vary greatly should be excluded as intrinsically variable.

If these observations were to be done on a medium sized optical telescope, such as the 1-meter telescope at Cerro-Tololo, one might expect each photometric integration to take up about a minute (Hamuy and Maza 1987). A list containing

1000 source objects might then take on the order of 50 nights. A similar program, designed to detect AGN variability, was carried out by Hamuy and Maza. They observed 91 AGN in 35 nights obtaining 693 observations primarily using the Cerro-Tololo 1 meter telescope. The accuracy of the measurements would be on the order of 0.05 magnitudes.

Having to spend 50 nights to obtain a single photometric measurement of 1000 candidate AGN is prohibitive. Only if the time scale for microlensing was long, on the order of tens of years, would such a program yield sufficient time coverage for a microlensing detection. The total observing time needed to catch a lensing event is on the order of tens of years.

These observations might take less time were many AGN found on the same photographic plate. Koo and Kron (1982) find evidence for more than 10 QSOs per square degree brighter than 20th magnitude. A wide-field photograph might then catch many AGN in a single exposure.

A telescope capable of catching many AGN on a single plate is the 48-inch Schmidt. These telescopes have fields typically as large as 6 square degrees, and the ability to image 20th magnitude objects in a 1 hour exposure (Minkowski and Abell 1963). One might then be able to image 1000 AGN on a single night. Once this is done, computing techniques would enable the observer to record and remember the AGN positions and magnitudes. Subsequent observations with image processing techniques should be able to analyse a plate and record AGN changes to within an

error of 0.2 magnitudes per observation (Weedman 1986).

A problem with this is the original tedious task of discriminating the stellar images from the AGN images on the plate (Weedman 1986). This formidable preliminary project could be attempted with a discriminating technique involving color-color comparisons discussed by Koo and Kron (1982).

Those objects that are thought to be undergoing a microlensing event might be investigated spectroscopically to see if the broad emission lines are simultaneously undergoing a change that might be identified with microlensing. It is here that future telescopes might be of value.

The Hubble Space Telescope (HST), as well as the future large ground based telescopes, may be able to monitor candidate microlensing objects with high spatial and frequency resolutions. In particular, the High Resolution Spectrograph and the Faint Object Spectrograph on board HST may prove to be useful, as they expands the possible number of observable objects for which spectroscopic microlensing effects may be observed.

We point out that the Wide Field /Planetary Camera on board HST, as well as the Faint Object Camera are not good survey instruments with which to look for microlensing photometrically. The reason for this is that the number of AGN visible per field of view is less than for ground based Schmidt telescopes. Once an object is identified as a candidate microlensing source, however, the superior abilities of these instruments is useful in future observations of the candidate object.

Only one program which involves constant monitoring of stable AGN has come to our attention. Fiedler et al. (1987) have observed several QSO's in different radio frequencies on a daily basis over the time base of years. The QSO's they investigated were not known to be rapidly variable. They are, on the other hand, too few in number and too large in angular size (in the radio band observed) to be expected to undergo a microlensing variation during the observing program described. They found occasional dips in the light curve, which they claim is occultations by clouds inside our galaxy. Although these observations have brought forth no obvious microlensing candidate events, we believe it is these types of observations that are necessary to find microlensing phenomenon.

7.4) Conclusions

The physical basis on which the prediction of the gravitational microlensing phenomenon stands is well founded. There is no 'mysterious physics' that goes into the equations which result in microlensing predictions. That gravity affects light is not only a theoretical prediction but an experimental fact. Experiments that confirm the gravitational bending of light have been done repeatedly both on and off the Earth, verifying the predicted effect.

The astronomical tenets on which microlensing stands are also well founded. Stars are known to exist, and are known to have the ability to bend light. Galaxies are known to be made up of stars. The placement of AGN at cosmological distances has become accepted also. The number of dim stars in galaxies and the universe

is the unknown. But even in the most conservative case, with bright stars the dominant form of candidate microlenses, the microlensing phenomenon may still be sought.

The observational techniques needed to detect microlensing also exist already. Photometric and spectroscopic evaluation are the tools needed to detect microlensing, and they have been the proven work-horses of astronomy since the beginning of the modern era. No new technology need await development.

The positive detection of a microlensing event would be of general interest to astronomy. The information it could tell us about the number, motions, and masses of compact lenses, and the structure and dynamics of AGN might revolutionize our understanding of everything from the cosmology of the universe to power source of QSO's. Among the possible results it might yield are direct detection of the form of dark matter in galaxies and the universe.

Why, then, has microlensing not been actively sought and detected? What, in the past, has prohibited the detection of microlensing is at least two impediments. First and foremost are the amounts of time and resources that would be needed to undertake a program that would have at least a reasonable chance of making a microlensing detection. The second prohibitive factor is a general lack of knowledge as to what to look for.

It is hoped that this thesis can bring closer the night of a microlensing detection. We feel our research helps reduce the barriers against microlensing detection in at

least 5 ways. 1) We have outlined the most probable places to look for microlensing. This was done in Chapters 2 and 3. 2) We have added reasons an observer might want to search for microlensing. This was shown in Chapter 4 by outlining how important lens and source information could be recovered from a microlensing detection. 3) We added to the ability of the observer to distinguish microlensing photometrically. This was accomplished in Chapter 5 by the presentation and discussion of double-star light curve signatures. 4) We have added another feature of microlensing that an observer can look for. This was done in Chapter 6 by the introduction of possible emission line changes that might be expected by microlensing. 5) We have also outlined possible observing programs that might yield a microlensing detection. This has been done in the present Chapter.

Microlensing can be an important tool to the informed observer. There is much information it can tell us, and many ways it could manifest itself. If detected, microlensing could prove to be an valuable resource in the quest to understand the universe around us.

References

Bond, J. R., Efstathiou, G., Silk, J. 1980, *Phys. Rev. Lett.* **45**, 1980.

Chang, K., and Refsdal, S. 1979, *Nature* **282**, 561.

Chang, K., and Refsdal, S. 1984, *A. Ap.* **132**, 168.

Deguchi, S. and Watson, D. 1986, *Phys. Rev. D* **34**, 1708.

Fiedler, R. L., Dennison, B., Johnston, K. J., and Hewish, A. 1987, *Nature*, **126**, 675.

Gott, J. R. III 1981, *Ap. J.* **243**, 140.

Greiger, B., Kayser, R., and Refsdal S. 1986, *Nature* **324**, 126.

Hamuy, M., and Maza, J. 1987, *A. Ap. Suppl.* **68**, 383.

Kayser, R., Refsdal, S., and Stabell, R. 1986, *A. Ap.* **166**, 36.

Koo, D. C., and Kron, R. G. 1982, *A. Ap.* **105**, 107.

Liebes, S. 1964, *Phys. Rev. B* **133**, 835.

Minkowski, R. L., and Abell, G. O. 1963, Basic Astronomical Data, Ed.: Strand, K. Aa.

Monk, A. S., Penston, M. V., Pettini, M., and Blades, J. C. 1986, *M. N. R. A. S.* **222**, 787.

Nottale, L. 1986, *A. Ap.* **157**, 383.

Paczynski, B. 1986a, *Ap. J.* **301**, 503.

Paczynski, B. 1986b, *Ap. J.* **308**, L43.

Press, W. H., and Spergel, D. N. 1985, *Ap. J.* **296**, 679.

Refsdal, S. 1964a, *M. N. R. A. S.* **128**, 295.

Refsdal, S. 1964b, *M. N. R. A. S.* **128**, 307.

Refsdal, S. 1986, private communication.

Saslaw, W. C., Narasimha, D. and Chitre, S. M. 1985, *Ap. J.* **292**, 348.

Schild, R. E., and Cholfin, B. 1986, *Ap. J.* **300**, 209.

Schneider, P., and Wagoner, R. V. 1987, *Ap. J.*, in press.

Schneider. P., and Weiss, A. 1987, *A. Ap.* **171**, 49.

Ulrich, M. H., Boksenberg, A., Bromage, G. E., Clavel, J. Elvius, A., Penston, M. V., Perola, G. C., Pettini, M., Snijders, M. A. J., Tanzi, E. G., and Tarenghi, M. 1984, *M. N. R. A. S.* **206**, 221.

Weedman, D. W. 1986, Quasar astronomy.

Wiita, P. J. 1985, *Phys. Rep.* **123**, 117.

Index